AD NUMBER

AD851233

LIMITATION CHANGES

TO:

Approved for public release; distribution is unlimited.

FROM:

Distribution authorized to U.S. Gov't. agencies and their contractors; Critical Technology; FEB 1969. Other requests shall be referred to Air Force Materials Laboratory, Attn: MAMN)Wright-Patterson AFB, OH 45433. This document contains export-controlled technical data.

AUTHORITY

afml ltr dtd 7 dec 1972

AFML-TR-67-128
PART II

INVESTIGATION OF NONDESTRUCTIVE METHODS FOR THE EVALUATION OF GRAPHITE MATERIALS

AVCO GOVERNMENT PRODUCTS GROUP
SPACE SYSTEMS DIVISION
201 Lowell Street
Wilmington, Massachusetts 01887

TECHNICAL REPORT AFML-TR-68-128, PART II

FEBRUARY 1969

AIR FORCE MATERIALS LABORATORY
AIR FORCE SYSTEMS COMMAND
WRIGHT-PATTERSON AIR FORCE BASE, OHIO

NOTICES

When Government drawings, specifications, or other data are used for any purpose other than in connection with a definitely related Government procurement operation, the United States Government thereby incurs no responsibility nor any obligation whatsoever; and the fact that the Government may have formulated, furnished, or in any way supplied the said drawings, specifications, or other data, is not to be regarded by implication or otherwise as in any manner licensing the holder or any other person or corporation, or conveying any rights or permission to manufacture, use, or sell any patented invention that may in any way be related thereto.

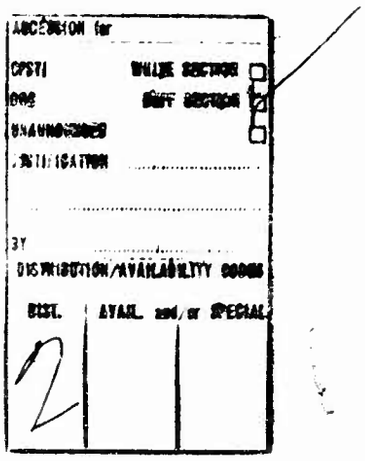

THIS DOCUMENT IS SUBJECT TO SPECIAL EXPORT CONTROLS AND EACH TRANSMITTAL TO FOREIGN GOVERNMENTS OR FOREIGN NATIONALS MAY BE MADE ONLY WITH PRIOR APPROVAL OF THE AF MATERIALS LABORATORY, WRIGHT-PATTERSON AFB, OHIO 45433.

Copies of this report should not be returned unless return is required by security considerations, contractual obligations, or notice on a specific document.

1100 - April 1969 - CO455 - 72-1592

AFML-TR-67-128
PART II

INVESTIGATION OF NONDESTRUCTIVE METHODS FOR THE EVALUATION OF GRAPHITE MATERIALS

R. C. STINEBRING
A. W. SCHULTZ
I. W ORNER

FOREWORD

This report was prepared by AVCO Corporation, Space Systems Division, Lowell, Massachusetts, under USAF Contract AF33(615)-3942. The contract was initiated under Project No. 7351 "Metallic Materials", Task No. 735109 "Nondestructive Methods". The work was administered under the direction of the Air Force Materials Laboratory, with Mr. W.L. Shelton, MAMN, acting as Project Engineer, and Mr. R.R. Rowand, Technical Manager for Nondestructive Methods.

This report covers work conducted from 15 April 1967 to 15 May 1968 at AVCO/SSD, Mr. R.C. Stinebring, Project Engineer, Mr. C.H. Hastings, Project Manager. The authors appreciate the contributions of Messrs. B.L. Killion, A.M. Chetson, S.A. LoPilato, and E.A. Proudfoot of the Nondestructive Test Evaluation Section.

Manuscript released by the authors May 1968 for publication as an AFML Technical Report. It is also assigned AVCO Document No. AVSSD-0236-68-RR.

This technical report has been reviewed and is approved.

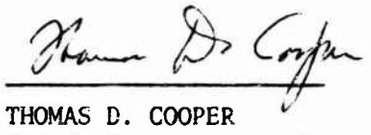

THOMAS D. COOPER
Chief, Processing and
Nondestructive Testing Branch
Metals & Ceramics Division

ABSTRACT

The objective of the program was to utilize the nondestructive testing information, correlations, and techniques, developed during the previous year, for characterizing and evaluating zirconium and hafnium diboride systems and aerospace graphite materials.

The program was divided into three distinct phases:

A. Characterization and Evaluation of Diboride Materials
B. Analysis of the Nondestructive Infrared Method for Measuring the Thermal Inertia ($k\rho C_p$)
C. Application of NDT Techniques for Evaluating and Predicting Properties in Aerospace Graphite Billets

During Phase A, over 800 billets of diboride systems were evaluated and characterized. Several important correlations are presented relating nondestructive test results to billet quality as well as mechanical and thermal behavior. Among the most effective NDT techniques for evaluating the diborides are ultrasonic velocity, ultrasonic pulse-echo, radiography, gamma radiometry, eddy current, thermoelectric and dye penetrant.

Phase B was concerned with the determination of limitations and influencing variables on the performance of the infrared radiometric techniques for determining thermal inertia ($k\rho C_p$). This technique offers several advantages, such as increased speed, non-contact with specimen and ability to evaluate actual structures.

The geometrical limitations, such as curvature, thickness, edge effects, as well as, range of thermal conductivities, etc., are discussed. Suggestions are made for improvements in the apparatus and for adapting it for field use.

Aerospace graphite (ATJ-S) used in a Philco-Ford nose cone program was characterized in the billet form in Phase C of the contract. The use of gamma radiometry and ultrasonic velocity data in a computer program allowed modulus to be monitored and density changes to be noted. Some work was also done on detection and characterization of flaws and anomalies, such as "calcium" deposits, parting lines, etc.; but their effects on material behavior were not studied. Recommendations are presented for improving this type of effort. These include the judicious use of such destructive test data as strain to failure, Poisson's ratio, ultimate tensile strength, modulus and effects of flaws for obtaining the most meaningful nondestructive test correlations.

CONTENTS

CONTENTS (Concl'd)

ILLUSTRATIONS

ILLUSTRATIONS (Cont'd)

ILLUSTRATIONS (Concl'd)

TABLES

PART A - APPLICATIONS OF NONDESTRUCTIVE TEST TECHNIQUES TO THE CHARACTERIZATION AND EVALUATION OF DIBORIDE MATERIALS

R. C. Stinebring

I. INTRODUCTION

Nondestructive test techniques for evaluating and characterizing various types of graphites have been developed on previous programs.[1,2] Of special significance was the development of correlations between mechanical properties measured destructively and nondestructively measured parameters of sonic velocity and density. The relationship, $V_L^2 d = E_D$, where:

V_L = longitudinal velocity

d = density

E_d = dynamic modulus

has correlated with the tensile modulus of graphite and other brittle materials.[3] Since the sonic velocity can be measured in an actual structure or material in bulk form and density can also be measured using a gamma radiometric technique, the variations in modulus and density can be monitored and predictions made on the behavior of the structure. This has obvious advantages over destructive sampling techniques that measure properties on specimens which may not be representative of the structure.

The information gained on the referenced programs was utilized for evaluating zirconium diboride and hafnium diboride materials with additions of such things as silicon carbide and graphite. The objectives of the program were threefold:

- to determine the effectiveness of the NDT techniques for evaluating and characterizing the diborides
- to give support and information to the Avco/SSD Metals and Ceramics Group for use in understanding and adjusting their process parameters
- to screen materials, make quality assessments, and supply information for the ManLabs programs being carried out under Air Force Contracts AF33(615)-3671 and AF33(615)-3859.

The diboride systems, mentioned above, were originally studied by ManLabs under Contract AF33(657)-8635, "Investigation of Boride Compounds for Very High Temperature Applications", and are briefly described in Reference 4. The usefulness of these materials for leading edges, nose cones, etc., for high velocity flight and reentry and methods for fabrication and scale-up are the subjects for the present ManLab's programs. These materials display considerable strengths and oxidation resistance at temperatures in excess of 2000°C. A listing of the materials evaluated on this program is given in Table I.

In addition to the ultrasonic velocity and gamma radiometry, other nondestructive techniques were applied to the evaluation and characterization of over 800 billets and specimens. These techniques are listed in Table II and are discussed in detail in the following text.

TABLE I

REVISED DIBORIDE COMPOSITIONS FOR SCREENING PHASE EVALUATION

Material No.	Designation	Remarks and Original Rationale for Specific Additives
I	ZrB_2	Zirconium diboride, no additive.
II	HfB_2	Hafnium diboride, no additive.
III	HfB_2 + SiC	Hafnium diboride with twenty volume percent silicon carbide to enhance oxidation resistance.
IV	HfB_2 + SiC	Hafnium diboride with thirty volume percent silicon carbide to enhance oxidation resistance.
V	ZrB_2 + SiC	Zirconium diboride with twenty volume percent silicon carbide to enhance oxidation resistance.
VI	HfB_2 + Hf-Ta	Hafnium diboride with four volume percent hafnium tantalum alloy additive, an oxidation resistant metallic binder phase, to enhance strength properties.
VII	HfB_2 + SiC	Discontinued. Boron rich HfB_2 with silicon carbide additive.
VIII	ZrB_2 + SiC + C	Zirconium diboride (56 volume percent) silicon carbide (14 volume percent) graphite (30 volume percent) composite with enhanced oxidation and thermal shock resistance.
IX	HfB_2 + HfSi	Hafnium diboride with twenty volume percent hafnium silicide additive to enhance oxidation resistance.
X	ZrB_2 + SiB_6	Zirconium diboride with twenty volume percent silicon hexaboride additive to enhance oxidation resistance.
XI	ZrB_2 + Cr	Zirconium diboride with eight volume percent chromium additive to enhance mechanical strength properties.
XII	ZrB_2 + C	Zirconium diboride with graphite additive to enhance thermal shock resistance.
XIII	ZrB_2 + W	Zirconium diboride with tungsten filament additive to enhance mechanical properties.

TABLE II

NDT TECHNIQUES APPLIED ON THIS PROGRAM

NDT Technique or Method	Property or Variable of Interest
1. Ultrasonic velocity	Elastic modulus, density, structure
2. Gamma radiometry	Density, homogeneity
3. Eddy Current	Electrical conductivity, structure, chemistry
4. Ultrasonic Pulse Echo	Flaws, i.e., cracks, inclusions, discontinuities, properties gradients, porosity
5. Dye Penetrant	Flaws, i.e., surface cracks, porosity
6. Radiography	Density, flaws, (i.e., inclusions, cracks, porosity)
7. Thermoelectric	Chemistry

II. PROGRAM RESULTS

A. FLAW DETECTION TECHNIQUES

1. Dye Penetrant

Among the simplest and often most informative NDT techniques for detecting surface cracks and porosity is that which employs a dye dissolved or carried in a penetrating oil. In this technique, the surface of a specimen is flooded with a dye penetrant which is drawn into cracks and porous areas by capillary action. Subsequent to rinsing the surface and applying fine developing powder, the dye bleeds out from the flaw areas and can be readily detected by visual or optical means.

Specimens which exhibited widespread cracking, such as seen in Figure 1, can be seen readily by normal visual observation and, of course, do not require dye penetrant techniques. However, more subtle cracking and porosity as shown in Figure 2 require the use of dye penetrant for effective detection.

Each billet was examined using this technique for screening and the information was used to eliminate billets from further processing and to make adjustments in processing parameters, such as pressure, temperature and time to minimize or eliminate the occurrence of these flaws.

It should be pointed out that the occurrence of cracked specimens was widespread in ZrB_2 and HfB_2 billets and the addition of other materials, such as SiC and graphite to the powders greatly reduced this propensity for cracking. Reference 4 indicates that the cracking condition may be due to impurity phases, such as metal oxides and carbides in the original powder. The addition of silicon carbide appears to act as a "getter" for these impurities and thereby improves the hot pressing characteristics of the powder.

The dye penetrant technique also proved useful in evaluating ZrB_2 material which had been subjected to a plasma arc high temperature test. Visual examination of the specimens indicated that they had survived the arc test without damage and plans were being made to put them through another high temperature cycle. However, the dye penetrant technique revealed the presence of widespread cracking due to thermal shock as shown in Figure 3. As a result, these specimens were removed from further testing. Other specimens (Figure 4) of HfB_2 were tested with dye penetrant and showed the presence of a porous band in the center of the specimen after the plasma arc test. Since these specimens had been fabricated by a facility other than Avco/SSD, and were supplied directly to ManLabs, no NDT tests were performed on the original billets and it was not known if this condition was present before the arc test. However, fragments of the original billets from which the arc test specimens were cut were dye penetrant tested and showed the presence of the porous band in the parent materials.

Billets of the diborides fabricated at Avco/SSD were tested with the dye penetrant and the other NDT techniques in two conditions -- the as-machined billet and as diametrical slices. Surface cracks and other conditions, such as seams, folds, and porosity were detected in the billet form; and if their severity

78-3849

Figure 1 GROSSLY CRACKED DIBORIDE BILLET

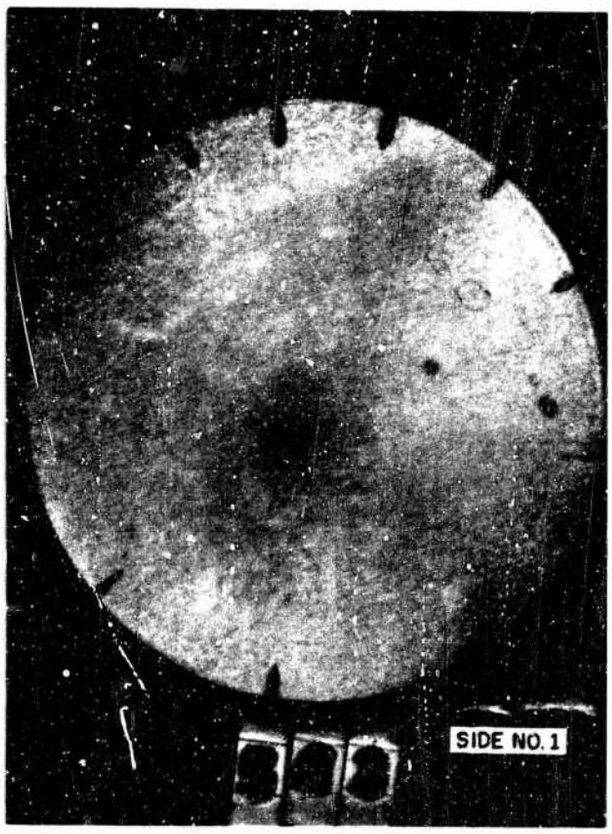

78-3850

Figure 2 CRACKS AND POROSITY DETECTED BY DYE PENETRANT TECHNIQUE

VISUAL APPEARANCE OF SPECIMEN AFTER
10 MW PLASMA ARC TEST

APPEARANCE OF SAME SPECIMEN AFTER DYE
PENETRANT TEST. NOTE THE EXTENSIVE
CRACKING AROUND DIAMETER AND ON THE
BOTTOM SURFACE.

Figure 3 CRACKING IN ZrB_2 SPECIMEN AFTER EXPOSURE TO 10 MW PLASMA ARC TEST

HfB_2 Specimen After 10 MW Arc Test
(Dark Band in Center Has Bluish Appearance)

Same Specimen Showing Dye Penetrant Test Results.
Strong Bleedout in Center Zone Indicates Gross Porosity

Figure 4 DETECTION OF BAND OF GROSS POROSITY IN ARC TESTED HfB_2 SPECIMEN USING A DYE PENETRANT TECHNIQUE

was judged to be minor, the billets were sectioned to obtain bend test and high temperature test specimens. The sections were then evaluated visually and with dye penetrant to detect any cracks or porous areas, which were previously subsurface. The results were recorded and described on a test summary sheet and were transmitted to the processing group for their information and action.

2. Ultrasonic Pulse Echo Technique

Techniques which use ultrasonic pulses and observations of the reflected pulses for interrogating materials are in widespread use for sensitively detecting such conditions as cracks, delaminations, inclusions, porosity, etc.

Billets of the diboride materials were evaluated using the equipment shown in Figure 5 and a map of each billet was made showing the locations of defect indications (Figure 6). These maps were supplied to the Metals and Ceramics Process Group to assist them in their sectioning plan and in making disposition of the material.

In addition, the effects of flaws on high temperature performance were considered to be important for establishing ultrasonic test and acceptance standards. Flaws detected by this technique generally fell into one of several categories:

- gross cracking (Figure 7)
- laminar cracks and segregation (Figure 8)
- voids and inclusions (Figure 9)
- porosity

Materials of the ZrB_2 + SiC series which contain flaws have been subjected to thermal shock conditions in high temperature test facilities located at Battelle Memorial Institute, Marquardt Corp. and Johns-Hopkins Applied Physics Laboratory. No deleterious effects have been traced to defects present in the material.

A leading edge specimen, subjected to the Marquardt hypersonic wind tunnel contained defects (voids) as great as 0.030-inch diameter and performed successfully. A ring specimen tested with a programmed increasing radial heat flux in the Battelle facility failed by cracking at a location approximately 1/4 inch away from an ultrasonically detected defect estimated to be approximately 0.020 to 0.030 inch (Figure 10).

Other flawed specimens tested in the plasma arc at Applied Physics Laboratory exhibited the same degree of success or catastrophic failure as materials without flaws. The high temperature test conditions and results will be discussed in forthcoming ManLabs reports and are preliminary at this time. This work is discussed only to illustrate the types of flaws being detected and the fact that their significance has not been established.

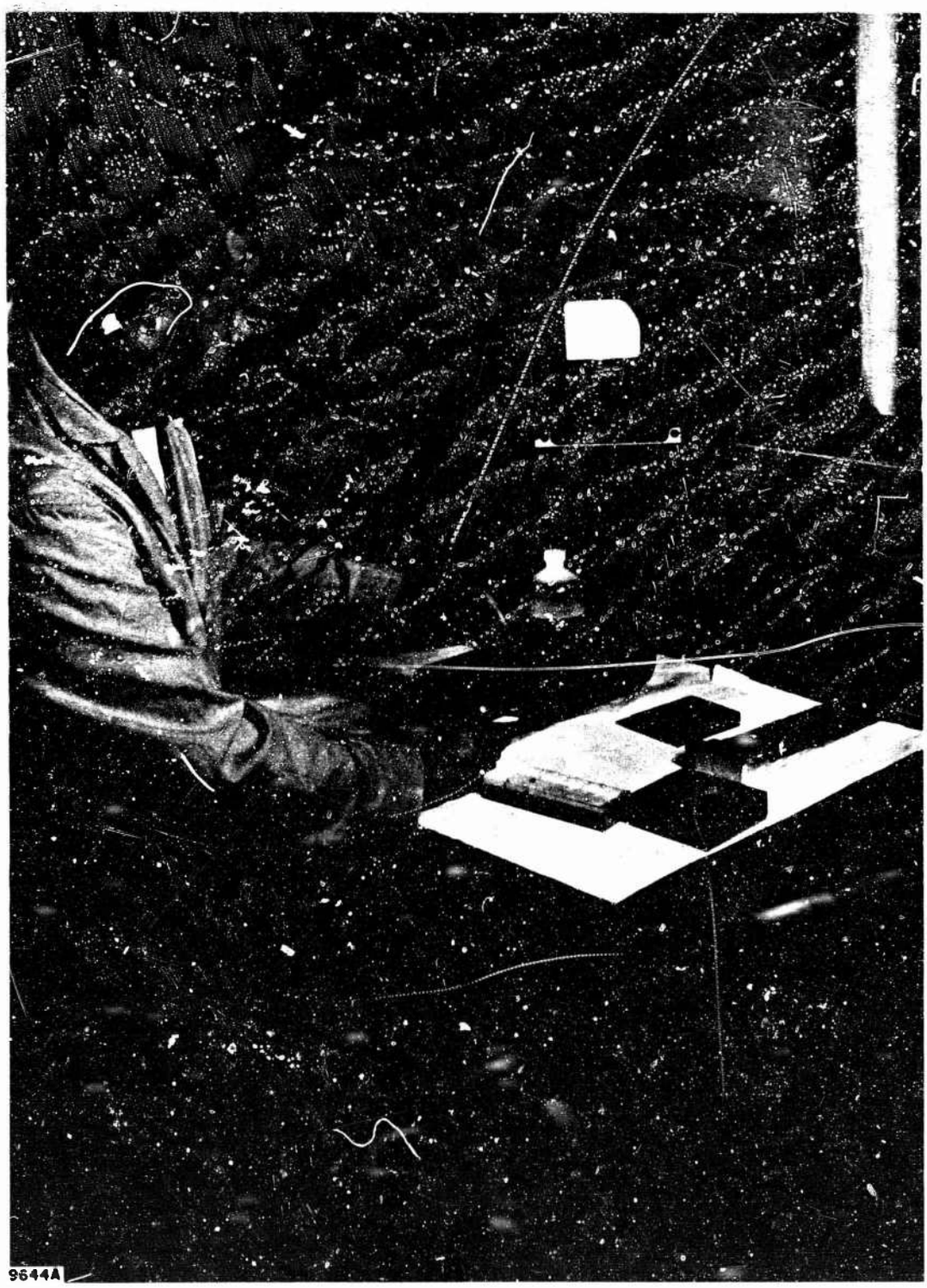

Figure 5 ULTRASONIC PULSE ECHO TEST METHOD AND APPARATUS

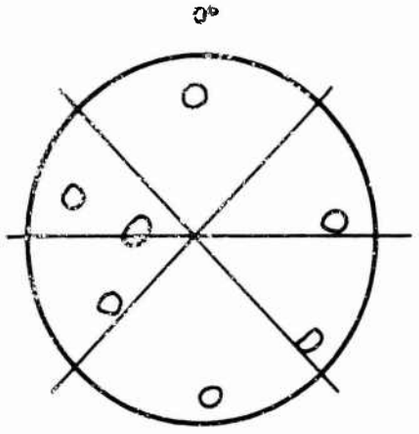

Figure 6 ULTRASONIC PULSE ECHO INDICATIONS NOTED ON MAP OF DIBORIDE BILLET

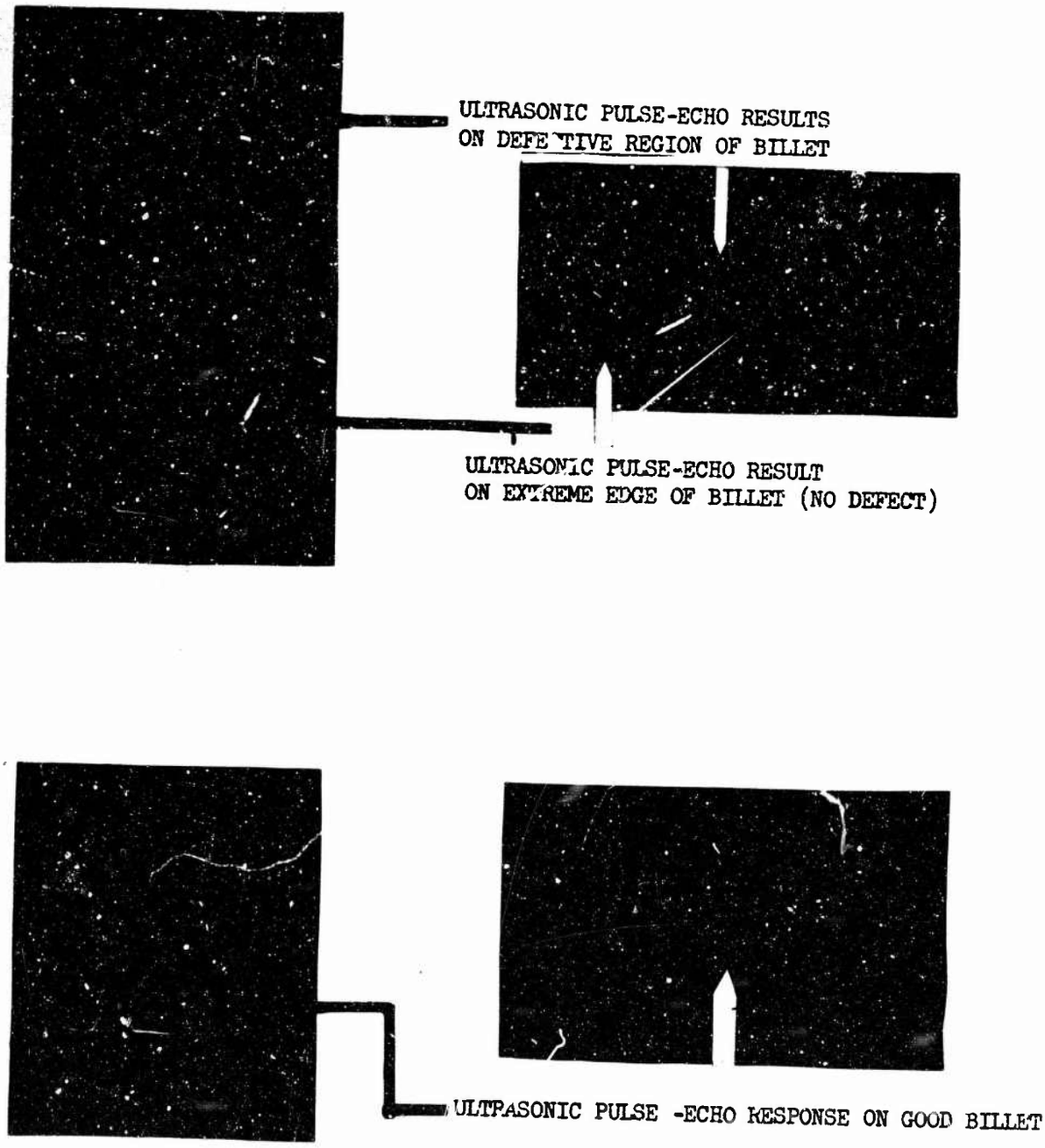

Figure 7 RESULTS OF PULSE-ECHO ULTRASONIC TEST TECHNIQUE ON ZrB_2/5 v/o GRAPHITE SHOWING TYPICAL RESPONSE TO DEFECTIVE AND NON-DEFECTIVE BILLETS

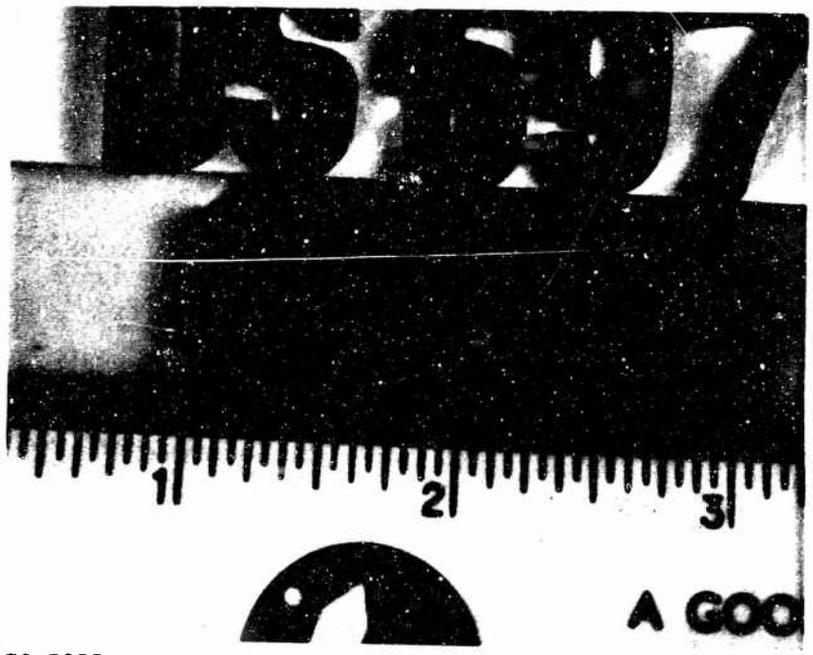

78-3855

Figure 8 LAMINAR CRACKS AND INCLUSIONS DETECTED BY ULTRASONIC PULSE ECHO TECHNIQUE

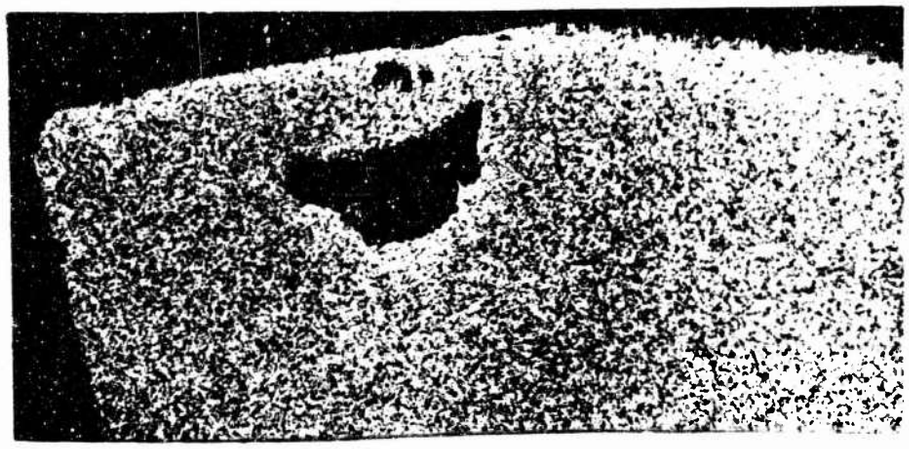

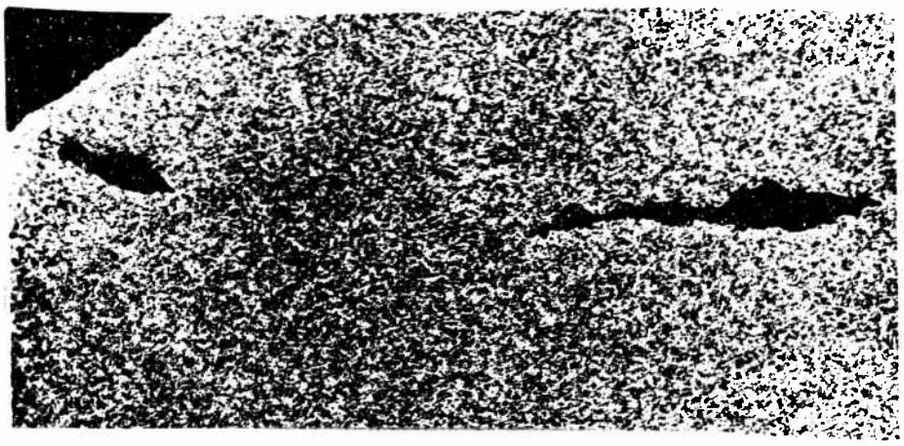

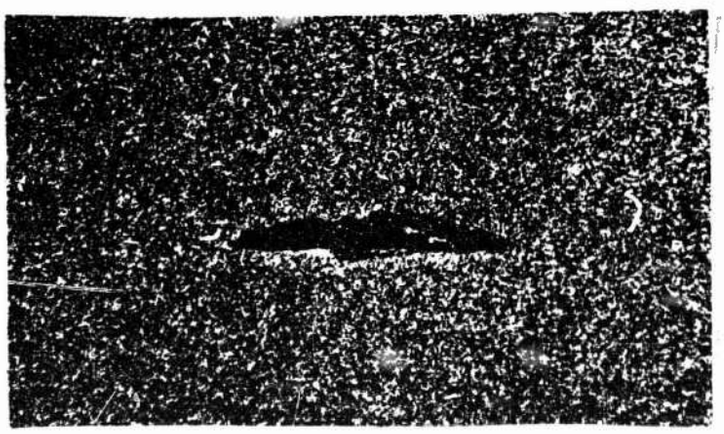

Figure 9 TYPICAL DEFECT SITE FOUND BY ULTRASONIC PULSE ECHO TECHNIQUE

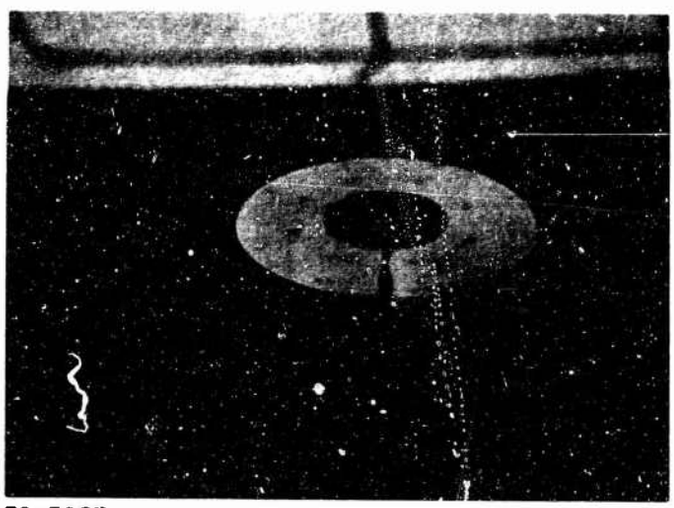

78-3857

CRACKED RING SPECIMEN AFTER EXPOSURE TO BATTELLE HIGH TEMPERATURE THERMAL SHOCK TEST (X MARKS THE LOCATION OF ULTRASONICALLY DETECTED DEFECT)

Figure 10 POST-TEST APPEARANCE OF DIBORIDE RING AFTER EXPOSURE TO BATTELLE THERMAL SHOCK TEST

Porosity in the billets can be detected by observing a loss of the back reflected pulse. While grossly porous material (greater than 10 percent) has not been tested for high temperature bend strength, it is interesting to note that homogeneously distributed porosity resulting in density differences of as much as 10 percent from theoretical density do not have a demonstrable effect on the room temperature or high temperature bend strength, although a small gram size may be compensating for the increase of porosity. However, porosity (or low theoretical density) does influence the modulus and, therefore, is a helpful parameter to monitor. The effect of density on modulus and sensitive techniques for measuring both density and modulus nondestructively will be discussed in a later section.

3. Radiography

Film radiography was used to detect the presence of voids, inclusions and local gross changes in composition such as gross segregation. The through transmission method is used with the x-ray source on one side of the specimen and a film (detector) on the other side. The equation describing x-ray (and gamma-ray) absorption in travelling through the specimen material is:

$$I = I_0 e^{-(\mu/d)\, dr} \qquad (2)$$

It will be noted that absorption is a function of the chemistry (upon which the value of μ depends), the density and the thickness. When several elemental components are present, the value of I observed depends on the density and the percentage of each element present and the wavelength or "voltage" of the incident radiation. Since monochromatic beams are not easily obtainable, the value of μ usually observed is an effective value for polychromatic beams. If chemistry, density, and thickness are constant, the amount of radiation passing through the specimen will be constant and the film will be uniformly exposed. However, if I changes locally, as in the case of foreign included material or of segregation of the elemental constituents, or if the thickness changed (as in the case of a void) then the amount of radiation impinging on the film is less than the surrounding image. Hence, voids, inclusions, and segregations can be detected by this procedure. Radiographic sensitivity depends on the source and the detector system used, but optimum combinations yield intensity differences on the order of 1 percent.

An example of a high density inclusion detected by this technique is shown in Figure 11. This inclusion is probably an agglomeration of ZrB_2 particles present in the starting powder.

Among other flaws which have been detected are cracks, voids, and density variations from edge to center of many billets.

B. PROPERTIES EVALUATION USING NDT TECHNIQUES

1. Gamma Radiometry

Radiometric density gaging is basically similar to radiography, consequently an equation similar to (2) applies. In radiometric density gaging, a collimated source of radiation (gamma rays, for this application) is used, and a

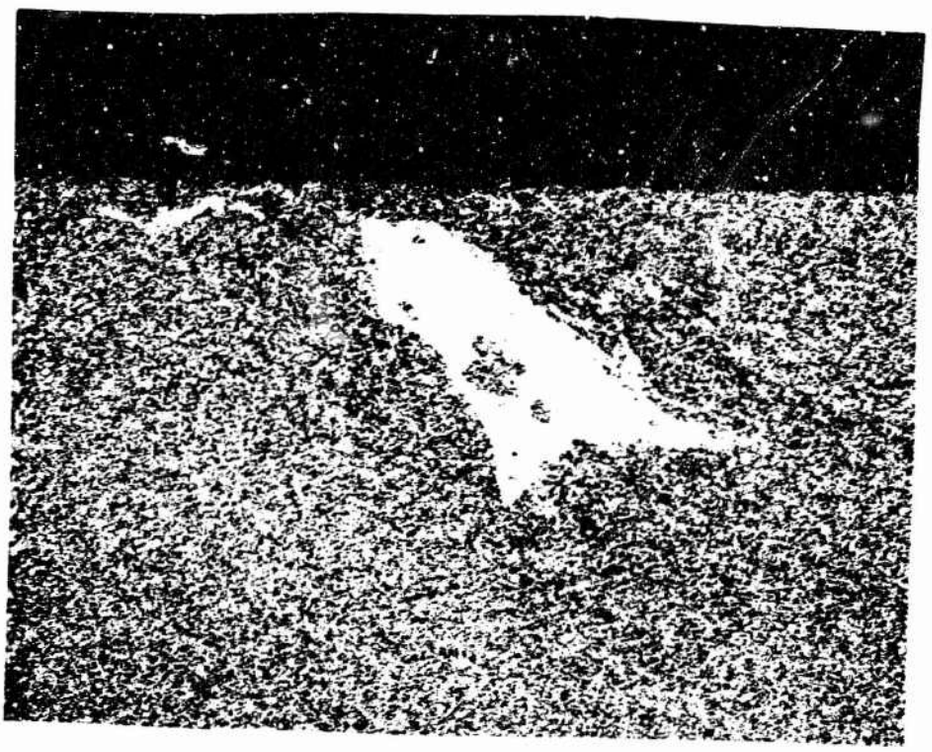

Figure 11 HIGH DENSITY INCLUSION IN ZrB_2 + SiC BILLET DETECTED BY RADIOGRAPHY

confined beam is directed through the specimen impinging on a scintillation detector. The output of the detector is fed to a scintillation counter. By accurately counting scintillations over a fixed time interval, small differences in radiation intensity from point-to-point or from specimen-to-specimen can be detected. Through suitable calibration procedures, specimen or local density can be determined. In practice, most radiometric gaging applications are based on the assumption of constant chemistry and only concern themselves with the thickness and/or density aspects of Equation 1. Since the value of transmitted intensity I is a function of both of these, it is necessary that one be fixed or known if the other is to be unambiguously determined. Hence, it can be quite important to radiograph materials, prior to density gaging, if voids, inclusions, etc., are likely to occur. Sensitivity of gaging devices to transmitted intensity changes is again about 1 percent and while normal operations usually have resolution on the order of 0.5 in^2, resolution much greater than this is attainable, depending on materials, configurations, reasonable counting times, etc.

The diboride billets have been radiometrically monitored at 20 locations and the results have been plotted graphically to illustrate the pattern of density variations. Figure 12 shows the results of monitoring a ZrB_2 billet which varies from edge to center. In this particular case, the density varies from approximately 5.73 gms/cc at the edge to about 6.05 gms/cc in the center with the average density (gravimetric) being 5.898 gms/cc or a total range of 5 percent. Since bend test specimens are taken from the central portion of the billet, the destructive test results of modulus and strength are only representative of this high density area in the gage length.

The radiometrically determined density is useful not only for monitoring the high temperature and pressure fabrication process but also can be used with the ultrasonic velocity results to nondestructively monitor modulus variations which will be discussed in detail in a later section.

2. Thermoelectric Technique

The use of a thermoelectric technique for detecting chemistry variations in diffusion-formed coatings is discussed in detail in Reference 5. It was reported that chemistry variability due to processing techniques and coating thickness were highly important to the oxidation behavior of coated refractory alloys. Because of the high sensitivity of the techniques, as well as simplicity of operation, it was applied to the diborides evaluation and characterization program for monitoring or detecting chemistry variations. As stated previously, the starting powders contained impurities that affected the fabrication parameters.

The effect on the billet density of HfB_2 specimens can be seen from Table III with the Wah Chang supplied material yielding a consistently lower density than the Shieldalloy powder.

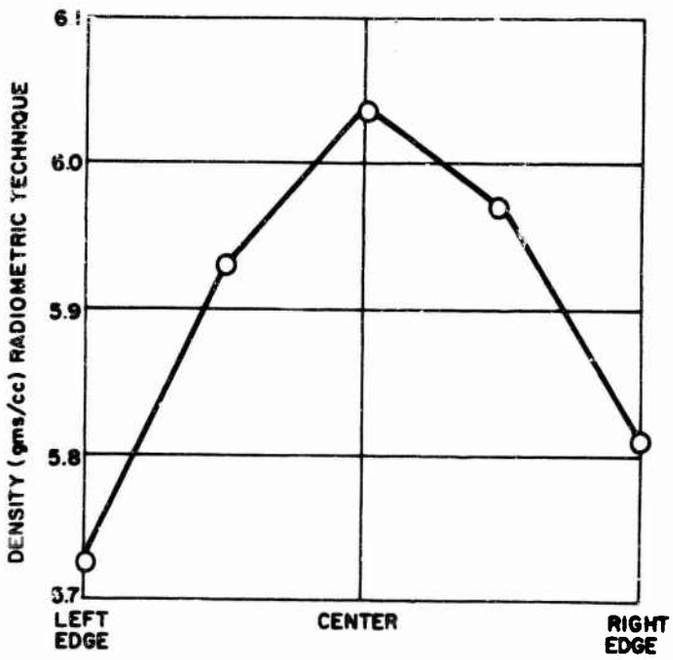

Figure 12 DENSITY VARIATIONS IN ZrB_2 + SiC BILLET USING RADIOMETRIC DENSITY GAGING

TABLE III

MATERIAL II FABRICATION CONDITIONS AND RESULTS (HfB_2)

Material Designation	Temp. (°C)	Pressure (psi)	Time (min)	Density (gm/cc)	Powder Supplier
II06 D0373	2200	4000	55	11.10	Shieldalloy
II06 D0374	2100	4000	42	11.17	
II06 D0375	2000	4000	68	11.15	
II06 D0376	1900	4000	145	11.14	
II06 D0379	1800	4000	130	10.84	
II06 D0383	2000	4000	40	11.17	
II05 D0399	1900	4000	100	9.10	Wah Chang
II05 D0409	2000	6000	180	9.80	
II05 D0413	2100	2500	124	9.54	
II05 D0423	1900	6000	180	9.26	
II05 D0425	2000	4000	153	9.45	
II05 D0427	2100	4000	108	9.57	

These effects are further demonstrated by the incidence of cracked specimens resulting from these powders (see Table IV).

TABLE IV

CRACK INCIDENCE VERSUS POWDER SUPPLIER ($Hf B_2$)

Supplier		Type of Cracks	No. Cracked/No. Tested	Percent Cracks
II Wah Chang	05	severe cracks/total examined	3/24	13
	05	edge cracks/total examined	4/24	17
	05	total cracked/total examined	7/24	29
Shieldalloy	06	severe cracks/total examined	4/5	80
	06	edge cracks/total examined	0/5	0
	06	total cracks/total examined	4/5	80

The thermoelectric technique test instrument shown in Figure 13 was applied to specimens made from powder representing three HfB_2 suppliers and the resultant thermoelectric emf was observed. These results are shown graphically in Figure 14, and it can be seen that the materials separate into three distinct groups according to the powder supplier. Note, also, that additions of SiC to as much as 35 percent do not affect the thermoelectric readings and the suppliers can still be identified. The reason for the differences in thermoelectric reading may be explained by comparing the starting powder chemistry assays. The Wah Chang powder exhibited lowest impurities, while Shieldalloy powder showed highest. Figure 15 shows a graphical plot HfO_2 assay for each powder and appears to correlate with the thermoelectric test results. The presence of 5 percent HfO_2 in the Shieldalloy powder may also explain the higher density for this material when compacted.

Chemical analysis of several powder batches of ZrB_2 did not reveal significant differences in chemistry with each exhibiting about 5 percent impurity level (chiefly ZrO_2) (Reference 4). These materials also did not show differing thermoelectric response.

3. Ultrasonic Velocity and Dynamic Modulus Results

The measurement of velocity presents a means for determining properties of interest by direct calculation using well known equations where applicable, and by establishing correlations between quantitative NDT measurements and material properties. In regard to elastic properties, for example, the relationship between wave velocities and physical properties can be seen from several equations such as:

$$V_L = \left[\frac{Y}{d} \frac{(1-\sigma)}{(1+\sigma)(1-2\sigma)} \right]^{1/2} \tag{3}$$

$$V_T = \left[\frac{Y}{d} \frac{1}{2(1+\sigma)} \right]^{1/2} = \left[\frac{\mu}{d} \right]^{1/2} \tag{4}$$

where:

V_L = longitudinal wave velocity

V_T = transverse wave velocity

Y = Young's modulus

σ = Poisson's ratio

d = Density

K = Bulk modulus

μ = Shear modulus

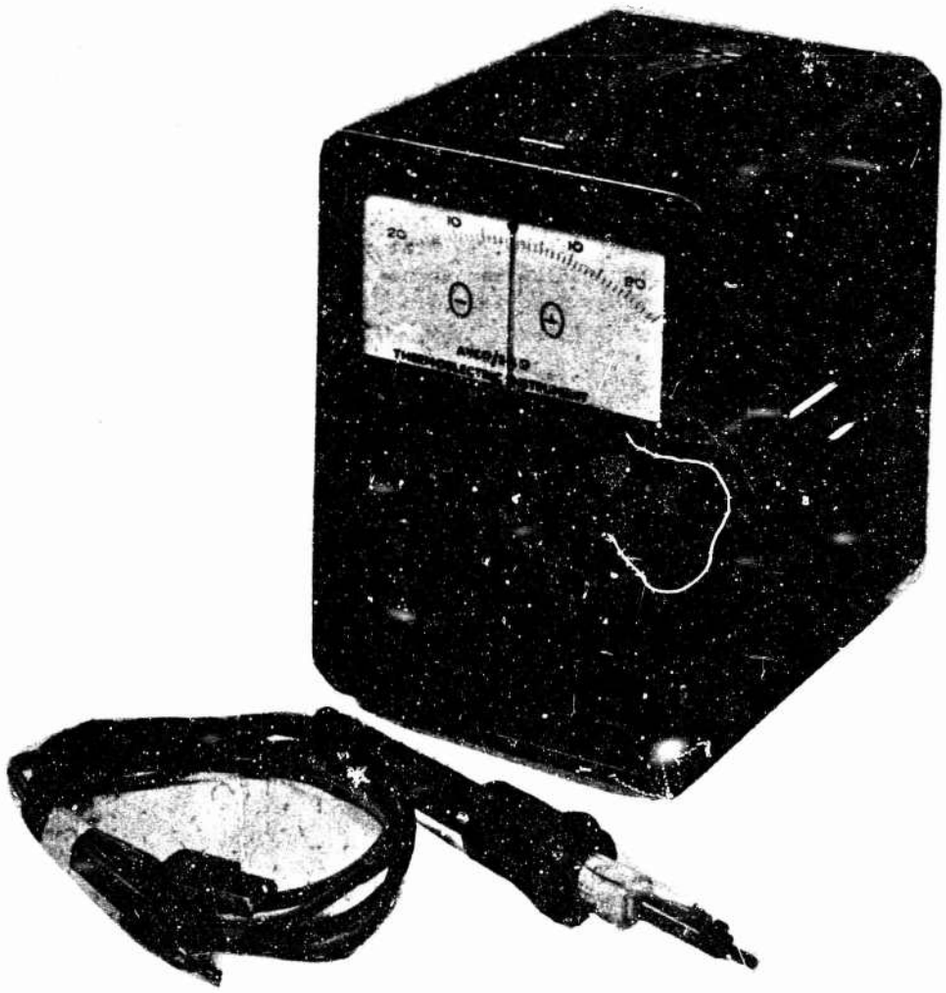

Figure 13 THERMOELECTRIC TEST INSTRUMENT

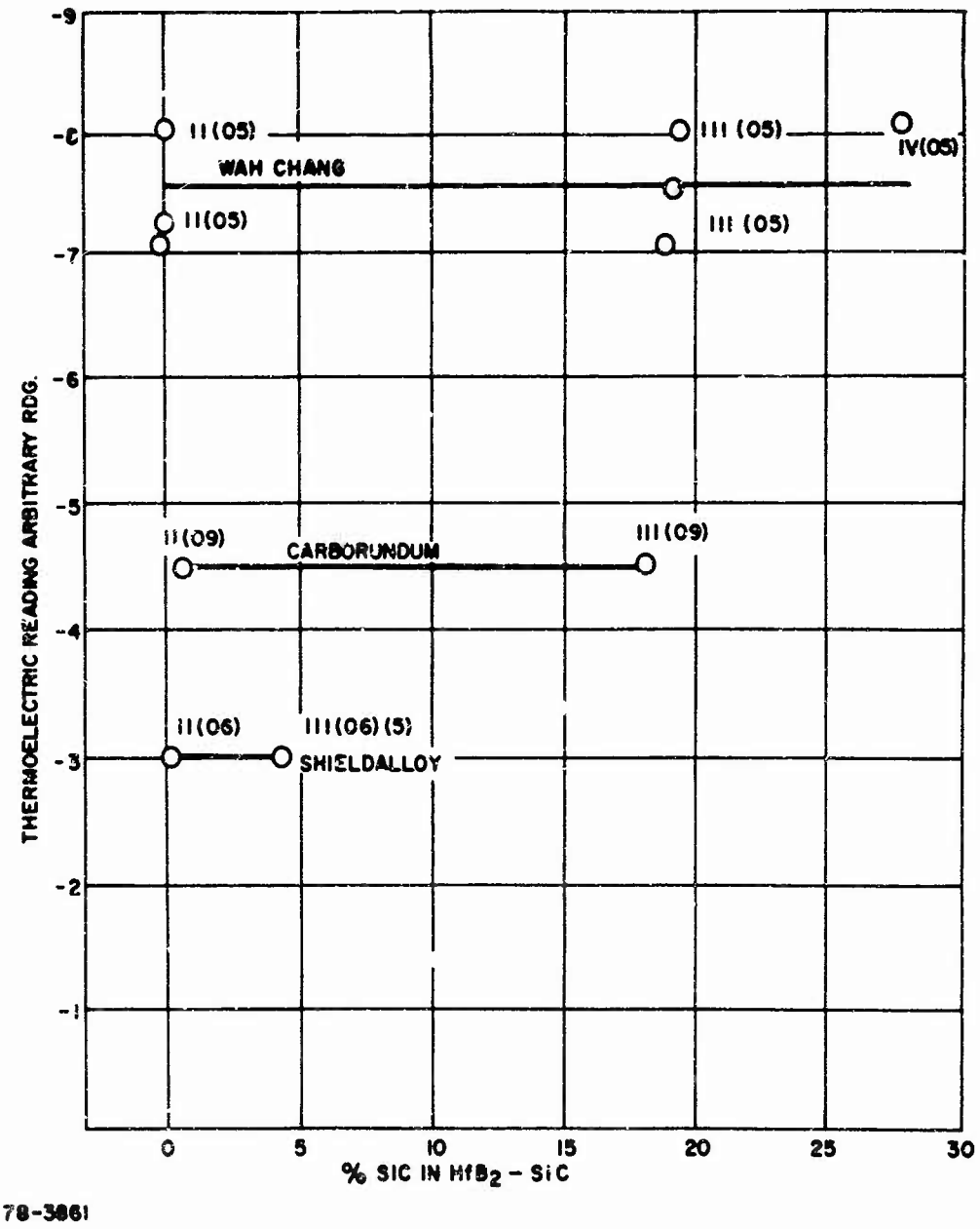

Figure 14 THERMOELECTRIC RESPONSE VERSUS POWDER SUPPLIER AND PERCENT ADDITIVE

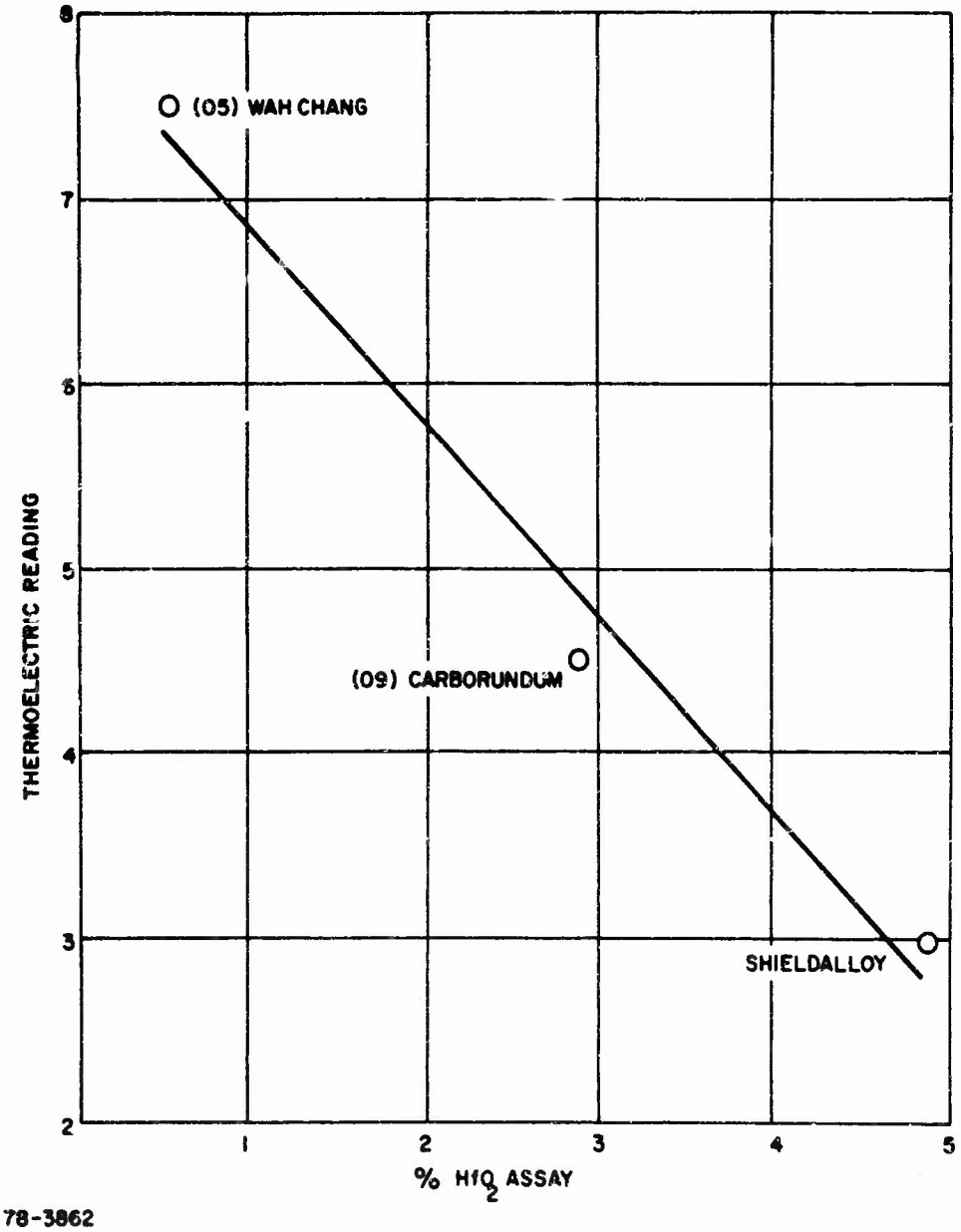

Figure 15 CORRELATION BETWEEN THERMOELECTRIC READING AND CHEMISTRY (HfO_2) IN HfB_2 BILLETS

While the above equations are written for extended isotropic media and represent an over-simplification when "non-ideal" materials are considered, empirical correlations between the nondestructively determined wave velocities and the destructively determined physical properties are to be expected. Equation 3 is of particular interest.

Since V_L is primarily responsive to the modulus-density ratio, process variation leading to modulus changes, either total or in a given direction (such as preferred orientation in elastically anisotropic materials or small amounts of "stiffening" impurities), will show up as a change in sound velocity. In some materials, depending on the stress-strain relationship, variation in internal stress levels will also be indicated. While not of immediate interest in this program, velocity-tensile strength determinations are also common for brittle materials. The present velocity measuring system is capable of making velocity determinations to a precision of about 1 percent (Figure 16).

It can be seen from Equation 3 that the substitution of 0.2 or less for σ will result in the approximate relationship of Equation 1. The value of σ can be determined by making longitudinal and transverse velocity measurements and solving the equation:

$$\sigma = \left[\frac{1 - \left(\frac{V_T}{V_L}\right)^2}{2 - \left(\frac{V_T}{V_L}\right)^2} \right] \qquad (5)$$

This was done for various specimens of ZrB_2 plus SiC and graphite and the Poisson's ratio was found to be approximately 0.1. Figure 17 shows the sonically measured Poisson's ratio in the pressing direction as a function of ZrB_2 plus SiC. Using this value in Equation 3 for σ, the product of $V_L^2 d$ very closely approximates the modulus. Empirical relationships were also established and are presented in Table V. Each specimen of the different material types was evaluated using sonic velocity and density and the results are given below.

a. Group I (ZrB_2)

The billets of ZrB_2 were evaluated over a density range of 5.3 gms/cc to 6.0 gms/cc representing a spread from 83 percent to 99 percent theoretical density. The data presented in Figure 18 show the marked decrease in dynamic modulus as a function of density. These data agree very well with the mechanical test data given in Reference 6 where the modulus decreases from 68.7 x 10^6 to 47 x 10^6 psi over a range of densities from 100 to 80 percent theoretical.

b. Group V (ZrB_2 + SiC)

It was mentioned previously that additions of SiC improved the fabricability of ZrB_2 base billets without apparently degrading strength or

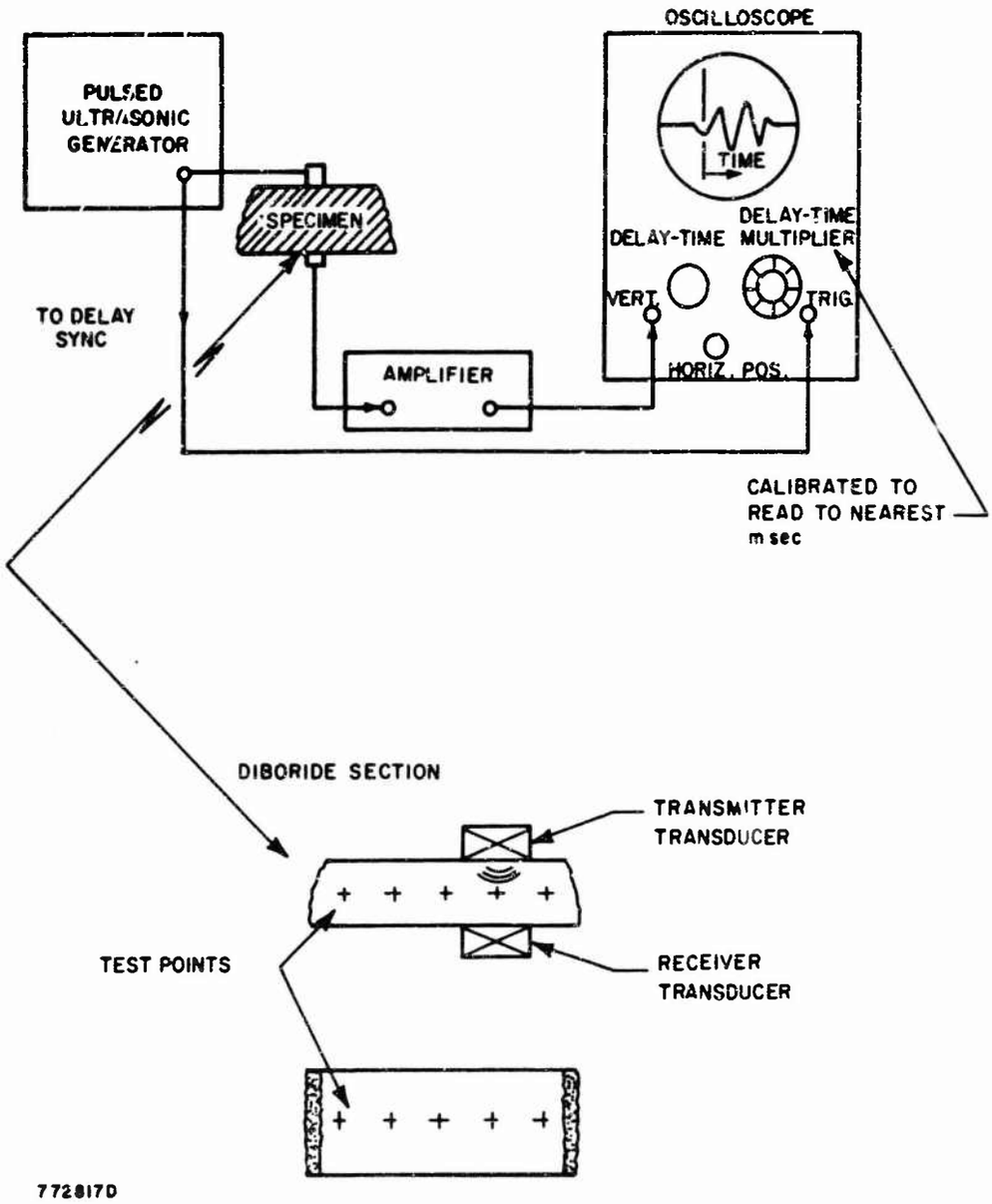

Figure 16 DIAGRAM OF ULTRASONIC VELOCITY MEASURING APPARATUS

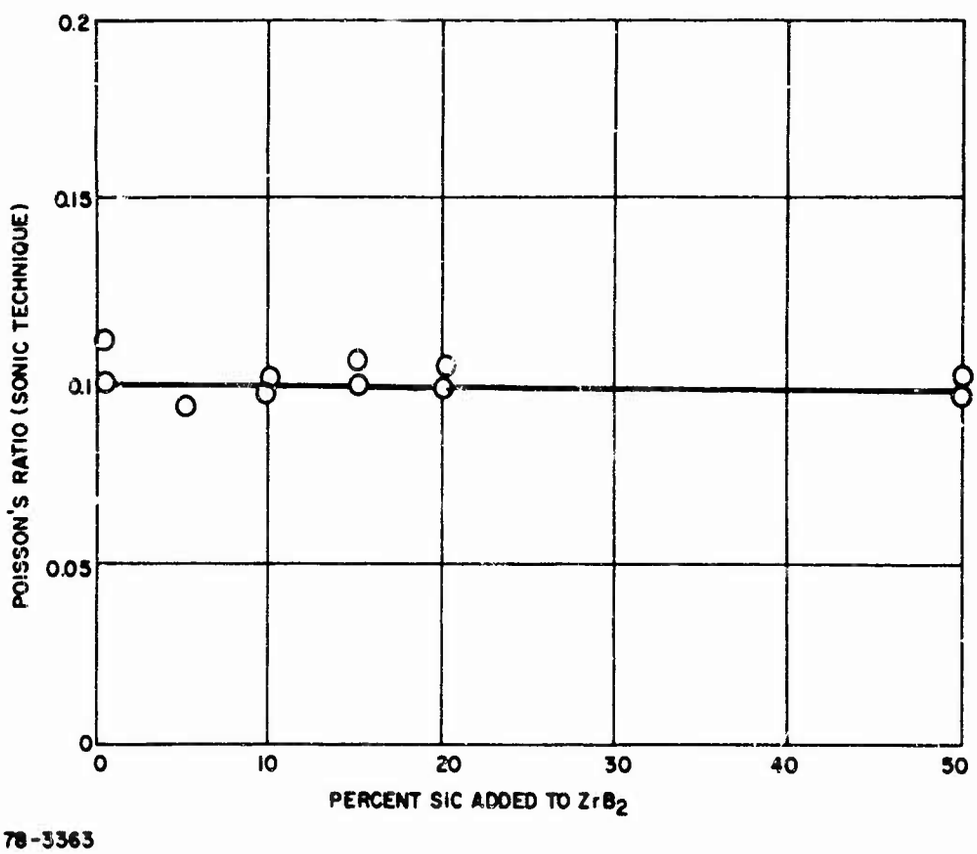

Figure 17 EFFECT OF SiC ADDITIONS TO ZrB_2 ON POISSON'S RATIO

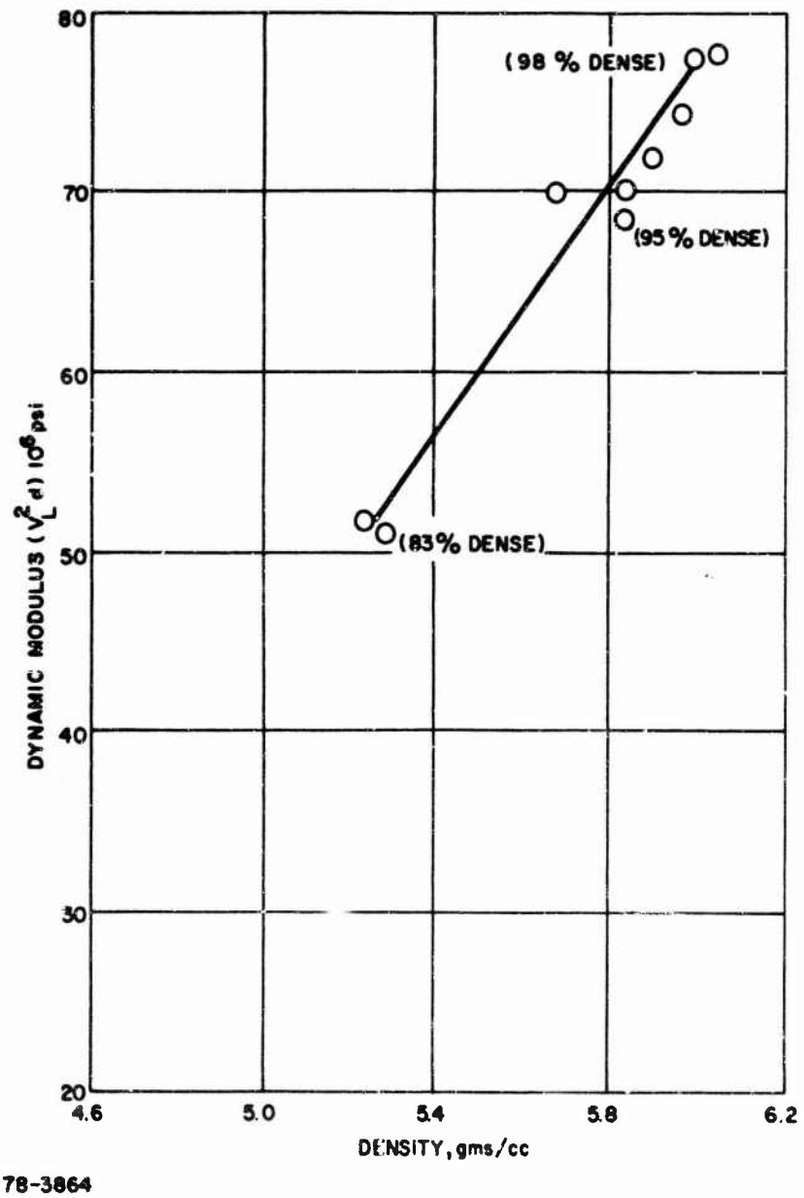

Figure 18 EFFECT OF DECREASING DENSITY (DUE TO POROSITY) ON DYNAMIC MODULUS

oxidation resistance while reducing the density thereby giving a more favorable strength to weight ratio. Billets of this type were studied extensively and were thoroughly characterized using NDT techniques.

In order to properly identify variability and the effects of such variables as porosity and additions of SiC the billet densities were plotted graphically as a function of theoretical density. Figure 19 shows this presentation with an approximate 100 percent theoretical density line based on the rule of mixtures. It should be noted from these data that numerous specimens are considerably less than 100 percent theoretical density and therefore contain appreciable void volume in addition to the SiC. Another point of interest is that the billets made from 05 powder (Shieldalloy Corp.) yield a consistently high density while 07 (U. S. Borax Corp.) and 02 (U.S. Borax Corp.) powders yield numerous lower density billets. Mechanical testing of selected specimens showed that modulus decreases with density as a function of the void or porosity volume (Figure 20). A comparison of these data with the dynamic modulus determined in the NDT Laboratory shows the same trends (Figure 21).

Those specimens of ZrB_2 plus SiC which are close to 100 percent theoretical density yield a high and constant modulus as shown in Figure 22. The numbers in parentheses on the graphs are the percentages of SiC that have been added to the ZrB_2 powder.

c. Group XII Material (ZrB_2 + Graphite)

The additions of graphite to the ZrB_2 decreases the density and modulus while improving machinability and high temperature bend strength. Graphite also appears to be an aid in densification, since most specimens approach the 100 percent theoretical density figure regardless of the original powder lot (Figure 23).

As mentioned above, the graphite addition to the ZrB_2 behaves much differently from SiC in its effect on modulus. Figure 24 shows this effect using two lots of ZrB_2 powder in preparing the billets.

d. Group VIII Material (ZrB_2 + SiC + Graphite)

This complex composition results in a high strength, lower density, oxidation resistant material with a lower modulus and improved machinability. As a result of this fortunate combination of properties, it may find considerable use in high temperature applications where thermal shock is a prime consideration.

The dynamic modulus for this material has been plotted as a function of density and additives and is presented in Figure 25. It should be noted that the modulus decreases as a function of the graphite only. The volume ratio of ZrB_2 to SiC was held constant at 4 to 1 for all the compositions in Figure 25.

When comparing the data for all three combinations discussed above (Figure 26), it can be seen that additions of either or both SiC and graphite decrease the density while only graphite additions affect the modulus.

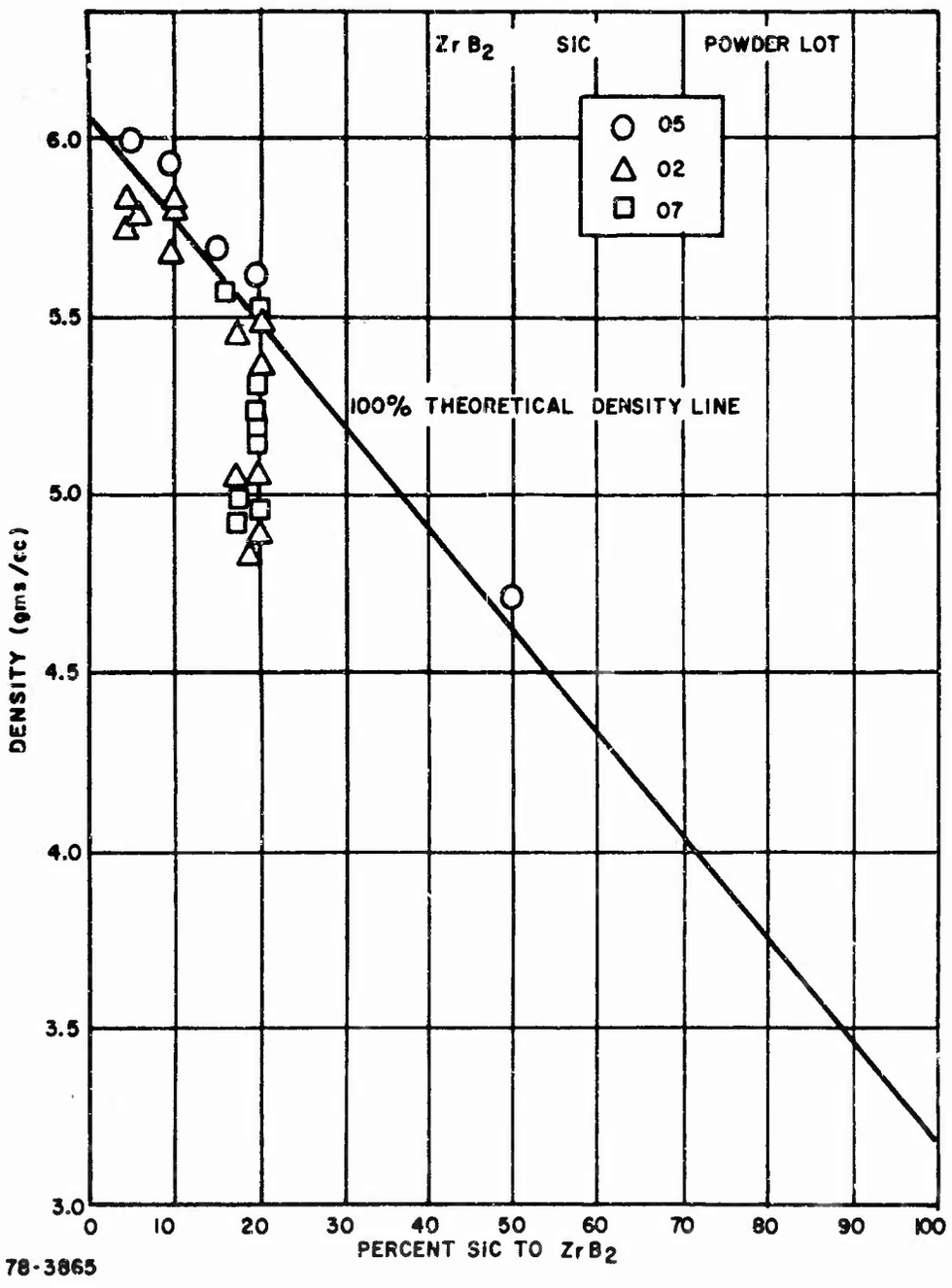

Figure 19 EFFECT OF SiC ADDITIONS TO ZrB_2 ON DENSITY OF BILLETS

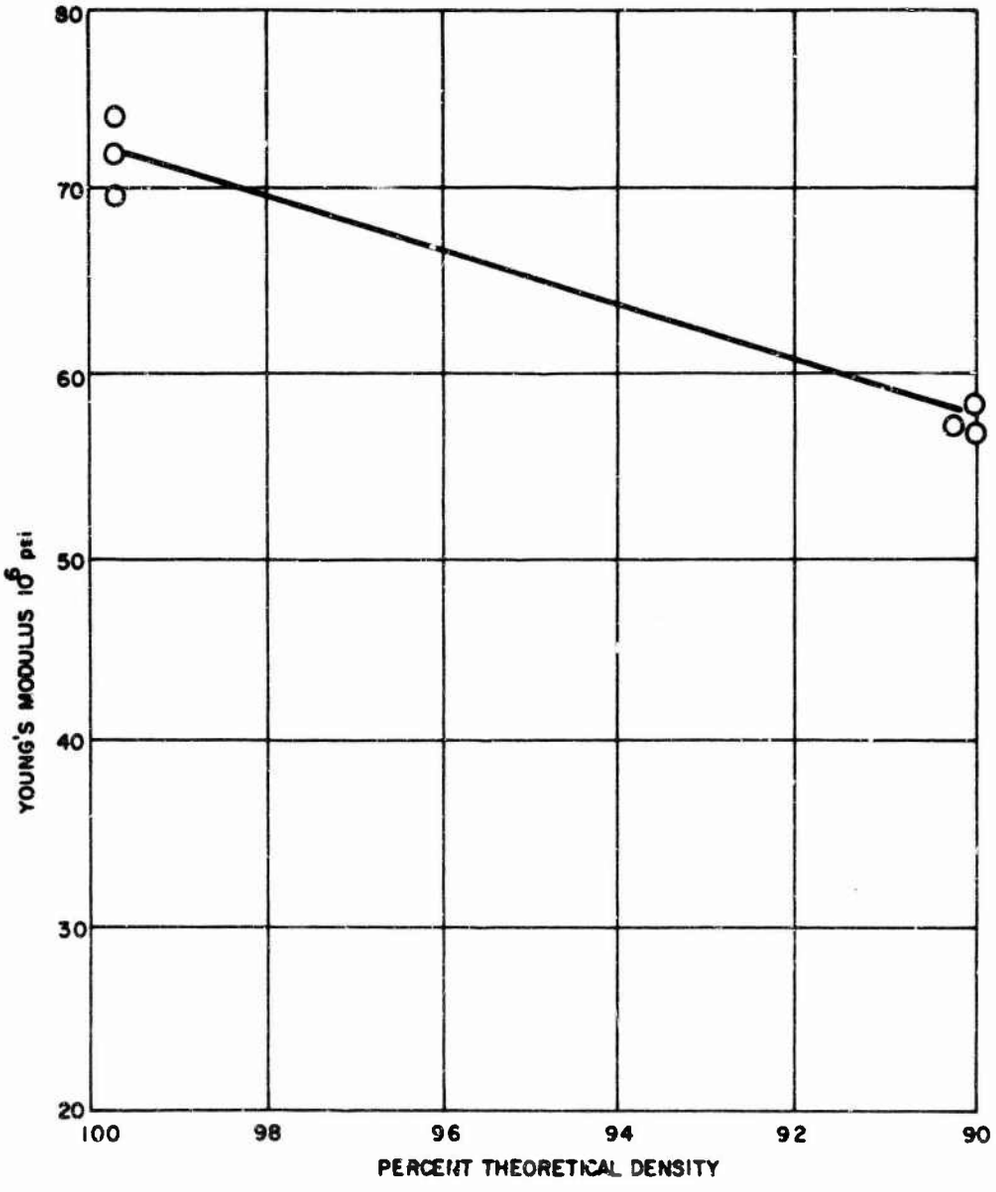

Figure 20 YOUNG'S MODULUS VERSUS DECREASING DENSITY (POROSITY) IN ZrB_2 + 20 PERCENT SIC

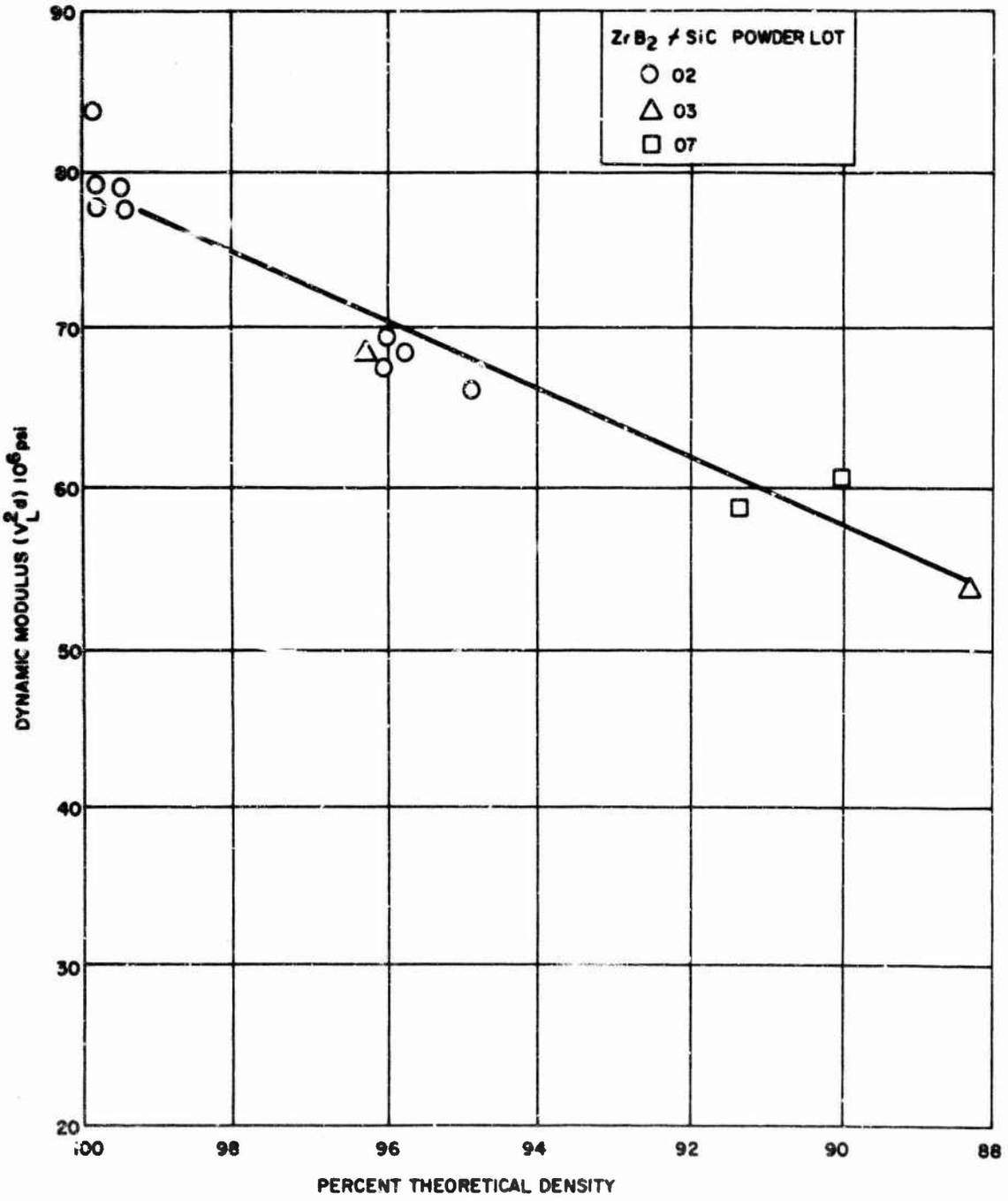

78-3867

Figure 21 DYNAMIC MODULUS VERSUS DECREASING DENSITY (POROSITY) IN ZrB_2 + 20 PERCENT SiC

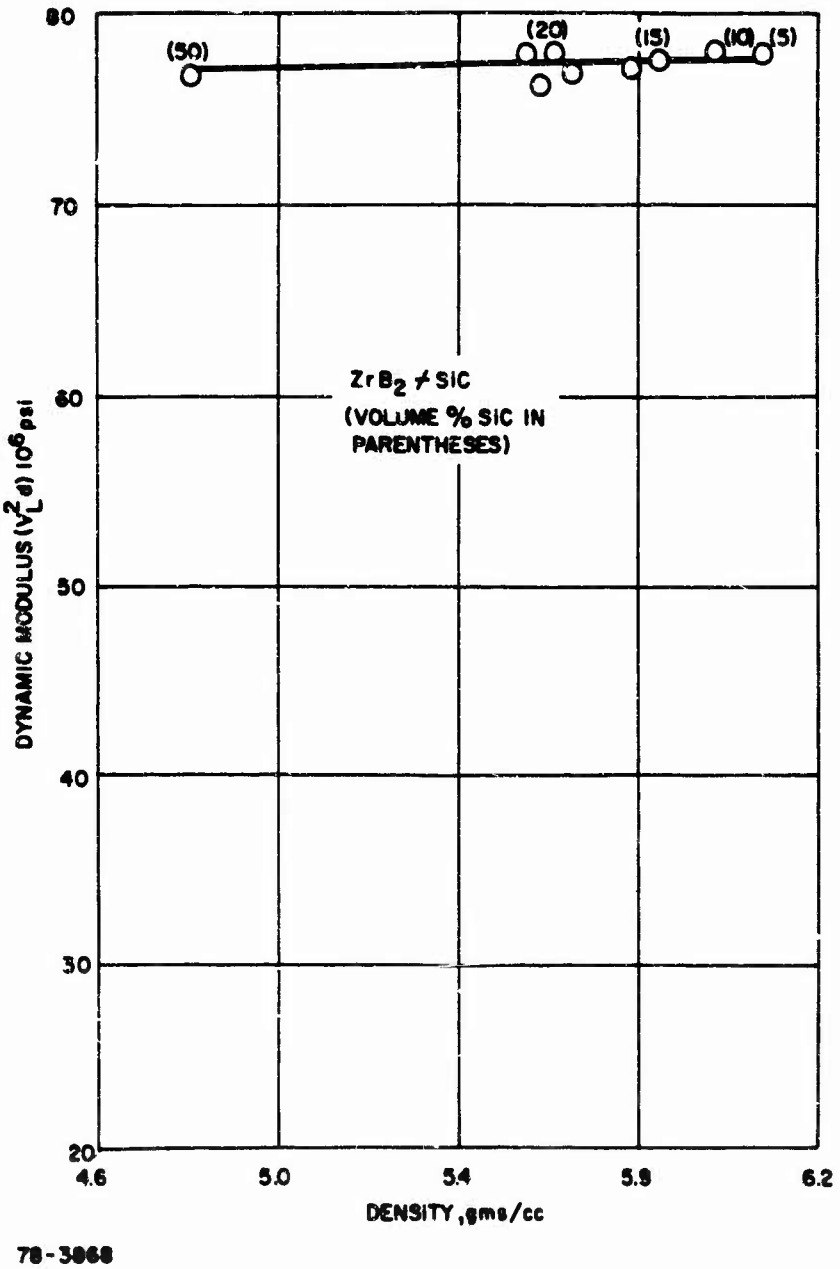

Figure 22 EFFECT ON DENSITY OF ADDITIONS OF SIC to ZrB_2 AND EFFECT ON DYNAMIC MODULUS

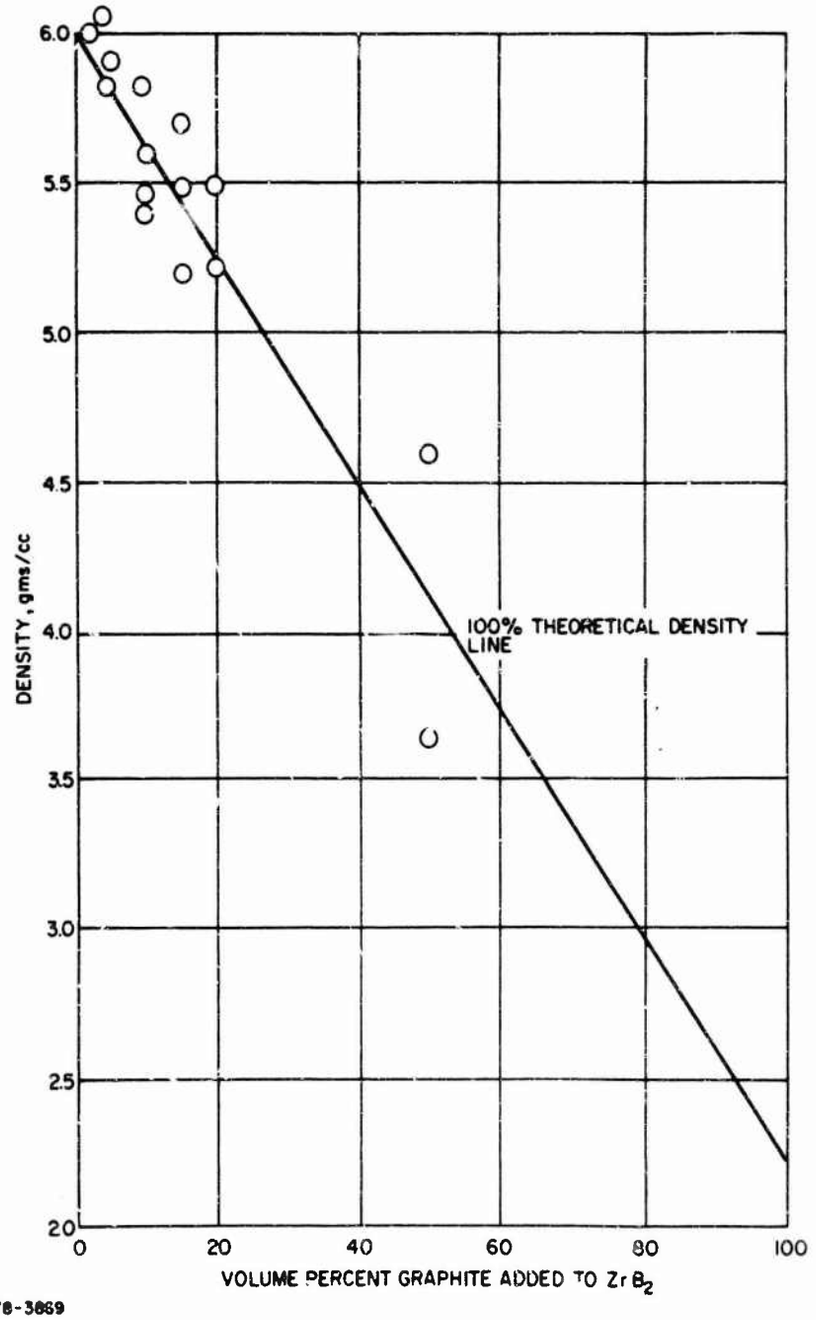

Figure 23 EFFECT OF ADDED GRAPHITE ON ZrB_2 BILLET DENSITY

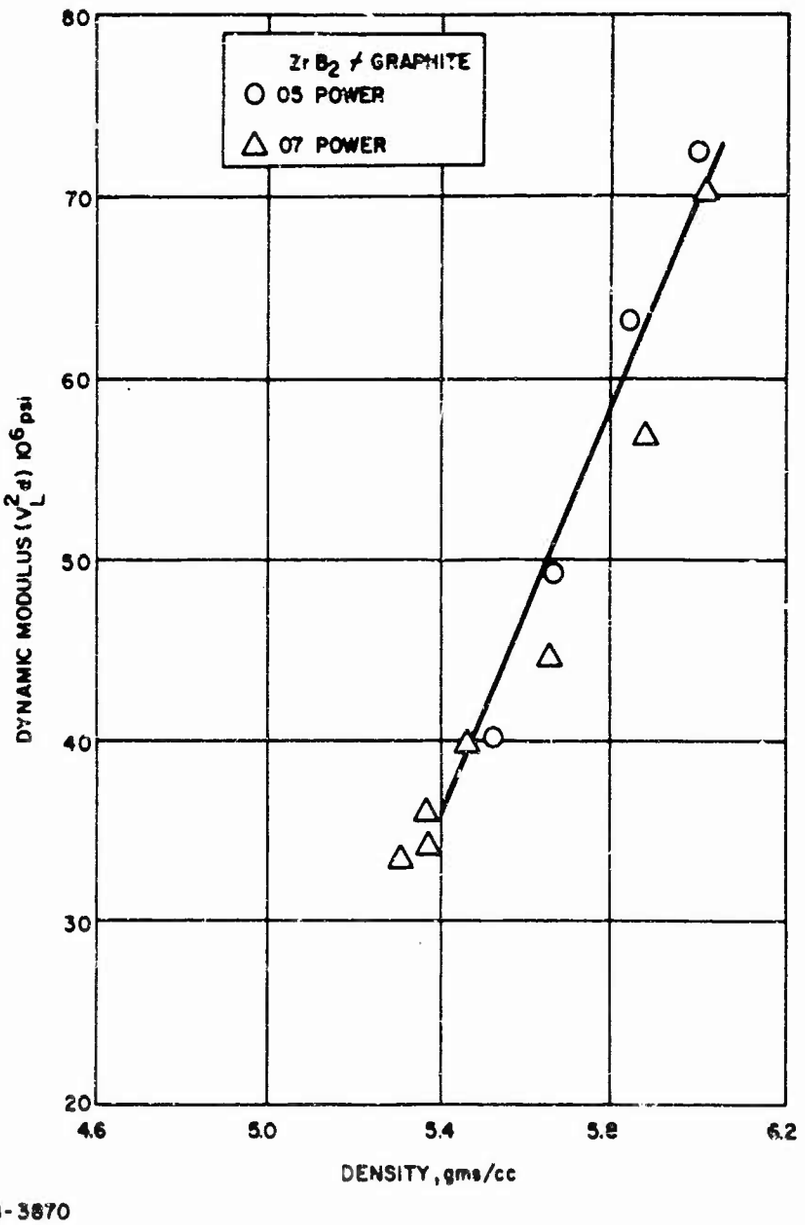

Figure 24 EFFECTS OF GRAPHITE ADDITIONS TO ZrB_2 ON DYNAMIC MODULUS

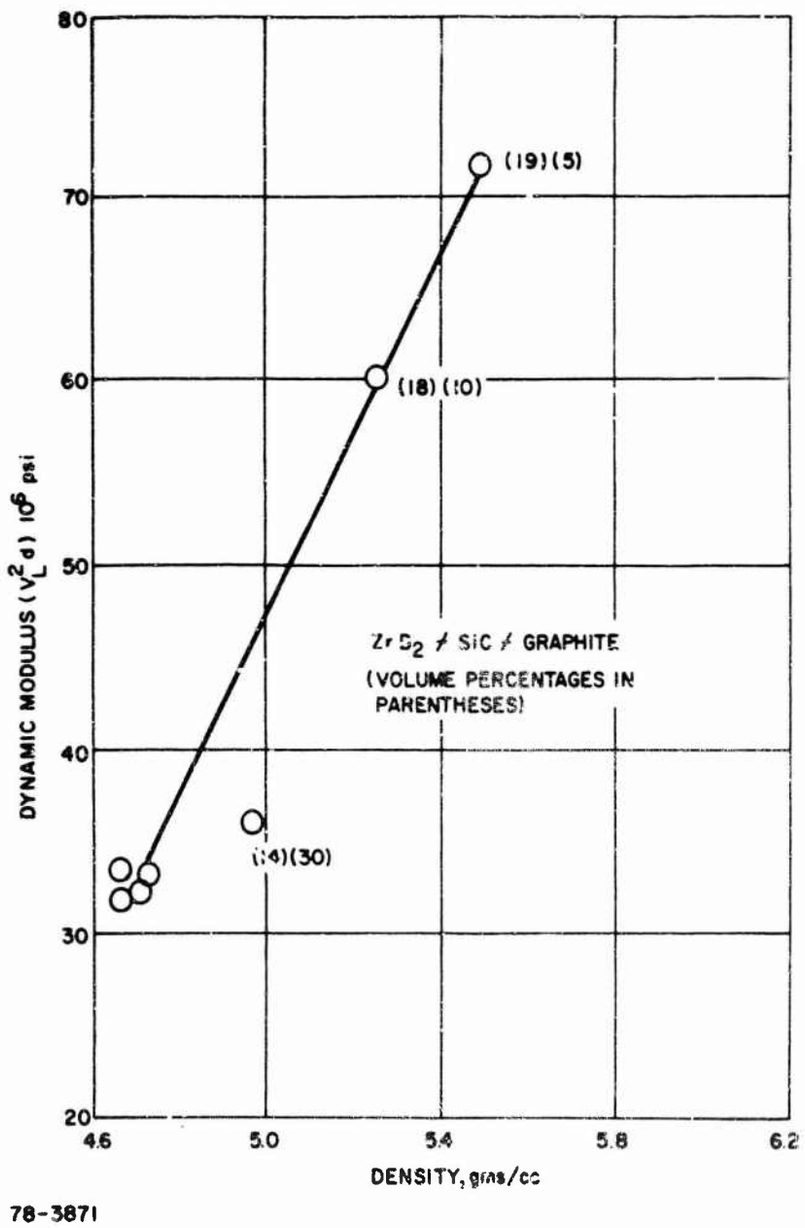

Figure 25 EFFECTS OF ADDITIONS OF SiC AND GRAPHITE TO ZrB_2 ON BILLET DENSITY AND DYNAMIC MODULUS

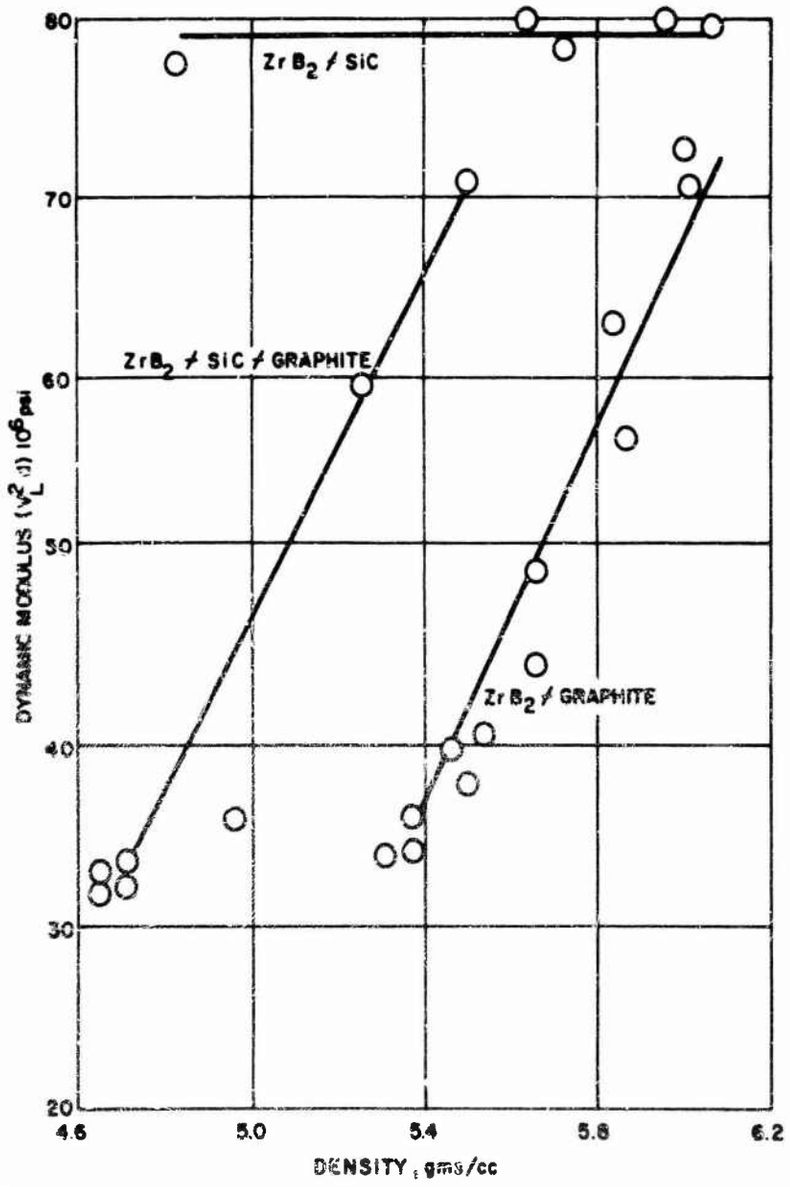

Figure 26 EFFECTS OF ADDITIONS OF SiC AND/OR GRAPHITE TO ZrB_2 ON DYNAMIC MODULUS

It should also be noted (Figure 27) that additions of air (porosity) to the ZrB_2 powder also decreases the dynamic modulus in the same manner as graphite additions.

e. Groups III and IV (HfB_2 + SiC)

The high incidence of cracking in the HfB_2 billets has resulted in low numbers of usable specimens and a lack of data for this material. However, on the basis of data obtained from HfB_2 plus SiC and the similarities with ZrB_2 plus SiC it can be assumed that HfB_2 and ZrB_2 behave similarly.

The density resulting from additions of SiC to HfB_2 follows approximately the rule of mixtures and most specimens were close to 100 percent theoretical density (Figure 28). As in the case of Group V material, the HfB_2 plus SiC billets show no significant changes in modulus as a function of percent additive (Figure 29).

4. Eddy Current Electrical

Variations in chemical composition, phases present, distribution of phases, hardness and internal stress result in changes in the electromagnetic properties of electrically conductive materials. These same factors may well have an influence on oxidation resistance; hence, the measurement of electromagnetic properties especially in the near surface layers, could provide a measure of relative oxidation resistance. This measurement is made by a coil carrying an alternating electrical signal which is brought into proximity with the electrically conductive specimen. Eddy currents are induced in the specimen, and some of the energy contained in them is dissipated through the action of the resistivity of the material encountered. That energy remaining is reflected back to the exciting coil and is seen by it as a back impedance. Hence, by measuring the coil current (phase, amplitude, or both) information is obtained regarding the electromagnetic properties of the material in the field induced by the coil. The depth of penetration of this field is defined as the depth at which the induced field strength falls to 1/e (37 percent) of its value at the surface and can be calculated from:

$$\delta = \frac{3.5}{f^{1/2}} \left[\frac{\rho}{\rho_o} \mu_{rel} \right]^{1/2} \qquad (6)$$

where:

δ = depth of penetration

f = exciting frequency in cps

ρ/ρ_o = ratio of resistivity of material to that of copper

μ_{rel} = relative permeability of material

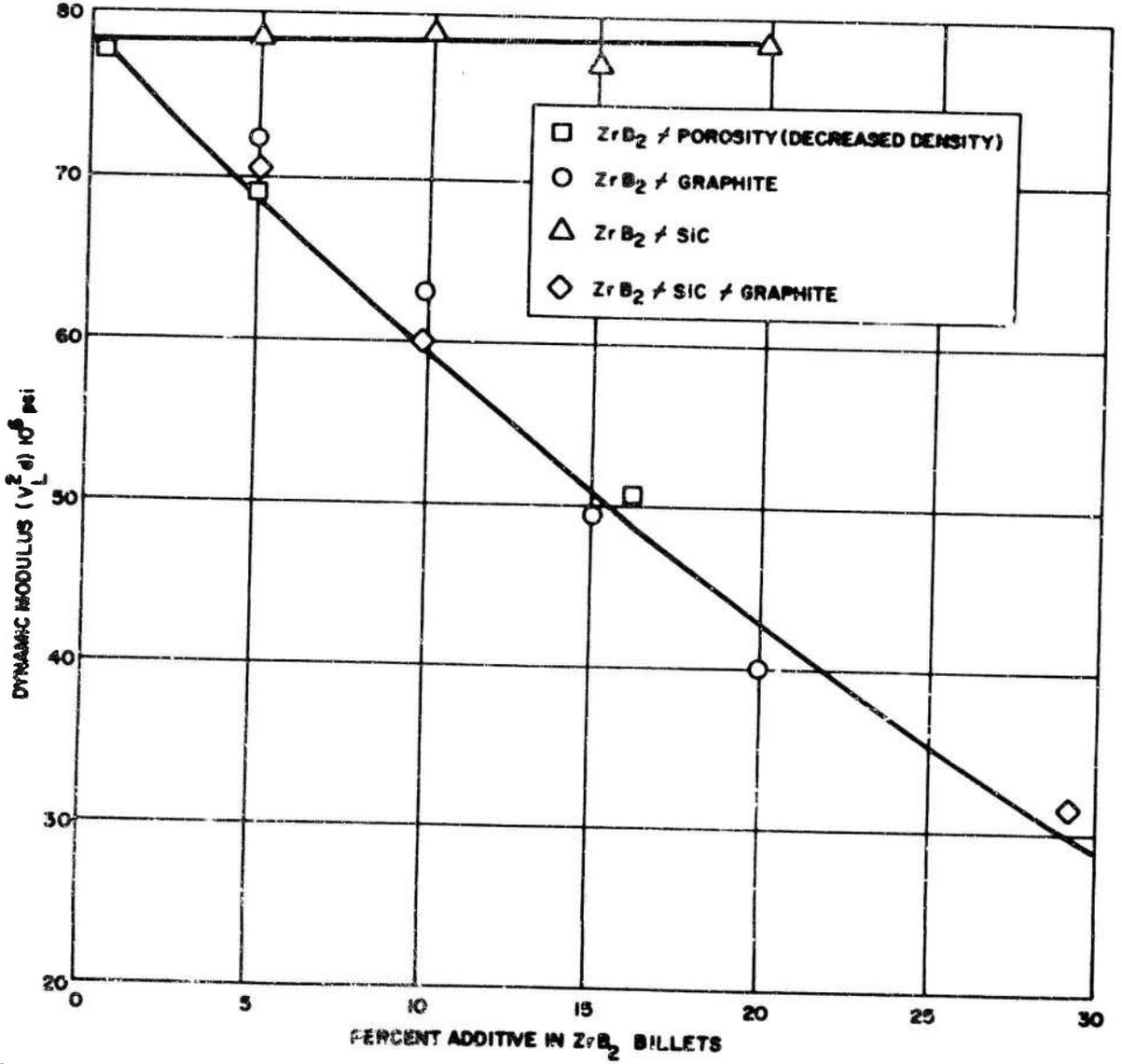

Figure 27 DYNAMIC MODULUS VERSUS PERCENT ADDITIVE IN ZrB_2 COMPOSITE BILLETS

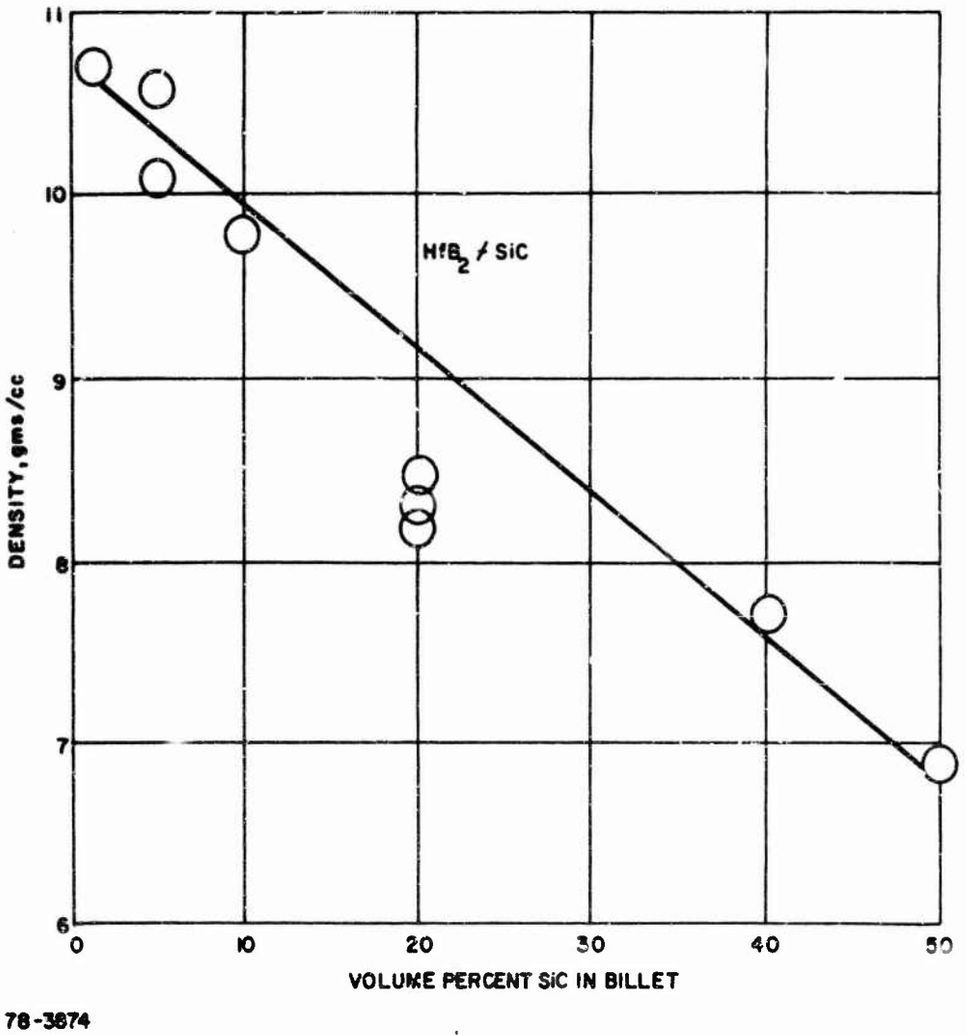

Figure 28 EFFECTS OF SiC ADDITIONS TO HfB_2 ON BILLET DENSITY

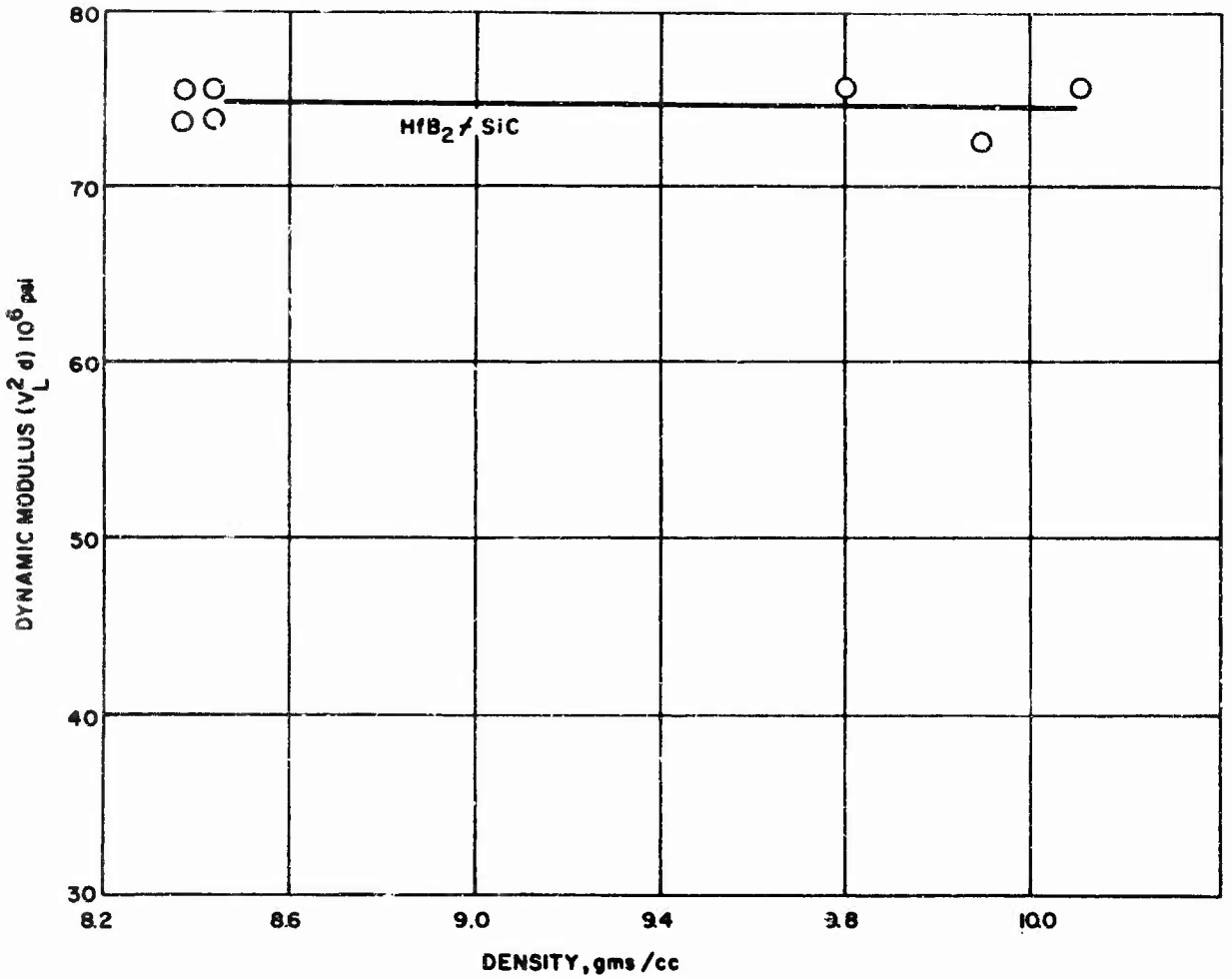

Figure 29 DYNAMIC MODULUS VERSUS DENSITY IN HfB_2+ SiC BILLETS

Each specimen was evaluated using a standard 60 KHz eddy current conductivity unit and data were analyzed to separate out effects due to material additives, porosity, and starting powder variations. It was noted that the latter variable (starting powder) resulted in differing electrical properties for the materials. For example (Figure 30), it was determined that billets made from 02, 03, and 07 material supplied by U. S. Borax all give a higher electrical conductivity than the 05 material supplied by Shieldalloy Corporation indicating either a structural or chemical difference. Data supplied in Reference 4 indicate that chemistry does vary according to supplier with U. S. Borax material having approximately 94.5 percent ZrB_2 by assay while Shieldalloy material has approximately 95 percent ZrB_2. This difference could explain the conductivity variations as well as the difficulty in achieving 100 percent dense billets from powders of 02, 03 and 07 material as mentioned previously while billets made from 05 powder were of consistently high density (Figure 31). This difference is also noticeable and consistent when SiC or graphite are added to the ZrB_2 as shown in Figures 32 and 33. It is not known how this effect is reflected in the Group VIII material (SiC and graphite), since only 07 powder has been used in preparing this material at this point (Figure 34). However, it is probable that differences in the electrical conductivity would also be present in this material.

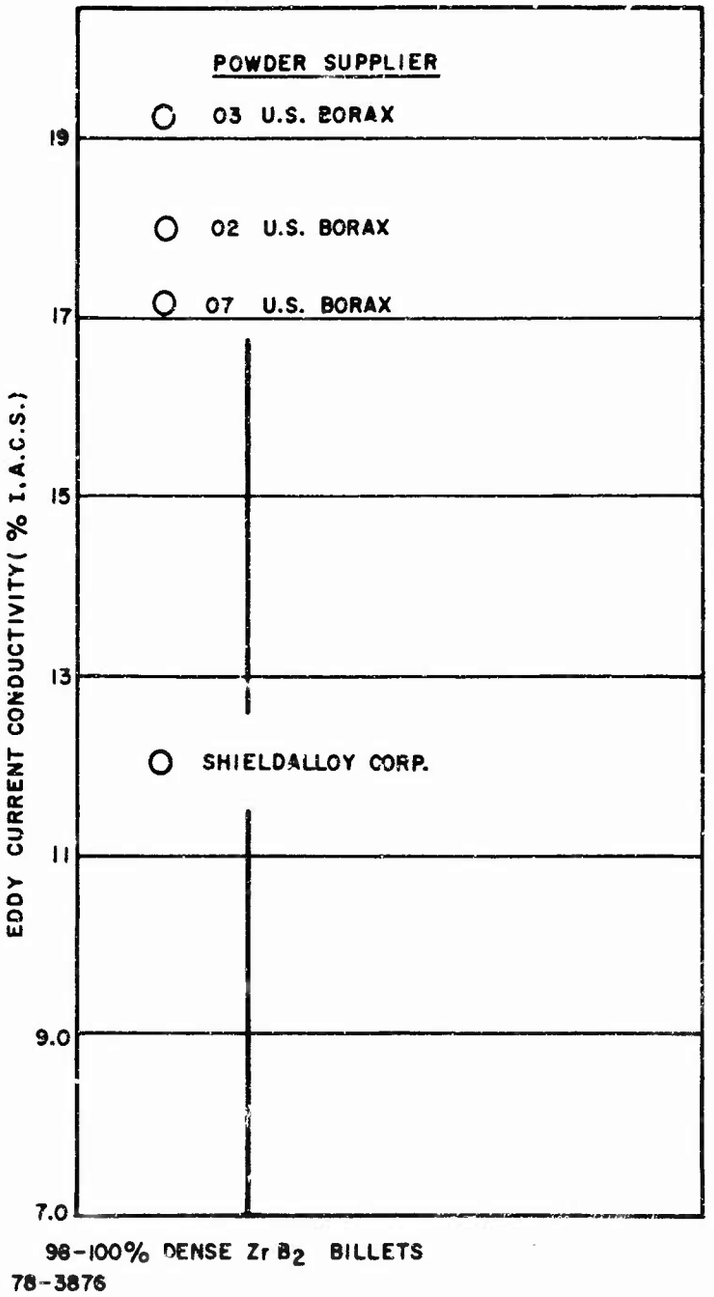

Figure 30 ELECTRICAL CONDUCTIVITY OF ZrB_2 BILLETS AS A FUNCTION OF POWDER SUPPLIER

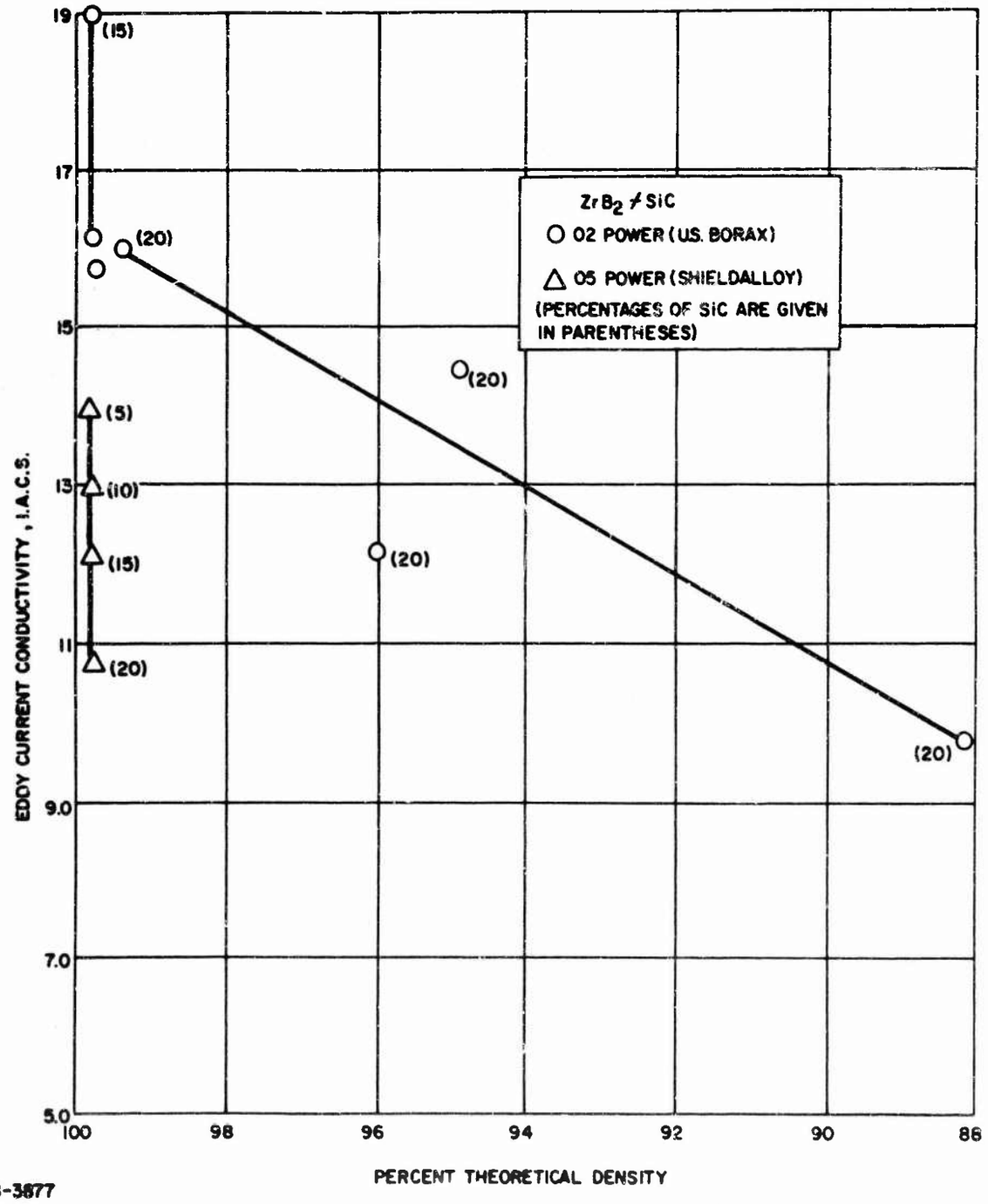

78-3877

Figure 31 ELECTRICAL CONDUCTIVITY VERSUS PERCENT THEORETICAL DENSITY (FOR TWO POWDER LOTS)

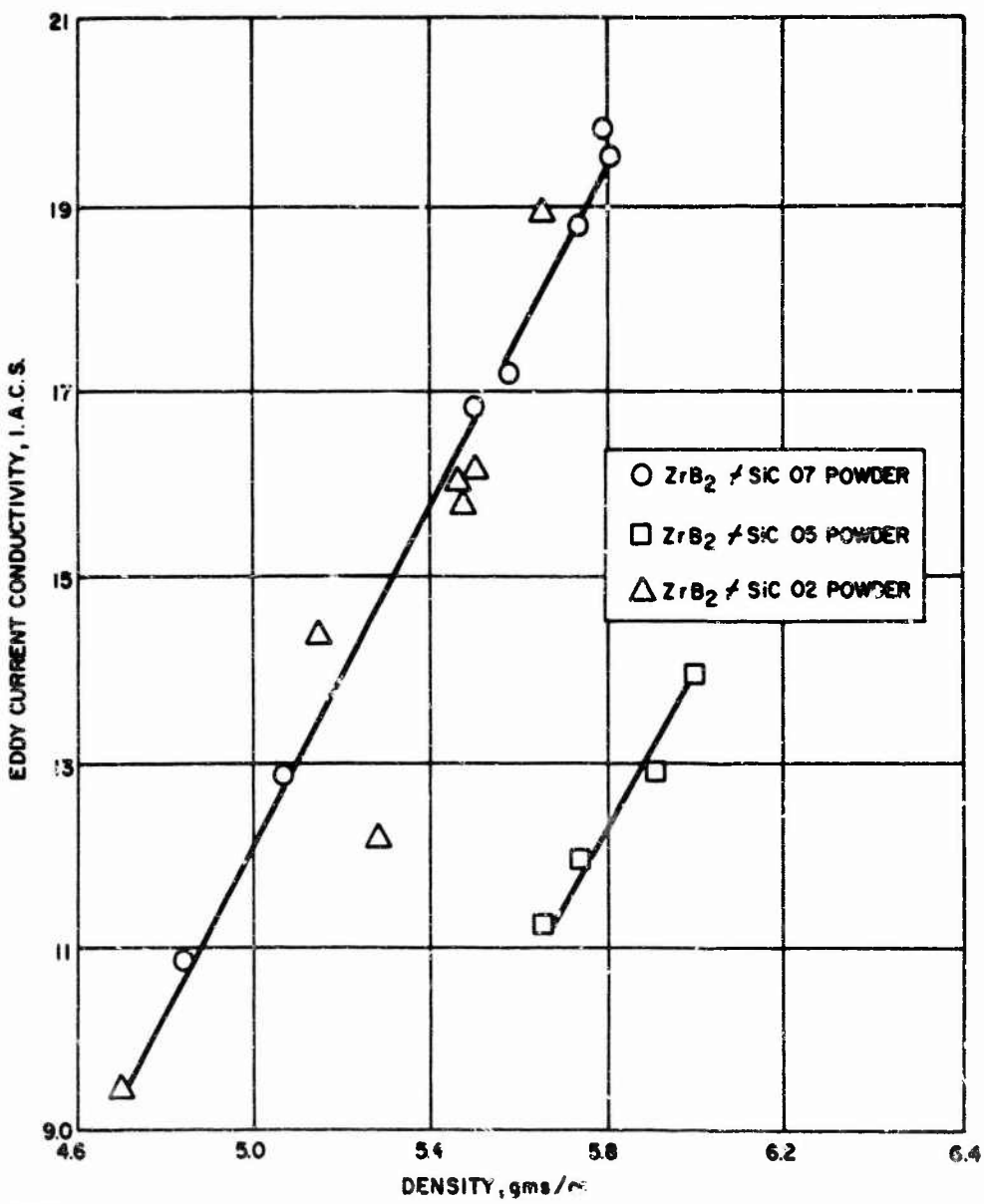

Figure 32 ELECTRICAL CONDUCTIVITY VERSUS DENSITY

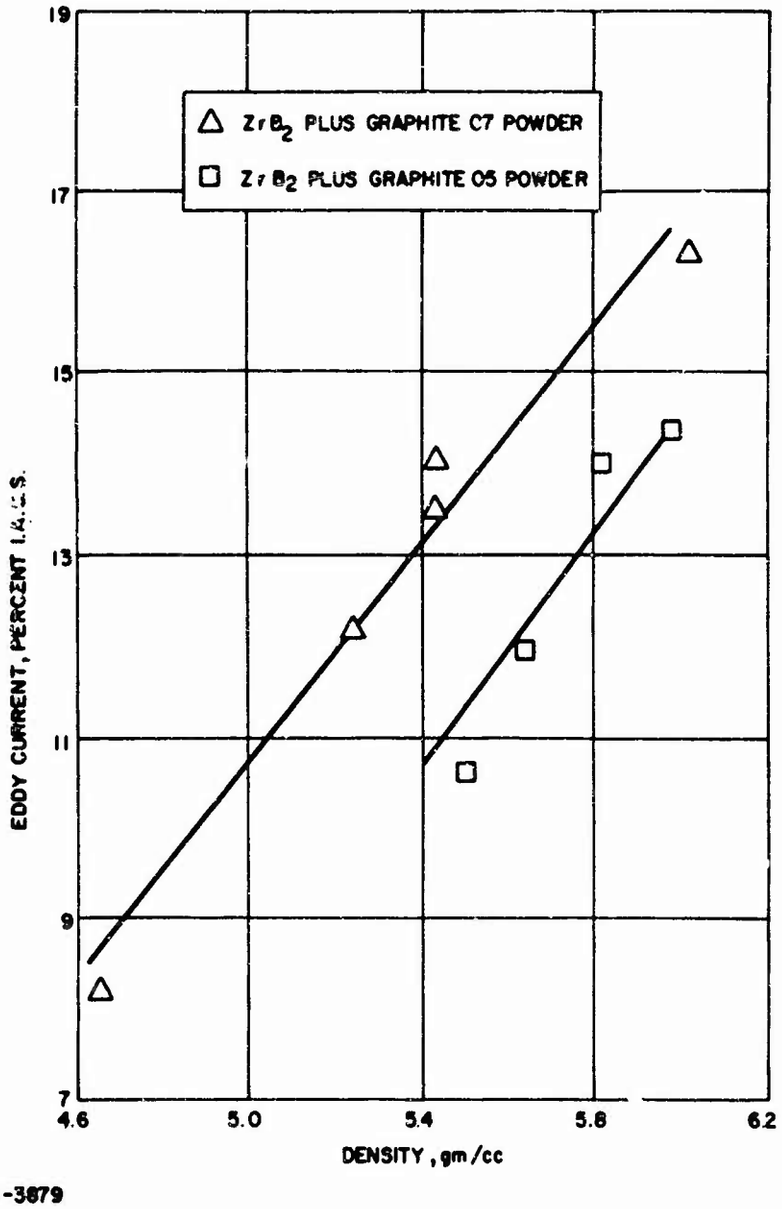

Figure 33 ELECTRICAL CONDUCTIVITY VERSUS DENSITY IN ZrB_2 PLUS GRAPHITE

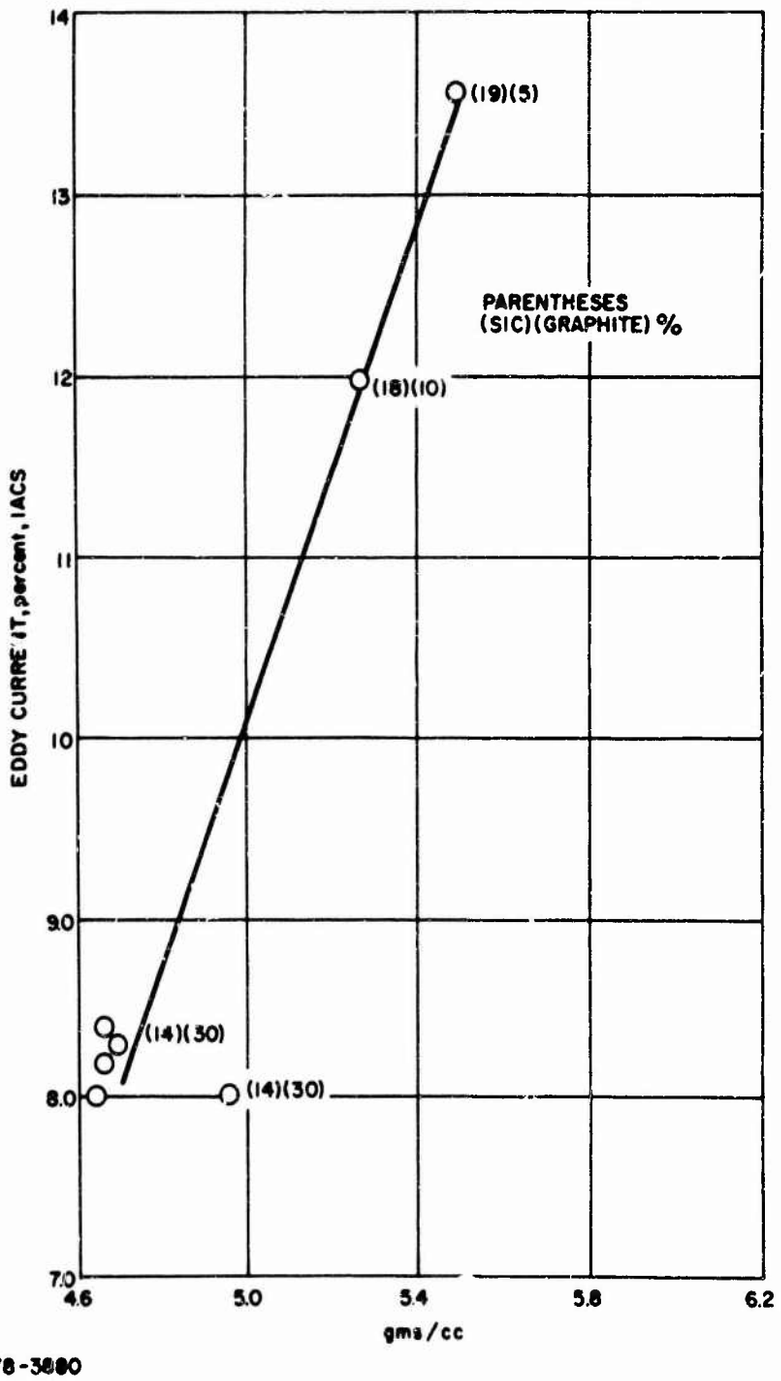

Figure 34 GROUP VIII (SIC PLUS GRAPHITE IN ZrB_2) ELECTRICAL CONDUCTIVITY VERSUS DENSITY

TABLE V

COMPARISON OF NDT DYNAMIC MODULUS AND MECHANICAL TEST TENSILE MODULUS

Material Type	Dynamic Modulus $V_L^2 d \times F_D$ (10^6 psi)	Tensile Modulus Reported by Mechanical Testing
I (ZrB)	68.7	72.0, 75.7
II (HfB_2)	67.11	73.6
III (HfB_2 + 10% SiC)	76.4	70.1
(HfB_2 + 20% SiC)		77.5
IV (HfB_2 + 30% SiC)	76.2	73.6, 74.2
V (ZrB_2 + 5% SiC)	68.3	
(ZrB_2 + 10% SiC)	71.25	69.8
(ZrB_2 + 20% SiC)	79.4	78.9
(ZrB_2 + 50% SiC)	76.8	72.0
VIII (ZrB_2 + 14% SiC + 30% Graphite)	36.0	33.9
(ZrB_2 + 19% SiC + 5% Graphite)	71.5	70.9
X (ZrB_2 + 5% SiB_6)	73.2	
(ZrB_2 + 10% SiB_6)	75.0	
(ZrB_2 + 15% SiB_6)	74.3	
XII (ZrB_2 + 5% Graphite)	54.5	
(ZrB_2 + 10% Graphite)	45.4	
(ZrB_2 + 15% Graphite)	49.3	50.0

TABLE VI

EFFECTIVE NDT TECHNIQUES FOR DIBORIDE BILLETS

Effective NDT Technique	Variable Detected or Monitored	Effect on Properties
Radiography	Cracks, porosity, inclusions	lower ultimate strength, changes in modulus
Dye Penetrant	Cracks, porosity, (open to surface)	degradation of mechanical properties and modulus
Ultrasonic Pulse-Echo	Internal cracks, inclusions, voids	not established yet
Thermoelectric	Chemistry (impurities content in HfB_2)	decrease in fabricability with increased impurity, affects crack incidence in billets of HfB_2
Ultrasonic Velocity	Changes in velocity or density	changes in dynamic modulus - correlates with tensile modulus
Radiometric Gaging	Changes in density (radiation transmitted), chemistry	changes in modulus
Eddy Current	Chemistry, structure, electrical conductivity, density	not established yet

III. CONCLUSIONS

1. Effective NDT methods are available for:

   - characterization of the diborides-material systems
   - monitoring material variability
   - predicting mechanical properties
   - detecting flaws, such as cracks, porosity, voids, inclusions, etc.

Table VI lists the tests used and the material property which was monitored.

2. Additions of materials such as SiC and/or graphite to the diborides affect the mechanical properties in different ways. These effects can be conveniently and nondestructively monitored using techniques described in this report.

3. No substantial evidence has been presented by workers performing mechanical testing data that room temperature or high temperature bend strength is affected by density/porosity where materials representing 85 to 100 percent theoretical density have been evaluated. (Note - may be due to a small grain size microstructure). In addition, the effects of discrete voids or other flaws on thermal shock properties have not been established and, indeed, materials containing flaws, easily discernible by standard NDT techniques, did not behave differently from flaw-free material when subjected to radial heat flux, high velocity wind tunnel, and plasma arc exposure.

4. Characteristics of the starting powder can be seen by the nondestructive tests employed and their effects on billets can be monitored. Electrical conductivity measurements allow billets of equivalent nominal composition and density to be sorted according to powder supplier and impurity level. A thermoelectric device is especially sensitive to chemistry variations, in billets of HfB_2 and additives, traceable to the starting powder and supplier. These chemistry variations affect the mechanical properties and fabricability of the billets, as discussed in this report and in referenced literature.

IV. RECOMMENDATIONS

1. The high temperature materials being characterized and studied on ManLabs and other programs should continue to be characterized and evaluated by NDT techniques. Greater emphasis should be placed on the NDT properties and flaw detection data in selecting specimens for characterization by high temperature exposure and mechanical testing.

2. The effects of flaws on behavior under thermal shock conditions should be more thoroughly studied. Materials containing discrete flaws of known size, as determined by NDT, should be included in the high temperature test program to determine the effects of cracks, voids, inclusions (high and low density), segregation, etc.

3. When structures, such as nose cones, leading edges, etc., are designed and fabricated, NDT should be included as an integral part of the program to determine and monitor variations in modulus, density, and chemistry, as well as flaws.

4. During the scale up portion of the program for fabricating large specimens of bulk diborides, the NDT techniques developed on this contract should be applied to detect possible changes in properties or introduction of flaws due to changes in processing techniques.

5. The effects of impurities on mechanical and ultimate properties should be determined by using NDT characterization techniques and destructive test correlations. Specifications should then be written to guide the supplier in amounts and types of impurities allowable.

V. REFERENCES

1. Lockyer, G. E., E. M. Lenoe, and A. W. Schultz, Investigation of Nondestructive Methods for the Evaluation of Graphite Materials, AFML-TR-66-101, Air Force Materials Laboratory, Wright-Patterson AFB, Ohio (24 May 1966).

2. Lockyer, G. E., A. W. Schultz, S. Serabian, and S. W. Carter, Investigation of Methods for Evaluating Graphite Materials, Part II, AFML-TR-67-128, Air Force Materials Laboratory, Wright-Patterson AFB, Ohio (June 1967).

3. Lockyer, G. E., and E. A. Proudfoot, Nondestructive Determination of Mechanical Properties of Refractory Materials, AVSSD-0068-66PP, Avco Space Systems Division, Lowell, Mass. (June 1966).

4. Clougherty, E. V., D. Kalish, and E. T. Peters, Research and Development of Refractory Oxidation Resistant Diborides Semi-Annual Report No. 1, ManLabs, Inc., Cambridge, Mass. (May 1967).

5. Stinebring, R. C. and R. Cannon, Development of Nondestructive Methods for Evaluating Diffusion-Formed Coatings on Metallic Substrates, Air Force Materials Laboratory, Wright-Patterson AFB, Ohio AFML-TR-67-178 (June 1967).

6. Hill, R. J. and W. H. Rhodes et al, Research and Development of Refractory Oxidation Resistant Diborides - 18th Monthly Report, Avco Space Systems Division, Lowell, Mass.

PART B - AN ANALYSIS OF A NONDESTRUCTIVE INFRARED METHOD FOR MEASURING THE THERMAL PARAMETER ($k\rho C_p$)

A. W. SCHULTZ

I. INTRODUCTION

The theory, several facets of the method, and initial experimental results have been detailed in the final report for last year's effort, which was performed under Contract AF33(615)-3942.[1] The substance of that thermal measurement study was to demonstrate that a thermal parameter for a solid (with emphasis on graphite) could be nondestructively and uniquely determined near room temperature by monitoring the temperature history generated by a surface while it was being subjected to a radiant flux. Analysis of this history and comparison of it with that for a "standard" material yielded the "semi-infinite" thermal parameter $k\rho Cp$ (k = thermal conductivity, ρ = density, and Cp = specific heat). This parameter is often termed "thermal inertia." The thermal conductivity and diffusivity ($\alpha = k/\rho Cp$), of the solid are then determined if other nondestructive techniques are used to obtain its density (such as gamma-ray radiometry), and a characteristic specific heat value for its chemistry is selected. The overall results of that work indicated that the method is capable of accurately determining $k\rho Cp$ for good thermal conductors ranging from copper to lead (including graphite). The degree of accuracy of these measurements is comparable to that resulting from the individual accuracies associated with typical destructive measurements used to obtain k and Cp, and from which the product $k\rho Cp$ can be calculated.

Since much of last year's effort was primarily directed toward demonstrating the feasibility of the method, additional work has been performed this year to explore its limitations, to improve upon the technique, to obtain measures of its usefulness and to attempt to coalesce the results into a technique that would prove useful for field testing hardware, again with special emphasis on graphite. The following presentation provides convincing evidence of the wide application and advantages that this method offers compared to other existing methods.

The above-referenced report contains all background information necessary for an understanding of this method, and it will be assumed that the reader is sufficiently acquainted with it so that its duplication here is unnecessary. Suffice it to say that the temperature rise of a solid's surface is monitored by an infrared radiometer and, in turn, by a recorder. The resultant recorder deflection as a function of time is directly proportional to the observed temperature history and is characteristically of parabolic shape. The magnitude of the latus rectum of one of these parabolas is directly proportional to the radiant energy absorbed by the solid's surface and is inversely proportional to the square root of $k\rho Cp$. Consequently, the square of the measured recorder deflection (temperature difference) within a certain time interval for a solid is inversely proportional to its inertia, where the proportionality in this case is "emissivity-normalized" to a "standard" reference material, such as Armco iron, within this same analysis time interval. By "emissivity-normalized" is meant that solids' surfaces are coated with a black, mat coating to achieve nearly uniform emittance/reflectance properties, and resultant small differences are normalized to a mean emissivity value. In the course of generating a history on the recorder, a simultaneous recording is also made on a second channel of the surface reflectance of the test material.

To be discussed first in this report are certain important characteristics of the measuring system leading to geometrical limitations to be imposed on materials. These limitations are necessary in order to satisfy conditions of "semi-infiniteness,"

which in turn must be adhered to in order that comparisons between inertia values may be regarded as valid. The accuracy of the technique is discussed next, which in turn leads into the range of application of the method. Finally, implications of the experimental results are viewed from the standpoint of practical application.

II. DISCUSSION

A photograph of the apparatus is shown in Figure 35; its schematic diagram is shown in Figure 36. The apparatus, as shown, is of laboratory design, is not portable, and represents about $10,000 in equipment costs. The design and quality of the apparatus is better, in many respects, than is necessary to obtain satisfactory results. Consequently, a great reduction in cost and analysis time, and portability can each be achieved in a redesign for use in the field. This will be discussed later. Figure 35 will serve here to describe the system used for the results to follow.

A. SYSTEM CHARACTERISTICS

Shown in Figure 37 are relationships between reflection amplitude and Variac setting and between the corresponding radiance and Variac setting. This reflection is that observed by the radiometer from the solids' surfaces which have been coated with 3M Velvet Black, No. 101-C10. Since the voltage applied to the two 1000 watt focused lamps relates linearly to Variac setting between 20 and 126 volts, it is significant to note the linearity that also obtains for the reflection and the radiance as functions of Variac setting. It is seen that, for example, a twofold increase in applied voltage (Variac setting) gives rise to a twofold increase in radiance and approximately the same increase for the reflection. This equivalence supports the original contention that the reflectance of the coating is reasonably constant over the 1 to 10 micron wavelength region of interest in this work. This is not unexpected. The principal constituents of the coating used are carbon black and silicon dioxide. Reflectance data reported for these substances in this wavelength region are essentially constant. Had reflectance varied over this wavelength region, a nonlinear relationship between reflection amplitude and lamp filament voltage would have resulted. Furthermore, it should be remarked that the reflection relationship in the figure was constructed from measurements performed on several different coated materials. The repeatability of these measurements over the indicated voltage range is extremely good (about 1 percent), indicating that coating application differences and effects of the substrate materials did not influence the analysis technique used for estimating reflectance values from the recorder charts.

Also included in Figure 37 is a relationship between the self-emitted recorder deflection for 1020 steel and Variac setting. This self-emitted component to the total radiation received by the radiometer arises from surface heating and is the history used to calculate the thermal inertia. The analysis interval used to construct this relationship was 0.25 to 1.0 second. The relationship is linear, thus providing the supporting evidence that the coating's emissivity is constant over the wavelength region of interest here. Moreover, it is observed that a twofold increase in relfection amplitude gives rise to a similar increase in the self emission amplitude. This indicates that a change in incident radiant intensity to a solid's surface results in a proportional change in the self-emitted radiation amplitude, thereby proving the previously proposed theoretical argument that the latus recta of the parabolic temperature histories are directly proportional to the incident radiant intensity, and thus are also proportional to the energy absorbed at the surface.

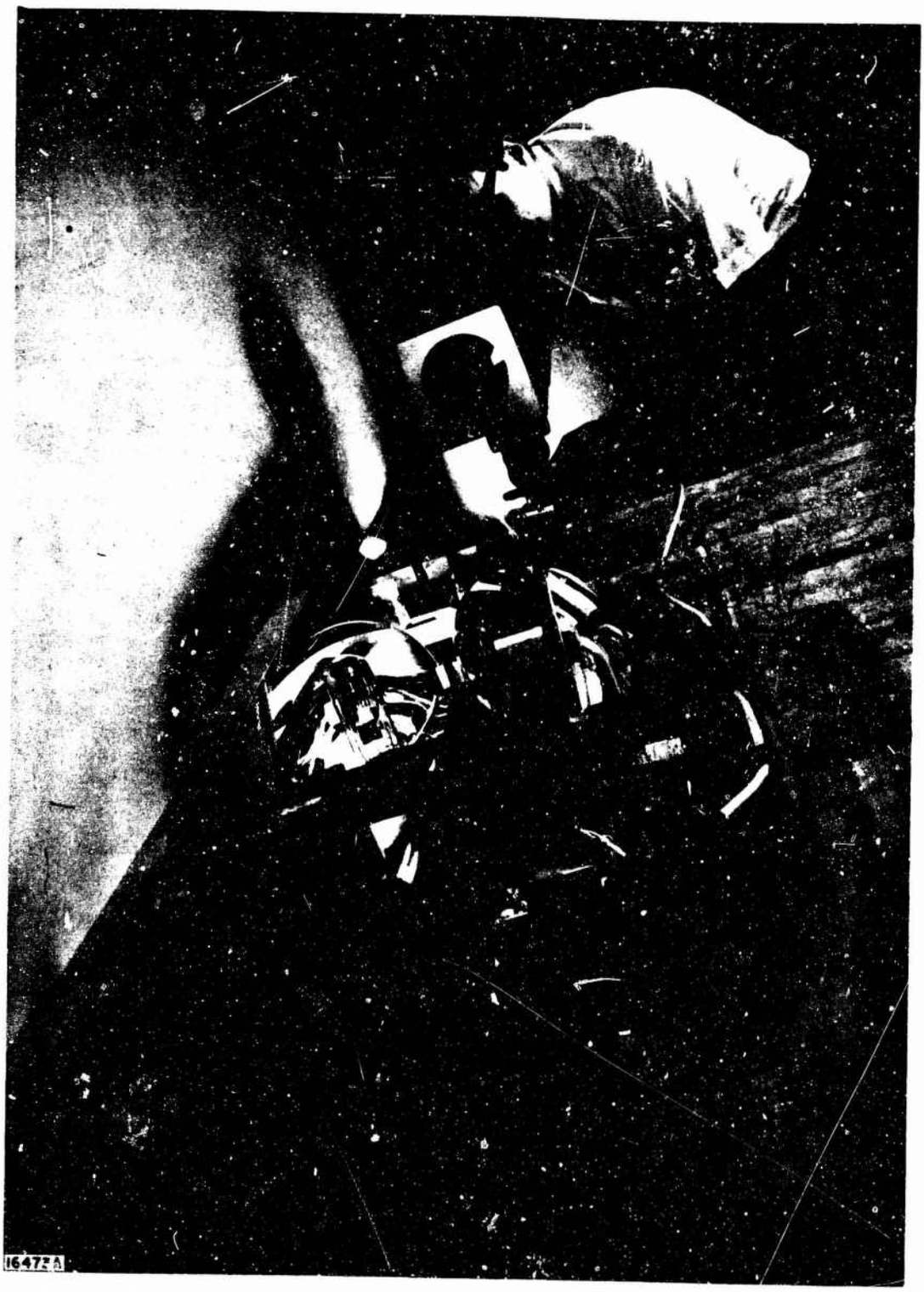

Figure 35 APPARATUS USED FOR MAKING INFRARED MEASUREMENTS

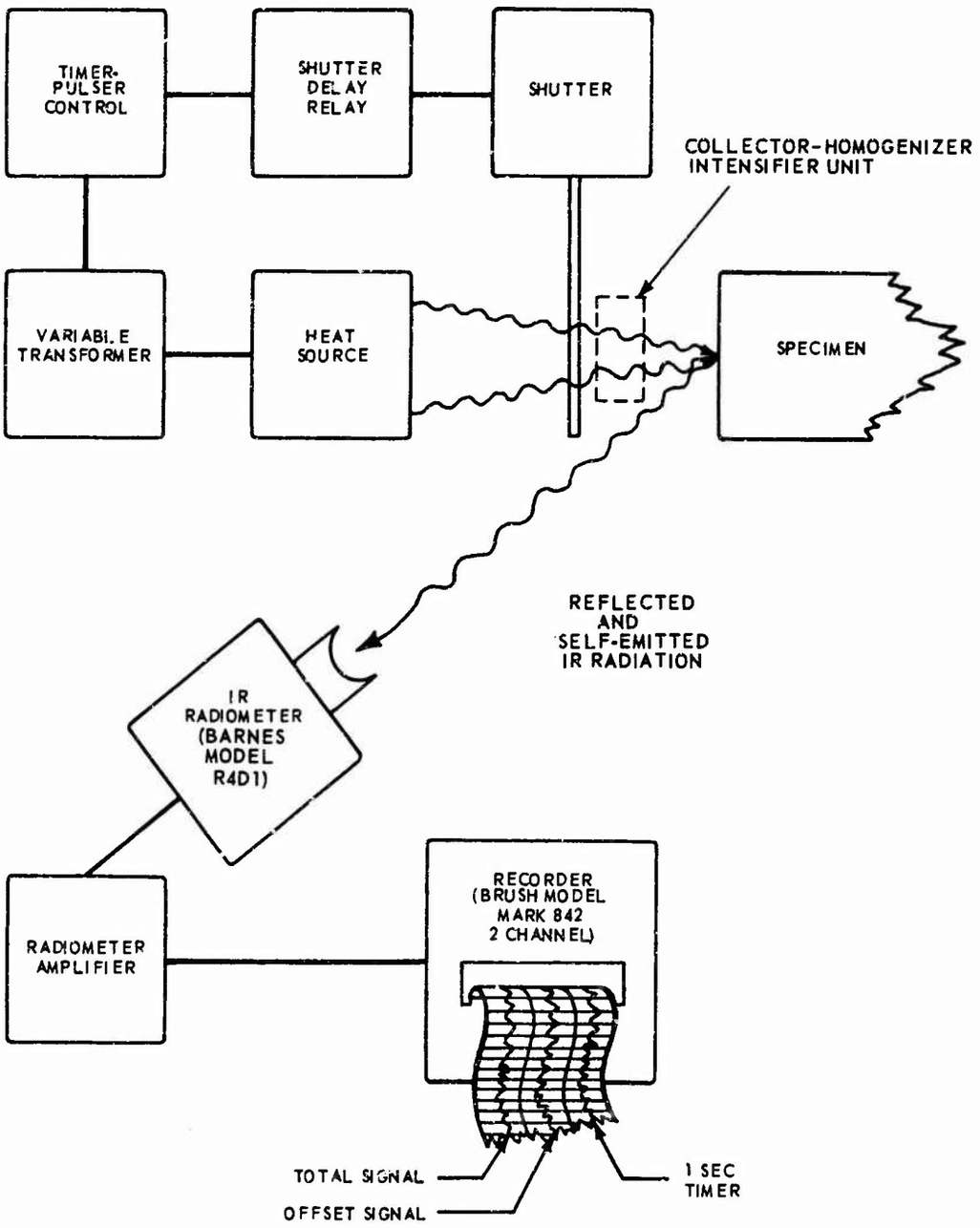

Figure 36 SCHEMATIC DIAGRAM OF THE EXPERIMENTAL ARRANGEMENT USED TO MEASURE THE THERMAL PARAMETER

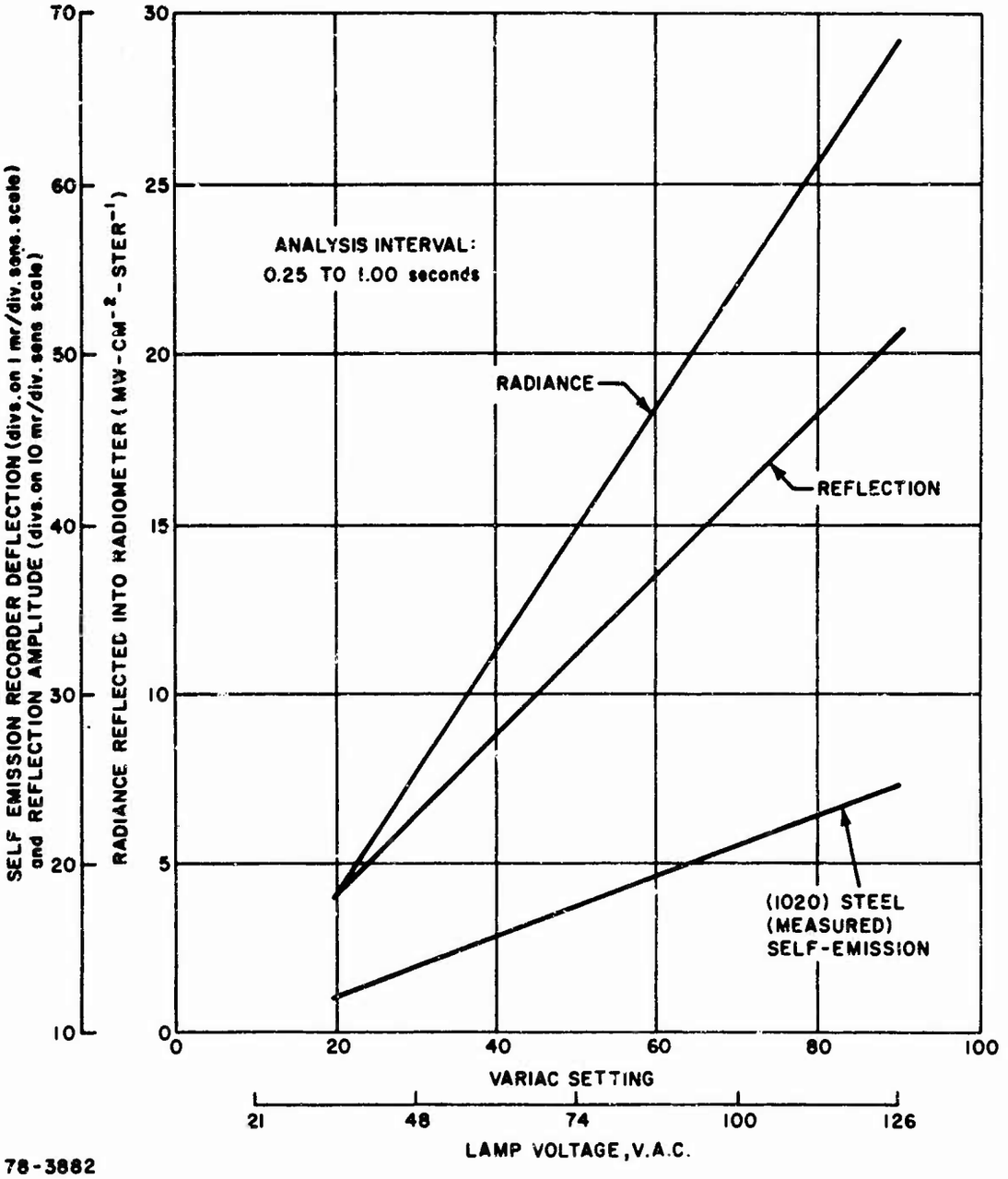

Figure 37 SELF EMISSION RECORDER DEFLECTION, REFLECTION AMPLITUDE AND RADIANCE REFLECTED INTO RADIOMETER AS FUNCTIONS OF VARIAC SETTING (LAMP VOLTAGE)

Shown in Figure 38 is the relationship between the apparent surface temperature of a solid and the measured reflection amplitude, or reflected radiance. This function is characterisitc of the radiometer when the emissivity of the coated surface is taken as 0.95. For the bulk of the measurements performed on the good conducting materials, the Variac setting used was 90 (126 volts), and the reflection amplitude ranged from about 17 to 25 divisions on the recorder chart, which corresponds to a reflected radiance range of 57 to 82 milliwatts per sq. cm. per steradian. This range is a consequence of differences in radiant intensity, coating application and similar variables present from test to test. Within this operating range, it is seen that the surface temperature is very nearly linear and related to reflection amplitude. This demonstrates the validity of the contention that recorder deflection (voltage output from the radiometer) is directly proportional to the temperature rise of the surface within the several degrees centigrade (about 10°C) above ambient temperature to which the surface is heated during the first second used for analysis of the history. It is this proportionality that results in the parabolically-shaped functions which are characteristic of the self-emission histories.

1. Emissivity Correction

The self-emission recorder deflection must be corrected for emissivity differences between the coated standard and the coated specimen. This correction has been concluded to be small regardless of application technique and after examining about 50 coated specimens. The only criterion required to achieve this nearly constant emissivity is that the coating be thoroughly dry before a measurement is made. Drying takes about 1/2 hour in air. To determine the correction factor by which a measured recorder deflection is to be multiplied to obtain a corrected deflection which can be compared with the standard, reference is made first to Figure 39. The reported value and our measured value of emissivity for 3M Velvet Black in the 1 to 10 micron region are in agreement at 0.95. This corresponds to a reflectivity of 0.05 for a reflection amplitude of 20 divisions at a Variac setting of 90 (126 volts). Consequently, each amplitude division change is equivalent to a change of 0.0025 reflectivity units. The range in reflectance amplitude for all coated specimens is between 17 and 25 divisions, so that emissivity values range between about 0.94 to 0.96. Even if the coating emissivity had been determined would have been 0.88 to 0.92. The point here is that it does not really matter what the actual emissivity value of the coating is, since it is the range of variability that is to be compared with the emissivity of the standard to establish a correction factor, if such correction is required.

Translating the relationships in Figure 39 to a format for graphically determining the emissivity correction factor, K_{Ry}, reference is now made to Figure 40.

The following expression has been used to construct these graphs:

$$K_{Ry} = \frac{(V_2 - V_1)_{20}}{(V_2 - V_1)\,y} = \left[\frac{\epsilon}{\epsilon - \frac{r}{RA}\,(y - 20)} \right]^2 , \qquad (1)$$

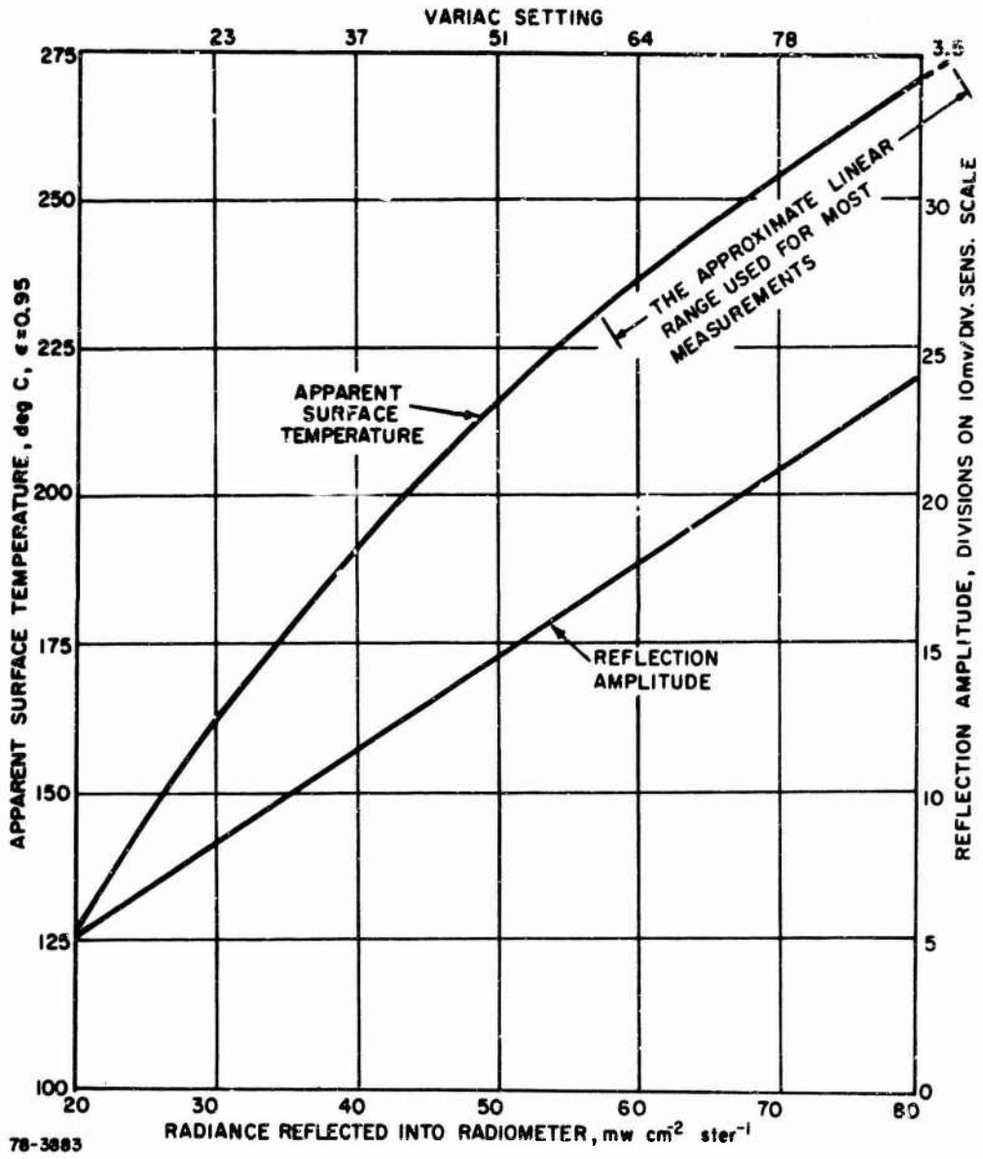

Figure 38 APPARENT SURFACE TEMPERATURE AND REFLECTION AMPLITUDE AS FUNCTIONS OF RADIANCE REFLECTED INTO THE RADIOMETER AND VARIAC SETTING

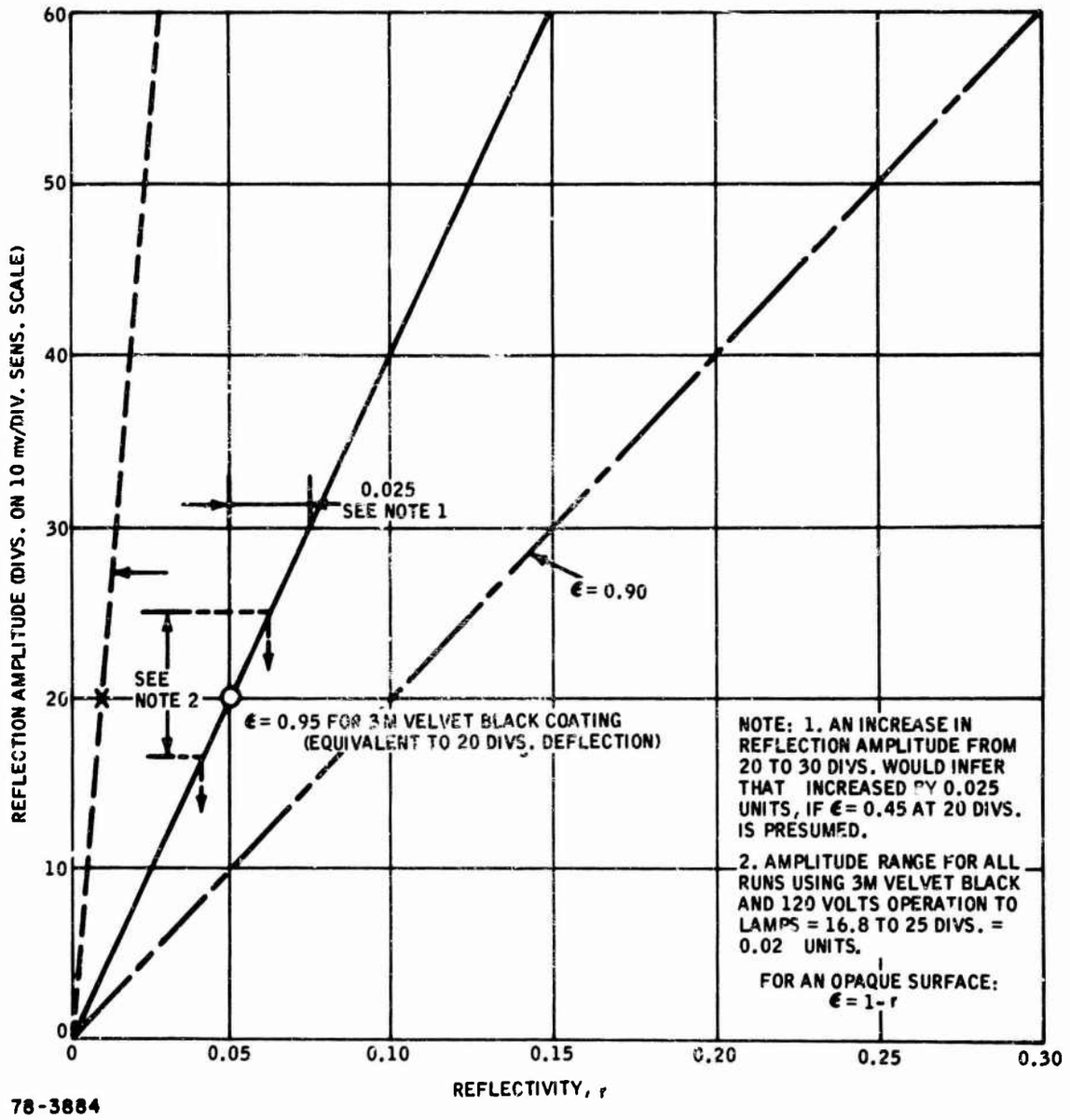

Figure 39 REFLECTION AMPLITUDE AS A FUNCTION OF REFLECTIVITY

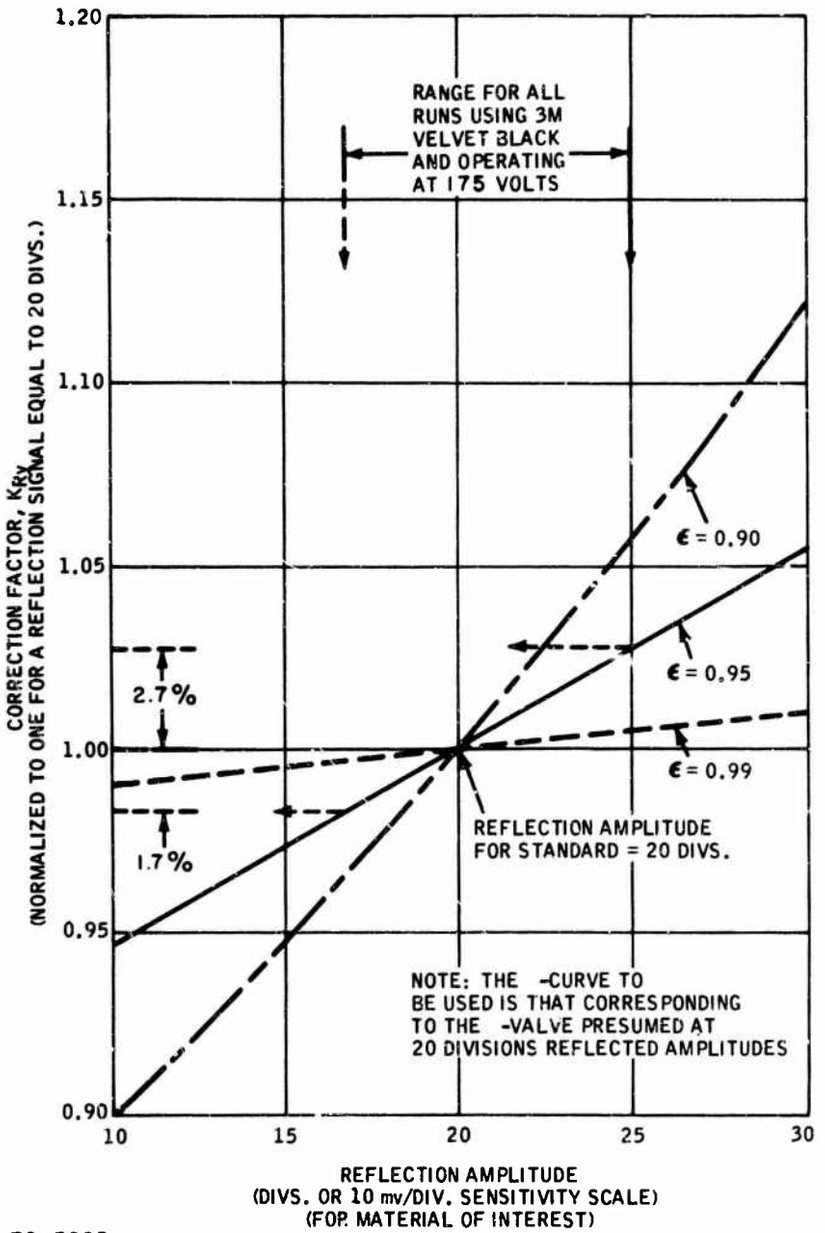

Figure 40 EMISSIVITY CORRECTION FACTOR, K_{Ry}, AS A FUNCTION OF REFLECTION AMPLITUDE

where $(V_2 - V_1)$ and $(V_2 - V_1)$ represent the self-emission recorder deflection amplitudes of 20 divisions and y divisions, ϵ represents emissivity, r/RA is the reflectivity divided by the reflection amplitude (RA) at 20 divisions, or 0.0025 r units per division reflection at $\epsilon = 0.95$ and a Variac setting equal to 90 (126 volts). It is y that ranges between 17 and 25 divisions. Within this range, it is seen that K_{Ry} varies between about 0.98 and 1.03, or about +3 to -2 percent, for $\epsilon = 0.95$. Had $\epsilon = 0.90$, then K_{Ry} would range between +6 to -3 percent of a normalized $K_{Ry} = 1$ at 20 divisions reflection amplitude. The large majority of reflection amplitudes lie within about 2 divisions of 20, so that the largest correction normally needed would be about 2 percent even if our emissivity measurements for the coating had been in error by 0.05 units, or about 6 percent.

2. Radiant Intensity Distribution

Theory requires a uniform radiant intensity distribution to be absorbed by the surface of a solid. In practice, a homogeneous flux is very difficult to obtain, and our present optical system is a tradeoff between optimizing intensity and homogeneity. Measurements of the radiant intensity distribution reflected from a surface positioned at the exit aperture of the collector-homogenizer-intensifer unit indicated that intensity varied by as much as 15 percent over the aperture from its center. Peak radiance was located at the center and diminshed gradually out to the aperture diameter (7/8 inch). This degree of nonuniformity did not have any significant effect on the inertia measurements for the materials tested, with perhaps graphite being the sole exception because of its anisotropic grain structure. This point will be discussed later.

3. Measurement Accuracy

The reading accuracy of the self-emission recorder charts is presented graphically in Figures 41 and 42. Because of the wide range of materials studied (in terms of thermal conductivity) radiant intensities and recorder sensitivities had to be adjusted to obtain an optimum readout. Referring to the dashed-line construction in the Figure 41, as an example of the use of the graphs in Figure 42, it is required, for a particular material, to decrease the maximum radiance (Variac setting = 90) to half its value (Variac setting = 42), and use a recorder sensitivity equal to 1 mv per chart division to obtain a 10 division measured deflection. Alternatively, maximum radiance and a sensitivity of 2 mv per division could be used. This self emission deflection will correspond to a true recorder deflection of 20 divisions when compared with the reference standard (Armco iron). The accuracy of the true deflection will be 4 percent. This is to say that the measured deflection of 10 divisions can be estimated to within 0.2 division at, say, 0.25 second and at 1.0 second, or within 0.4 division over the analysis interval. As noted in the figure, pyroceram had a true deflection of 32.7 divisions in the 0.25 to 1.0 second interval. Its measured deflection was 16.3 divisions for a sensitivity setting of 2 mv per division, and its reading accuracy is about 2.5 percent.

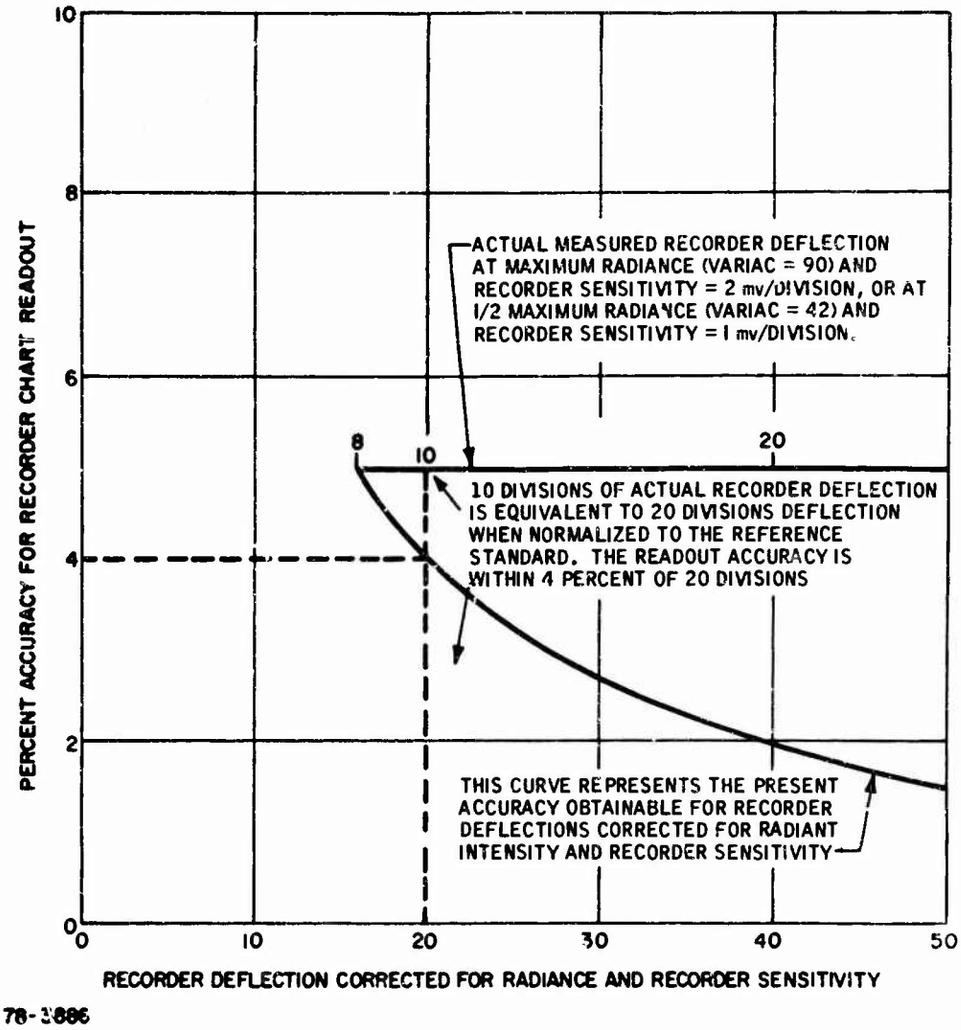

Figure 41 CONSTRUCTION USED TO ADJUST FOR RECORDER SENSITIVITY AND SOURCE RADIANCE CHANGES

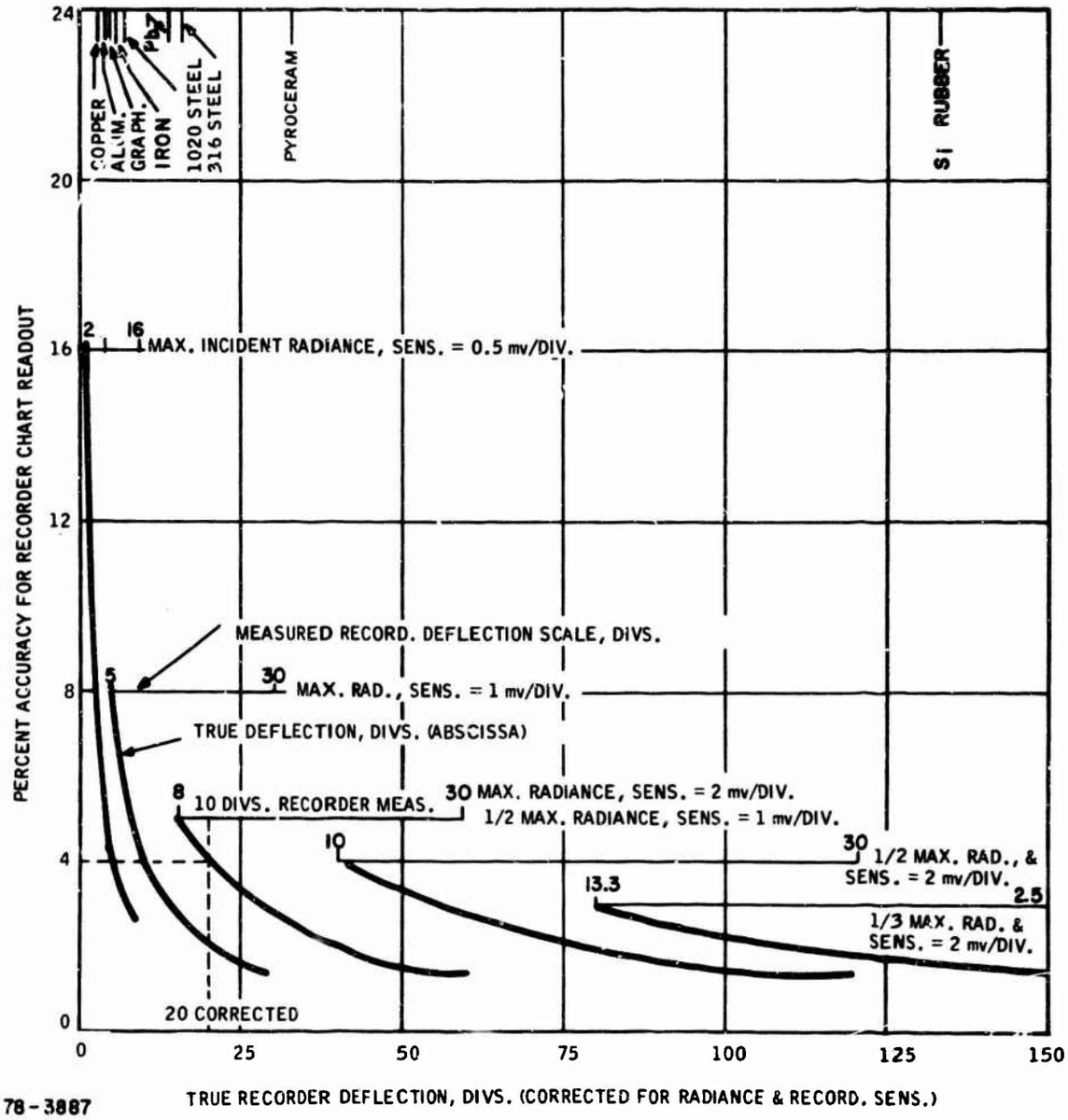

Figure 42 READING ACCURACY AS A FUNCTION OF RECORDER DEFLECTION

B. EXPERIMENTAL RESULTS

Listed in Table VII are the "handbook" thermal properties of the materials reported on here. These property values are considered to be the most consistent for the material grades used, as reported in the literature, or actually determined by facilities at Avco.

The ATJ graphite conductivity value listed is only approximate, since this property has been reported by several authors somewhat above room temperature, and extrapolation of their data (which is in poor agreement) results in values ranging from about 0.1 to 0.4 calories per cm.-sec.-deg. C. Of course, ATJ graphite today is not identical to that manufactured earlier, when much of the reported properties data were originally prepared. We selected the higher conductivity value for inclusion here, since recently produced material tends to have higher densities and other characterisitcs compared with material produced earlier.

The density values listed in the table were determined gravimetrically for the actual specimens studied. The thermal parameter (inertia) and the thermal diffusivity values were calculated from the individual values of ρ, Cp and k. It should be remarked that the conductivity values for the several materials studied span almost 4 orders of magnitude, as do the inertia values; this being an extraordinarily broad range of thermal values to be capable of studying using only a single measurement system.

1. Effect of Surface Roughness

Several specimen parameters were investigated to determine the effect they may have on recorder deflection. It is obvious that a geometrical parameter, for instance, that causes a greater deflection than normal, (i.e., for a semi-infinite section), will result in calculating a lower inertia value and a lower conductivity than the true values. The first effect investigated was surface roughness.

Surfaces of steel and graphite were prepared having different finishes ranging from a polished surface to about an 80 grit abrasive finish, and were then coated with 3M Velvet Black. Results indicated that these surface conditions did not effect recorder deflection, so that essentially a surface need only be coated without regard to roughness, at least to an 80 grit finish.

2. Effect of Thickness

Thickness was investigated next. Results for ATJ graphite are shown in Figure 43 for the two analysis intervals 0.25 to 1.0 second and 1.0 to 4.5 seconds. Since theory requires that a specimen appear semi-infinite in extent during the simultaneous heating and observation period for a valid comparison to be made against a standard without the need for correction, thinner sections can be measured for the earlier time interval. Thus, one would expect to observe semi-infiniteness, or a flattening of the curve for recorder deflection versus thickness, sooner for the 0.25 to 1.0 second interval than for the 1.0 to 4.5 seconds interval. This is borne out by the results shown in Figure 43, where it is to be noted that the later interval is plotted on a scale one-fifth that used for the earlier interval. Included

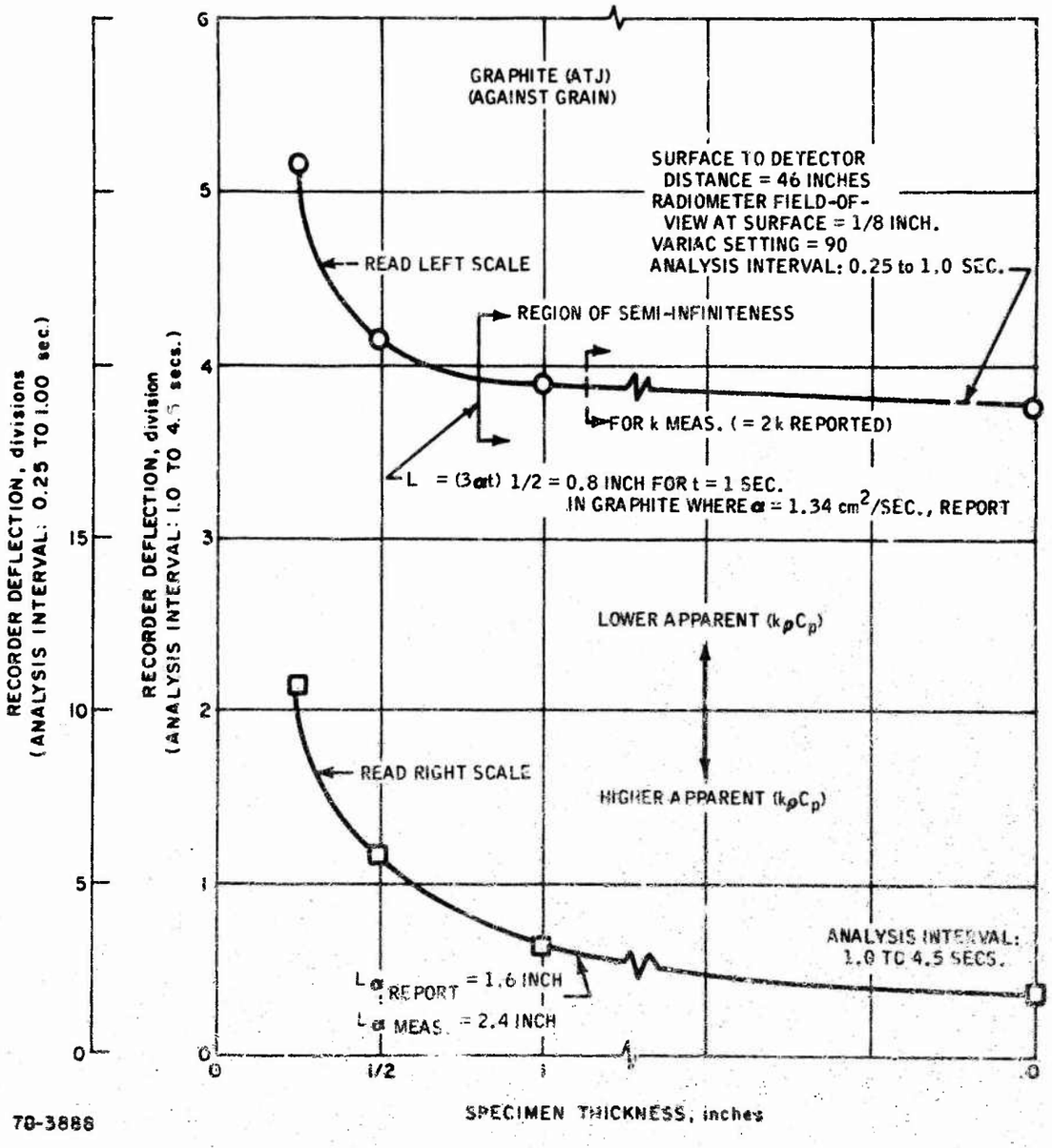

Figure 43 THE EFFECT OF SPECIMEN THICKNESS ON RECORDER DEFLECTION

TABLE VII

THERMAL PROPERTIES

Material	Density ρ (gm/cm^3)	Specific Heat Cp (cal/gm - ^oC)	Thermal Conductivity k (cal/cm -sec ^oC)	Volume Heat Capacity ρ Cp (cal/cm^3 - ^oC)	Thermal Parameter kpCp (cal/cm^4 -sec $^oC^2$)	Thermal Diffusivity $k/\rho Cp$ (cm^2/sec)
Copper	8.93	0.092	0.91	0.822	0.746	1.11
Aluminum (2024)	2.78	0.230	0.44	0.564	0.299	0.779
Graphite (ATJ)	1.73	0.172	0.4	0.298	0.12	1.34
Iron (ARMCO)	7.87	0.107	0.175	0.842	0.147	0.208
Steel (1020)	7.88	0.105	0.124	0.827	0.103	0.150
Steel (316)	7.96	0.108	0.0319	0.860	0.0274	0.0371
Lead (96Pb-45b)	11.03	0.031	0.073	0.342	0.025	0.213
Pyroceram (9606)	2.60	0.185	0.0096	0.481	0.00461	0.020
Rubber (NBS Silicone)	1.29	0.340	0.000661	0.439	0.000289	0.00151

in the figure are calculated semi-infinite thicknesses, L_∞, using reported and measured values of k to obtain the diffusivity values, α. For the 0.25 to 1.0 second interval, the L_∞-values for the reported and measured k-values are 0.8 and 1.1 inches, while for the 1.0 to 4.5 seconds interval, the reported and measured values for L_∞ are 1.6 and 2.4 inches. In each case, the tendency of the curves to flatten out nearer to the measured L_∞-values supports the choice of the higher k-value. Moreover, somewhat greater flattening of the curves occurs nearer to the measured k-value than the reported k-value, inferring that the true conductivity of the ATJ graphite specimens used is more likely closer to that measured than reported. A feasible argument to explain the difference between the measured and reported k-values for this graphite will be presented later.

3. Effect of Surface Curvature

The effect of surface curvature on recorder deflection was also investigated. Results for ATJ graphite, 1020 steel and lead (96 Pb - 45b) in the 0.25 to 1.0 second analysis interval are shown in Figure 44. As expected, recorder deflection decreases, i.e., the inertia appears to increase, as the radius of curvature increases toward infinity, or a flat surface. For ATJ graphite, a radius of curvature less than about 1.25 inches will affect inertia measurements. That is, the self-emission recorder deflection is greater than the reading accuracy error. A similar result obtains for 1020 steel. A much greater radius of curvature is required for lead to suppress this effect on recorder deflection. Of course, components having small radii of curvatures can still be measured using graphs, as in the figure, to correct the deflections to their semi-infinite values for comparison with the reference standard. A plot of recorder deflection as a function of curvature for a family of inertia values would suffice for correcting an unknown material to its semi-infinite geometry.

4. Effect of Specimen Edges

The proximity of the radiant beam (7/8-inch aperture diameter) to specimen edges was investigated. Results for ATJ graphite are shown in Figure 45 for a 2-inch-diameter x 1-1/2-inch-thick cylinder in two analysis intervals and for a semi-infinite rectangular block was not oriented. These two specimens were from different ATJ graphite billets. One would expect that recorder deflection will increase as an edge is approached, especially for good thermal conductors, and the experimental results confirm this. For the 0.25 to 1.0 second interval, recorder deflection is significantly effected when the center of the beam is positioned within 3/4 inch from an edge (the outside beam diameter being within 5/16 inch from an edge) for both the finite cylinder and semi-infinite block cases. In other words, the 2-inch diameter x 1-1/2-inch-thick cylinder appears semi-infinite both in thickness and diameter as long as the beam is positioned at the axis of the cylinder, and the analysis interval is 0.25 to 1.0 second. This is not the case for the cylinder, however, when the analysis interval is 1.0 to 4.5 seconds. The figure shows that the 7/8-inch beam diameter cannot be positioned even at the cylinder's axis without significantly affecting recorder deflection. In other words, the later analysis interval (1.0 to 4.5 seconds) cannot be used for measuring the inertia of this graphite cylinder without appropriate correction, since measurements will result in an apparently larger deflection than normal and the derived inertia and conductivity values will each appear less than actual.

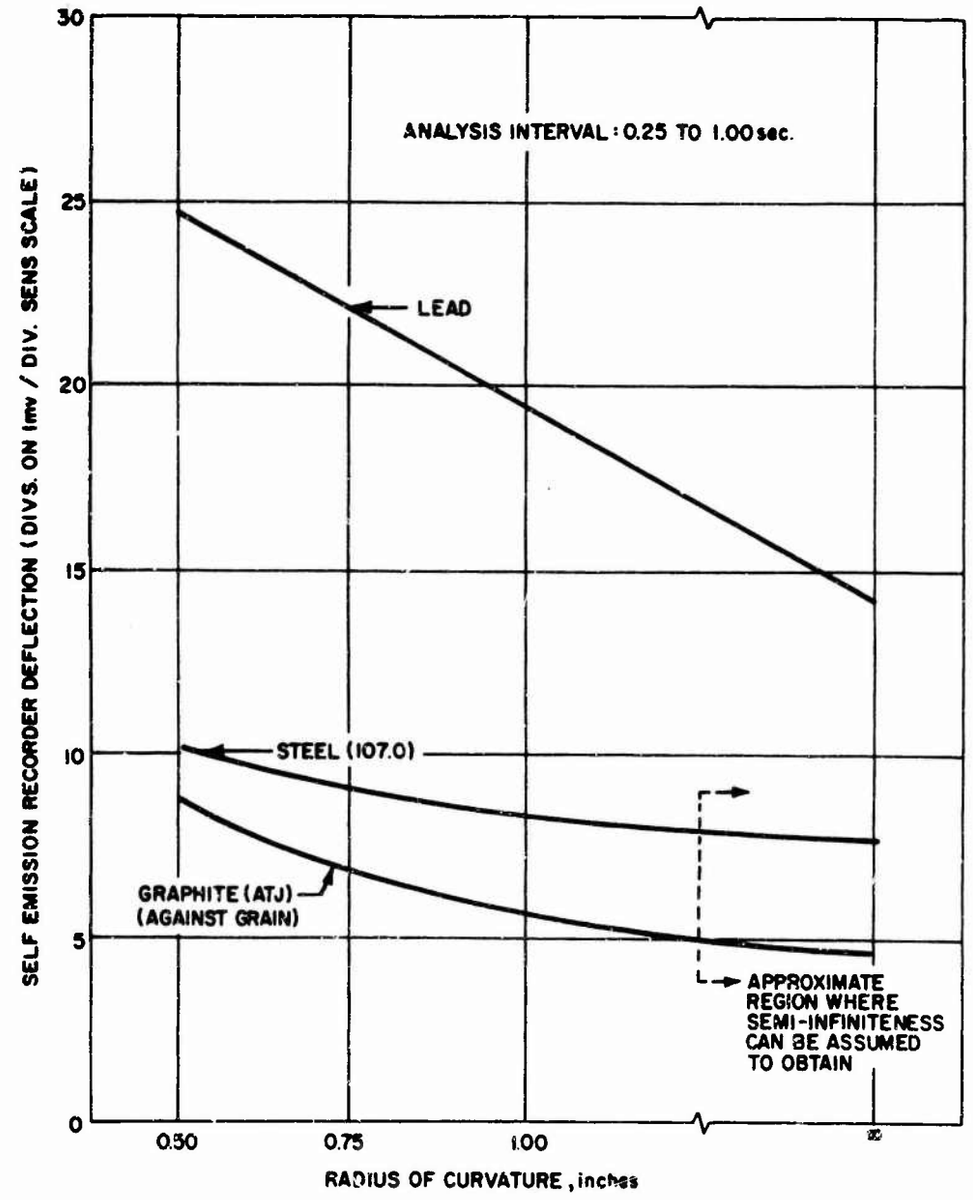

78-3889

Figure 44 THE EFFECT OF SURFACE CURVATURE ON SELF EMISSION RECORDER DEFLECTION

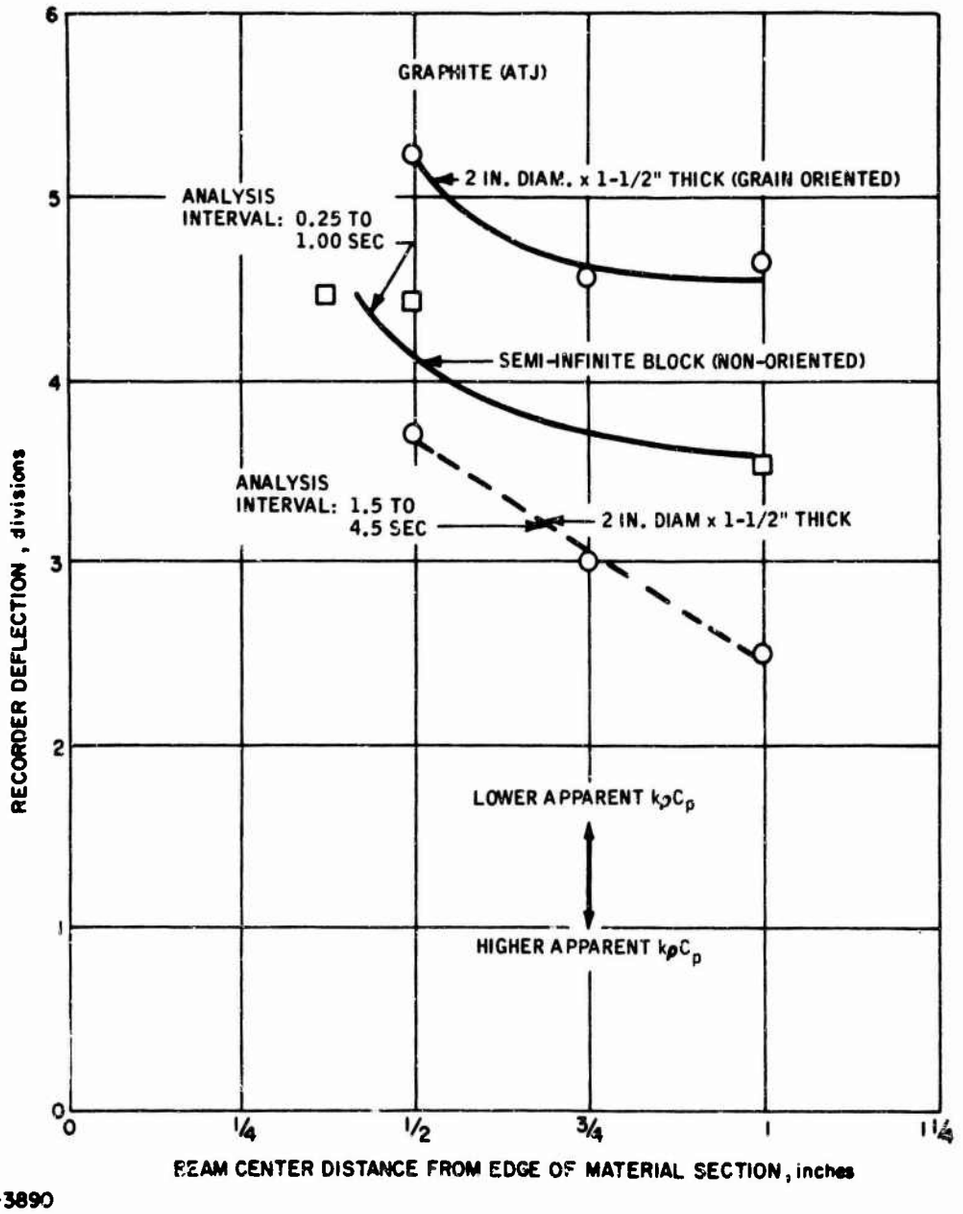

78-3890

Figure 45 THE EFFECT OF EDGES ON RECORDER DEFLECTION

5. Material Test Results

Using the foregoing and similar results for the materials listed in Table VII specimens were fabricated having semi-infinite geometries. All specimens were coated with 3M Velvet Black. Measurements of their recorder deflections were then made within the 0.25 to 1.0 second analysis interval. The results of these recorder deflections are listed in Table VIII. Also included in this table are the ratios of these deflections to that for the Armco iron reference standard, since these are inversely proportional to the inertia ratios. Shown in Figure 46 is a plot of the data calculated from the reported values of $(k\rho C_p)$ listed in Table VII. The agreement is seen to be excellent over about 4 orders of magnitude, with the exceptions of the ratios for ATJ graphite and 316 stainless steel, where the differences are noted to be 50 and 47 percent, respectively. Little in the way of explanation can be offered for the 316 steel discrepancy. If it is assumed that our measured value for this steel specimen is correct in view of the results for the other materials, then either the reported value for its conductivity is too high or its true conductivity is less than reported for most 316 steel bars. The more likely situation is the latter, wherein cold rolling, or other unique fabrication processes, may have altered the grain structure sufficiently to decrease its normal conductivity. Its volumetric heat capacity is not regarded as significantly alterable in any unique process as can be the conducitivity.

The discrepancy noted for ATJ graphite can be explained in two plausible and complimentary ways. First, the production methods used for manufacturing ATJ graphite are continually undergoing improvement in the graphite industry. This is to say that ATJ graphite today is, in fact, not identical to that produced, say, in 1962, although the two products are still called ATJ. This is because of certain characteristic physical and mechanical properties that generally remain within specified limits and because the basic process is essentially the same. Some reported values for STJ graphite in the literature were, in a sense, outdated even as they went to press. The graphite used in this study was manufactured recently. Since recently produced ATJ graphite generally has less porosity and smaller grain size than earlier stock, it is reasonable to expect that the thermal conductivity today is greater than values reported in the literature. The conducitvity measured in this study is about twice that reported, and discussions with knowledgeable persons lead this author to believe that our measured inertia value is not only consistent with the increasing trend in conductivity, but also with the approximate magnitude of difference noted in Figure 46.

As a second argument to explain the discrepancy noted for graphite, reference is made to the previous discussion of beam radiance nonuniformity. Since the beam's intensity was maximum at its center, the resultant instantaneous surface temperature distribution on any of the materials tested also exhibited a maximum at the center. This condition gives rise to lateral heat flow within the material outward from an axis concentric with that of the beam, or aperture. The heat loss tends to diminish the recorder deflection from the true deflection, which results when the thermal wave front travelled plane and parallel into the material. When comparing two homogeneous and isotropic solids to obtain a ratio, this effect due to thermal wave distortion is insignificant from the viewpoint of the overall results presented for the several materials.

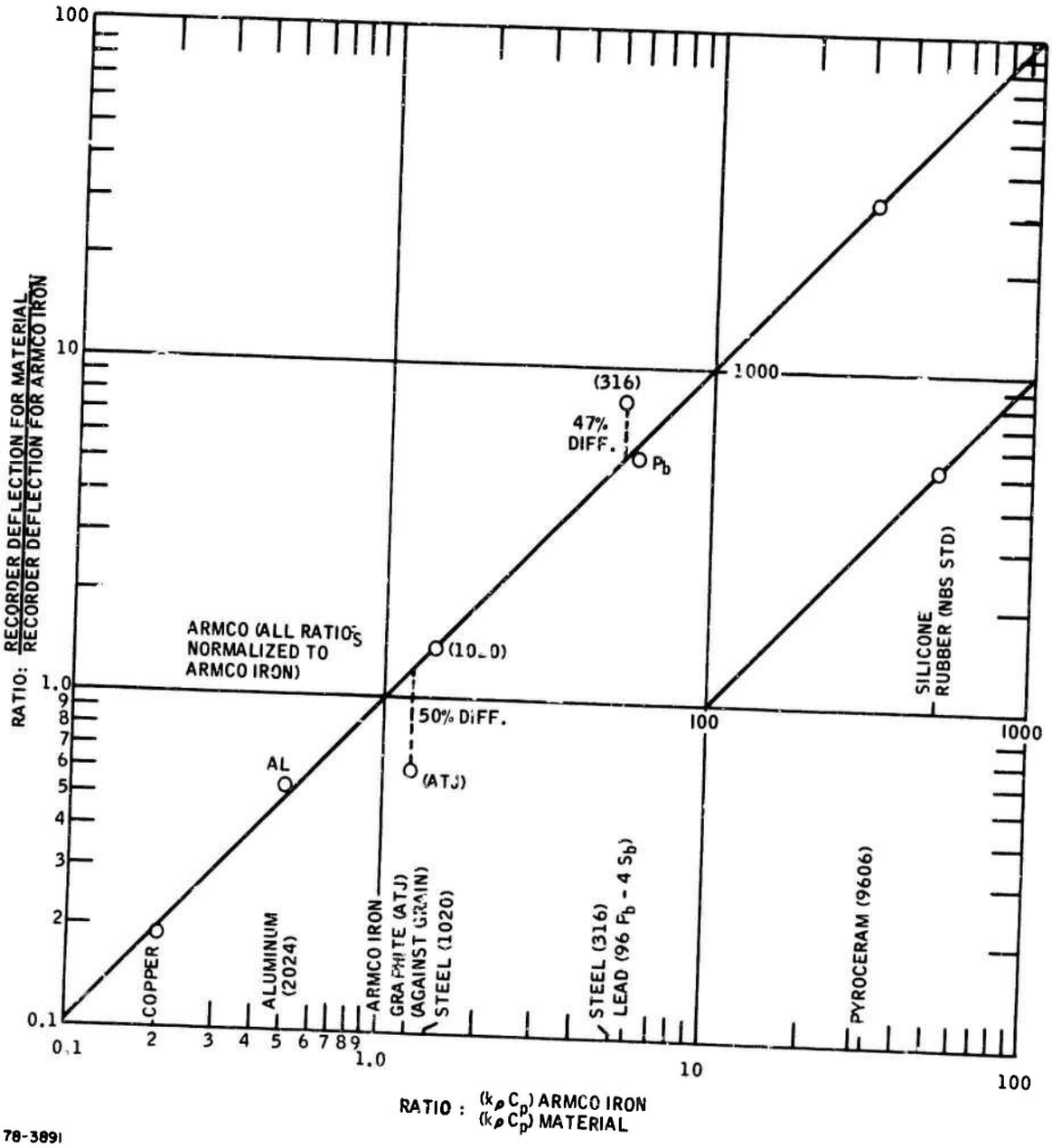

78-3891

Figure 46 COMPARISON BETWEEN MEASURED AND REPORTED RATIOS OF $k\rho C_p$

TABLE VIII

COMPARISON BETWEEN MEASURED AND REPORTED RATIOS OF THE THERMAL PARAMETER

Material	Dimensions (diam. x thick.) (inches)	Measured Self-Emission Recorder Deflection Between 1/4 and 1 seconds (divs.)	Ratio of Deflection for Material to That for ARMCO Iron	Ratio Squared	Ratio: $(k\rho Cp)$ ARMCO $(k\rho Cp)$ Material as Reported By Others
Copper	2 X 1-1/2	2.6	0.44	0.19	0.197
Aluminum (2024)	2 X 1-1/4	4.3	0.73	0.53	0.492
Graphite (ATJ) (Against Grain)	2 X 1-1/2	4.6	0.78	0.61	1.22
Iron (ARMCO)	1-1/4 X 3	5.9	1	1	1
Steel (1020)	2 X 1-1/2	7.0	1.18	1.40	1.42
Steel (316)	2 X 6	16.6	2.81	7.90	5.37
Lead (96Pb - 45b)	2 x 1-1/2	13.7	2.32	5.40	5.88
Pyroceram (9606)	1 X 2	32.7	5.55	31.3	31.8
Silicone Rubber (NBS Standard)	4-5/8 X 1/2	133	22.6	510	510

However, ATJ graphite is anisotropic and our meaaurements were performed in a direction such that the wave front travelled against the grain orientation. This means that lateral heat transfer along the grain direction would be abnormally high relative to transfer againat the grain direction. An even smaller recorder deflection would result for this geometry than would be expected for an isotropic material, ao that a comparison of the resultant deflection for the graphite with the deflection for Armco iron would be greater than a ratio calculated from reported values. The net effect would be to have calculated a conductivity greater than actual.

Also included in the table are percent differences between these values. Comparing these differences to the reported values, only the graphite and the 316 stainless steel differences cause concern. The above argumenta obtain here in explanation of this. The other differences (8 percent and less) can be directly attributed to either inherent readout and system errora, or to poor judgement in selecting and reported k, and posaibly Cp valuea, near room temperature, that were most representative of the actual materials used. Theae results are presented graphically in Figure 47. In general, the volumetric heat capacities, ρC_p, for the reported and the measured inertias are identical, so that Figure 47 ia essentially a plot of conductivity values. The thermal conductivitiea calculated from the measured inertia values are also included in Table IX.

Each of the above arguments for graphite, in themselves, can likely account for the 50 percent difference between the reported and measured inertia ratios. Moreover, the remarkable correspondence for the other materials (where Pyroceram 9606 and NBS silicone rubber are alao standard materials uaed in thermal testing laboratories, and were measured by a thermal test group at Avco) does lend great support to the method's capability. Consequently, the discrepancy for graphite is not regarded as a significant fault of either the method or of the measuring syatem, but rather one of inadequate information upon which an accurate judgement can be made.

Listed in Table IX are reported and meaaured values of ($k\rho C_p$) for the several materiala. The measured values were derived from the ratios using the inertia value for Armco iron as the reference.

C. IMPLICATIONS OF THE RESULTS

The immediate and most general statement that can be inferred from the above work is that this method will permit both laboratory and field measurements of the thermal inertia property of solids to be performed in a nondestructive manner near room temperature with an accuracy suitable for engineering and most scientific purposes. Moreover, the capability for measuring such a thermal property for materials in fabricated form would appear to have wide application. Furthermore, the extension of this method to include materials other than lids and for use at elevated temperatures appears to be feasible, after redesi of the present apparatus.

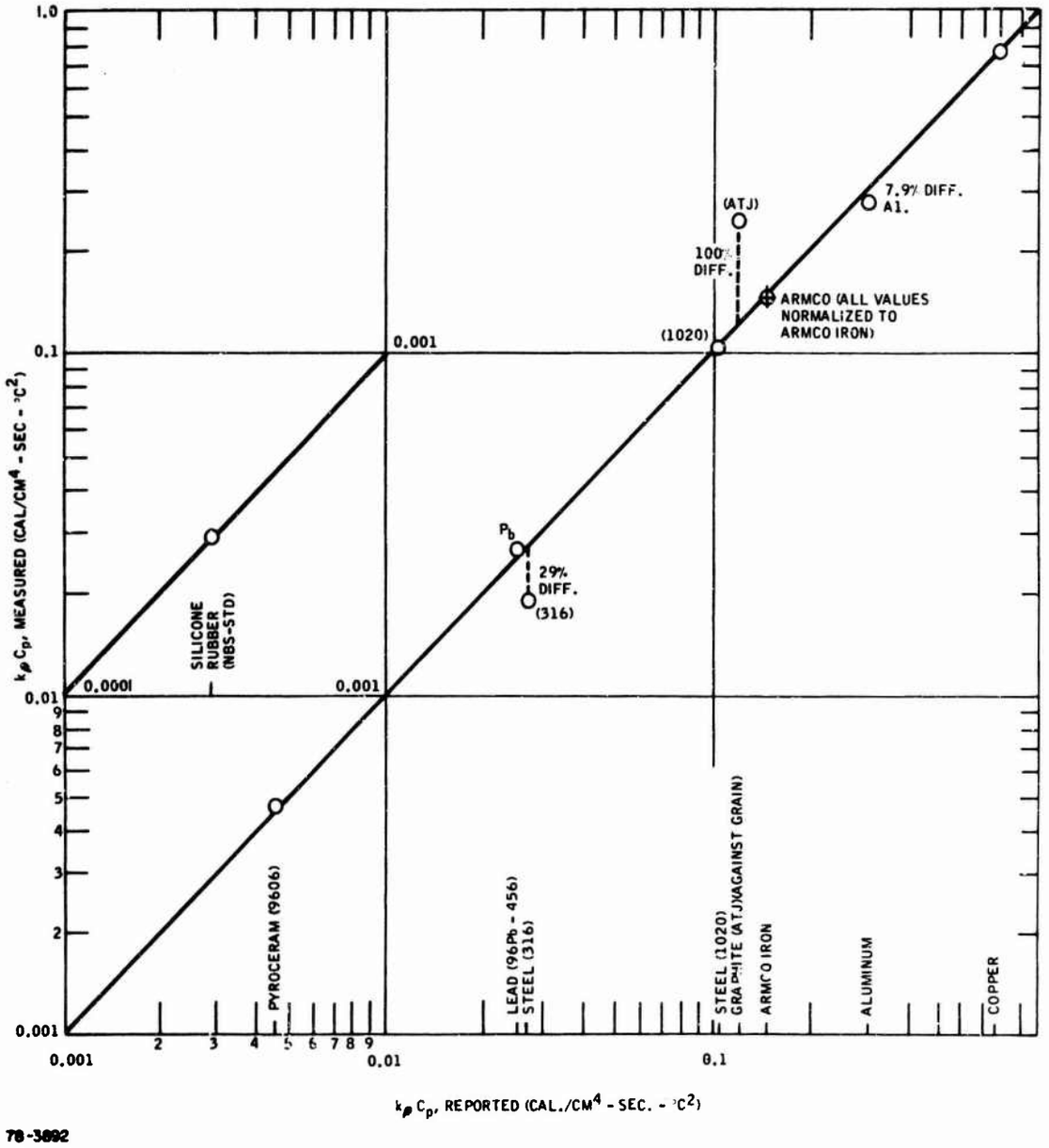

78-3892

Figure 47 COMPARISON BETWEEN MEASURED AND REPORTED VALUES OF $k\rho C_p$

TABLE IX

COMPARISON BETWEEN MEASURED AND REPORTED VALUES OF THE THERMAL PARAMETER, ALSO THE MEASURED VALUES OF THERMAL CONDUCTIVITY

Material	Reported[2] ($k\rho Cp$) (cal/cm^4 -sec - $^oC^2$)	Measured[3] ($k\rho Cp$) (cal/cm^4 -sec - $^oC^2$)	Percent Difference $\frac{\text{Meas. - Report.}}{\text{Meas.}}$	Percent Difference $\frac{\text{Report. - Meas.}}{\text{Report.}}$	Measured - Values[4] (Near Room Temp.) (cal/cm - sec -C)
Copper	0.746	0.757	1.5	-1.5	0.72 ± 0.18
Aluminum (2024)	0.299	0.276	-8.3	7.7	0.48 ± 0.08
Graphite (ATJ) (Against Grain)	0.12	0.242	50	-100	0.81 ± 0.14
Iron (ARMCO)	0.177	0.147	0	0	0.175 (Reference)
Steel (1020)	0.103	0.104	1	-1	0.126 ± 0.010
Steel (316)	0.027	0.019	-42	29	0.221 ± 0.018
Lead (96Pb - 45b)	0.025	0.027	7.4	-8.0	0.079 ± 0.006
Pyroceram (9606)	0.0046	0.0048	4.3	-4.2	0.0100 ± 0.0008
Silicone Rubber (NBS Standard)	0.00029	0.00029	0	0	0.000662 ± 0.000052

1. Normalized to ARMCO Iron

2. Calculated from Reported Values of k, ρ, and Cp Near Room Temperature

3. $(k\rho Cp)_{\substack{\text{Meas.}\\\text{Material}}} = (k\rho Cp)_{\substack{\text{ARMCO}\\\text{Report.}}} X\left(\frac{\text{Deflect. for ARMCO Iron}}{\text{Deflect. for Material}}\right)^2 = \frac{0.147 \times (5.9)^2}{(\text{Defl. Mater.})^2} = \frac{5.11}{(\text{Defl. Mater.})^2}$

4. Calculated using Measured ρ-Values, Reported Cp-Values, and the Measured $k\rho Cp$-Values.

The principal limitations imposed by the present system design are the response time and the available radiant intensity. Yet these limitations are of importance only when measuring the good thermal conductors, which includes graphite. The present response time and intensity make it necessary to use about a 1 second analysis interval to obtain a signal having an amplitude sufficiently great to achieve a reasonable accuracy for readout. As a consequence of this interval, geometries for the good conductors must be rather large (about 2-inches diameter by 1-1/4 thick, and a surface radius of curvature greater than about 1-1/2 inches) to approximate semi-infiniteness. Otherwise, preliminary experimentation is necessary to arrange for appropriate corrections to normalize for semi-infiniteness. A faster response time and higher intensity radiant source will permit smaller sections to be measured. These limitations are inconsequential, for the most part, for the poorer thermal conductors.

Two additional limitations of concern in any redesign of the system are the beam intensity distribution and the coating. The present system optics are inadequate for obtaining a uniform intensity across the beam diameter, and although the effect is negligible in most cases, for grain oriented solids uniformity in intensity may be a serious requirement. The coating that has been used is essentially a poor thermal conductor. Application of the coating to a good conducting solid creates a mismatch which can become most important if analysis intervals are shorter and/or earlier after radiant pulse initiation than the 0.25 to 1.0 second interval used here. Ideally, coatings should not be used. This may be a practical requirement for some applications, as well.

Another limitation, or operating inconvenience, which may be important in any redesign is the disproportionate time required for chart analysis when compared to the actual measurement time. At present, the measurement time takes just a few seconds. Using the recorder readout, which is a linear system, several minutes are required to determine a signal amplitude increment and to calculate an inertia value. A logarithmic display, or a direct digital readout, each preset to internally compare the reference standard with the material of interest would result in a more efficient operation when many measurements are to be performed.

Moreover, the present system is costly, is not portable, and is capable of making only laboratory measurements. In this author's judgement, redesign would enable a relatively inexpensive and portable system to be constructed. The optics can be simplified and made more efficient. The existing electromechanical shutter is massive, complex, noisy, and can create significant vibration. A rotating sectored-disc type shutter, or a movable tape, or tapes, containing appropriate aperture geometries, or a movable mirror arrangement appear to be more desirable. The infrared radiometer now used is more sophisticated, in many respects, than is necessary for simply generating a comparative signal. It is believed that a ruggedized unit containing the source, its optics, and the shutter can be constructed together with an infrared radiometric detector and readout analyzer, of comparable response to that used here, for about $5000, following, of course, design and development costs for constructing a prototype system. The present system consists of laboratory type equipment whose value is about $10,000. The cost of standard equipment for measuring k, ρ, and C_p independently in most thermal properties laboratories is about the same as the present system and requires specially prepared test specimens. The time required to generate these values can run into days compared to a few minutes using the infrared method. Experience and facilities at Avco/SSD are suited for designing and manufacturing a portable, infrared, measuring system for obtaining useful engineering data in the field.

III. CONCLUSIONS AND RECOMMENDATIONS

The method has been applied to the measurement of thermal inertia near room temperature for several materials ranging from copper, through aluminum, graphite, iron, steel, lead, and Pyroceram 9606 to NBS silicone rubber with excellent results over a conductivity range spanning about 4 orders of magnitude. Thermal conductivities have been determined from the measured inertia values with accuracies ranging from about 20 percent for copper, to about 15 percent for ATJ graphite, to about 8 percent for NBS silicone rubber. Better results can be expected if a more sensitive infrared radiation detector and a more intense source than used here are employed. These results, however, are sufficiently accurate for most engineering applications.

The time involved in making a measurement is only several seconds; analysis and calculation of inertia presently requires a few minutes.

The present system is not protable and must be redesigned for practical application in the field.

For the good thermal conductors, the present system imposes limitations on their geometrical configurations. To appear semi-infinite in the 0.25 to 1.0 second analysis interval, the good conductors, including ATJ graphite, must be at least 1-1/4 inches thick, have a diameter of 2 inches or greater, and have a surface radius of curvature greater than 1-1/2 inches. Smaller configurations require considerable correction to obtain a normalized value of recorder deflection for comparison with the reference standard. A high emissivity coating, such as 3M Velvet Black, must be applied to the surface being measured; no other special surface preparation being necessary, as long as its finish is at least equivalent to that produced by 80 grit energy paper or finer before coating. Geometrical limitations are considerably less severe for the poorer conducting materials.

It is recommended that a prototype system be designed and constructed for ruggedized field testing. Such a design should incorporate only those features necessary to achieve satisfactory accuracy for engineering applications, as well as a rapid readout and analysis capability.

IV. REFERENCES

1. Lockyer, C. E., A. W. Schultz, S. Serabian, and S. W. Carter, Investigation of Nondestructive Methods for the Evaluation of Graphite Materials, AFML-TR-67-128 (June 1967).

PART C - APPLICATION OF NONDESTRUCTIVE TEST TECHNIQUES FOR EVALUATING AND PREDICTING PROPERTIES IN AEROSPACE GRAPHITE BILLETS

John Orner

I. INTRODUCTION

A. NDT/MECHANICAL PROPERTIES CORRELATIONS AT ROOM TEMPERATURE IN GRAPHITE

Density, elastic modulus, and tensile strength have been identified as properties of general interest in graphite. In particular, density has been cited by many investigators to be the predominant property or variable which influences other design properties. However, since density determinations in bulk shapes by radiometric techniques have been noted to be insensitive to the anisotropy of graphite with respect to elasticity and strength, ultrasonic longitudinal wave velocity measurements, with and against the grain, play an important role in the nondestructive determinations of elastic modulus and tensile strength.

The measurement of density or thickness of materials by radiation gaging is well established in industry, especially for sheet materials, such as metals, paper, plastics, and rubber. Whether for determination of density or thickness, the basic principle is the same. As the ratio of transmitted to incident radiation is a function of the thickness-density product in accordance with the well-known relationship:

$$I = I_o e^{\mu_m d x} \tag{1}$$

where

I = intensity of transmitted radiation

I_o = intensity of incident radiation

μ_m = the mass absorption coefficient

d = density

x = material thickness

The mass absorption coefficient is a constant property of the material for a particular photon energy and, since the thickness, the incident intensity, and the transmitted intensity can all be measured, the density can be calculated from the expression:

$$d = - \frac{1}{\mu_m x} \ln \frac{I}{I_o} \tag{2}$$

The bulk velocity of longitudinal waves in an extended isotropic medium is given by:

$$V_L = \left[\frac{E}{d} \frac{(1-\sigma)}{(1+\sigma)(1-2\sigma)} \right]^{1/2} \tag{3}$$

where

V_L = longitudinal wave velocity

E = Young's modulus

σ = Poisson's ratio

However, for all practical purposes, it has been determined that for values of Poisson's ratio of 0.2 or less, such as occur in graphite, this expression can be simplified and written as:

$$V_L^2 = \frac{E_D}{d} \quad \text{or} \quad E_D = d V_L^2 \tag{4}$$

where

E_D = dynamic modulus

If a completely brittle material can be defined as a material for which the stress-strain curve is linear up to the point of rupture, then the ultimate tensile strength of such a material could be determined from the relationship:

$$UTS = E(\epsilon) \tag{5}$$

where

ϵ = total strain to failure

Thus, once the total strain to failure for such a brittle material has been determined experimentally, the ultimate tensile strength may be computed directly from nondestructive measurements of density and bulk velocity of longitudinal waves.

Graphite, however, does not conform strictly to the definition of a perfectly brittle material, as the stress-strain curve is not linear, but exhibits a definite curvature. Therefore, in order to make any predictions with respect to ultimate tensile strength, it is necessary to compensate for this curvature. This has been done by introducing the concept of the secant modulus, which is defined as a straight line on the stress-strain diagram joining the origin and the point of rupture. The ultimate tensile strength is then given by the relationship:

$$UTS = E_s(\epsilon) \tag{6}$$

where

E_S = secant modulus

All that is now needed for the computation of ultimate tensile strength in graphite is a derivation relating dynamic modulus, and secant modulus, and a knowledge of strain-to-failure values for the grades of graphite under consideration.

B. DENSITY COMPUTATIONS

The radiometric measurement of densities in graphite is subject to numerous experimental errors which have to be compensated for in order to achieve the required degree of accuracy. Predominant sources of error are associated with such factors as limitations of the instrumentation, superimposed background count, internal scattering of the radiometric beam by the material, edge effects. Edge effects, or errors due to a change in scattering coefficient as the radiometric beam traverses the material in close proximity to a surface of the billet can be avoided by choosing test points appropriately removed from the edges. Other sources of error can be either reduced to negligible proportions, or completely eliminated by making a determination of an adjusted, or effective coefficient of mass absorption applicable to the particular billet of graphite under test.

In practice, there is no need for actually computing the effective mass absorption coefficient as the density determinations for each test point on the billet are computed from the relationship:

$$d = \frac{d_g t_a \ln \frac{I_o}{I}}{t \ln \frac{I_o}{I}} \qquad (7)$$

where

d_g = gravimetric density of the billet as determined by physical measurements of weight and dimensions

t = thickness of billet at the test point under consideration

t_a = averaged thickness of the billet as obtained by averaging the thickness values for every test point in the dimension under consideration, e.g., diameter or length

I_o = incident radiation

I = transmitted radiation at the test point under consideration

I_a = averaged value of all transmitted radiation for every test point in the dimension under consideration

In effect, with this method, radiometry is not used to make an absolute density measurement; but rather, it is used to determine density variations from point to point, in the graphite billet, the absolute values of which are fixed such that their combined average is equal to the predetermined gravimetric density. In this way, a high degree of accuracy is maintained.

C. OTHER NONDESTRUCTIVE TESTS

Each graphite billet to be nondestructively characterized with respect to materials properties must also be subjected to other nondestructive tests in order to pinpoint any possible defective conditions which could degrade the performance of the material in any load-bearing application.

Each graphite billet evaluated at Avco/SSD is radiographed in at least two different directions in order to detect any material anomalies, such as voids, inclusions, cracks, lines of demarcation or any other condition detectable by this method.

Each graphite billet is subjected to an exhaustive ultrasonic defect detection procedure at both 1 MHz and 2.25 MHz frequencies in order to detect any material discontinuities or areas of abnormal attenuation, such as would be caused by areas of relatively high porosity. Material discontinuities detectable in this way include cracks, voids, inclusions, or any sudden change in material characteristics which would tend to reflect travelling stress waves. In order to detect any abnormal surface conditions, each graphite billet is also subjected to an alcohol penetrant test which effectively shows up surface cracking and areas of variability in porosity.

II. APPLICATION OF TECHNIQUES TO AEROSPACE MATERIALS

A. EVALUATION OF PHILCO-FORD BILLETS

During this phase of the program, a total of 31 graphite billets were nondestructively characterized at the request of the Air Force Materials Laboratory. These billets were evaluated for the Air Force by the Philco Ford Corp.

All destructive test data obtained on the Philco-Ford graphite to date have been tabulated and an attempt will be made here to correlate this information with the nondestructive characterization carried out at Avco.

In a discussion with Messrs. Bruce Thoeni, Bruce Linde, and Walter Olson, which took place at Philco-Ford, Newport Beach, California, on 28 and 29 February 1968, the following points were discussed:

Characterization data as being supplied by Avco on the Philco-Ford graphite billets have not been used for design purposes. As explained by Mr. Linde, the experimentally obtained values for strain-to-failure in the with-grain direction on ATJ-S graphite vary over a range of 0.0027 to 0.0053 inch per inch. Therefore, Philco-Ford feels that characterization data based on the lower limit of these boundaries would be more meaningful than the presently established value of 0.0034 inch per inch used by Avco for the computation of ultimate tensile strengths.

It was also stated by Philco-Ford that when graphite billets are cut, either for machining of components, or for destructive testing, no account is taken of the Avco nondestructive characterization except, of course, the flaw detection. The opinion was also expressed that the ultrasonic flaw detection technique was not giving sufficiently meaningful information with respect to either the size or the characteristics of the defects that were being reported.

In the Philco-Ford design of graphite nose tips and nozzles, the characteristic of major importance around which the design is based is the strain to failure value of the material rather than the ultimate tensile strength. The strain-to-failure used is the lower boundary of the experimental values observed on tensile specimens cut from the billet to be used. The values of modulus used to compute the strain are also determined experimentally rather than taken from the nondestructive test data.

In answer to questions on nose tip failures, the opinion was expressed that the failure mechanism involved was either thermal stress leading to cracking, or by break up initiated by localized gaging with subsequent burn through. It was also stated that none of the failures that had occurred could be correlated back to NDT data. One of the difficulties appears to be that the nose tip cannot be oriented back to the original billet positions and directions. Philco-Ford has had a nose tip failure in the Malta spin test of one of their blunt nosed units, but they feel the failure could have been due more to the test facility than to any anomalies in the graphite itself. The feeling is that the failure, in this case, was initiated by severe unsymmetrical gaging at a point near the tip which lead to complete burn through. There have not yet been any flight tests on nose tips made from Avco characterized graphite.

Philco-Ford agrees that the room temperature properties of graphite probably can be extrapolated to indicate high temperature properties, but they were quick to point out that they would not stake a design on it.

On the relative merits of ATJ and ATJ-S graphite, Philco-Ford pointed out that the strain-to-failure value is the same for both grades, but as the ATJ-S has a higher modulus and tensile strength. The same margin of safety exists for both grades. It was admitted, however, that the ATJ-S graphite would be the better material for applications involving purely mechanical loading.

It must be pointed out here that this statement by Philco-Ford is not in accordance with Avco's observations on the two grades concerned. Lockyer, Lenoe, and Schultz[1] report strain-to-failure values for ATJ graphite averaging 0.00448 inch per inch in the against grain direction, with high and low values of 0.0055 and 0.0036. In the with grain direction these values are 0.00348 inch per inch, 0.0043 and 0.0028, respectively. Strain-to-failure values being established for ATJ-S graphite are apparently considerably higher, and more variable, than the values previously established for the ATJ grade. It appears, in fact, that both the magnitude and the variability displayed by ATJ-S graphite are sufficient to seriously impair tensile strength correlations.

The graphite billets which have been rejected by Philco-Ford, and presently being held in storage, have been rejected mainly on the basis of heavy calcium deposits--not on Avco NDT characterization data. Slabs in thicknesses of 1/4 inch or less are cut from each billet and radiographed. In graphite sections of this thickness, the calcium deposites are easily seen. In addition, five billets have been returned to Union Carbide, one because of bad cracking, and four because of a line of demarcation visible on the Avco radiographs. It is interesting to note that chemical analysis, in some cases, shows a considerably higher calcium content on billets that appear to be relatively clear of calcium deposits, than on billets that have been rejected for high radiographic indication of calcium.

B. CORRELATION BETWEEN PHYSICAL AND NONDESTRUCTIVE TESTS

Destructive test data compiled by the Philco-Ford Corporation on graphite billets that have been subjected to the Avco NDT characterization has been made available by Philco-Ford and an attempt will be made to compare the results of the physical tests with the predicted values of the material characteristics. Most of the physical test data reported here have been extracted from the Philco-Ford Corporation, Space and Reentry Systems Division, Engineering Data Release No. 5108 entitled Properties of ATJ-S Graphite, prepared by Mr. H. B. Thoeni.

To date, only one of the characterized graphite billets (No. L-1-11) has been cut-up into test specimens that allow a fairly extensive correlation between actual and predicted properties on a one-to-one basis. Even in this case, however, many of the tensile coupons in the with the grain direction were cut on an angle which had not been characterized. Figures 48, 49, 50, and 51 indicate the cutting plans for the test coupons taken from billet L-1-11. It should be noted that a direct correspondence between Avco and Philco-Ford specimen numbers exists only for the axial (against the grain) coupons. The radial test coupons were cut at points which did not directly correspond to the Avco test points. For this reason, a direct correlation between predicted and measured property values will not be entirely meaningful in the case of the "with grain" directions. Predicted

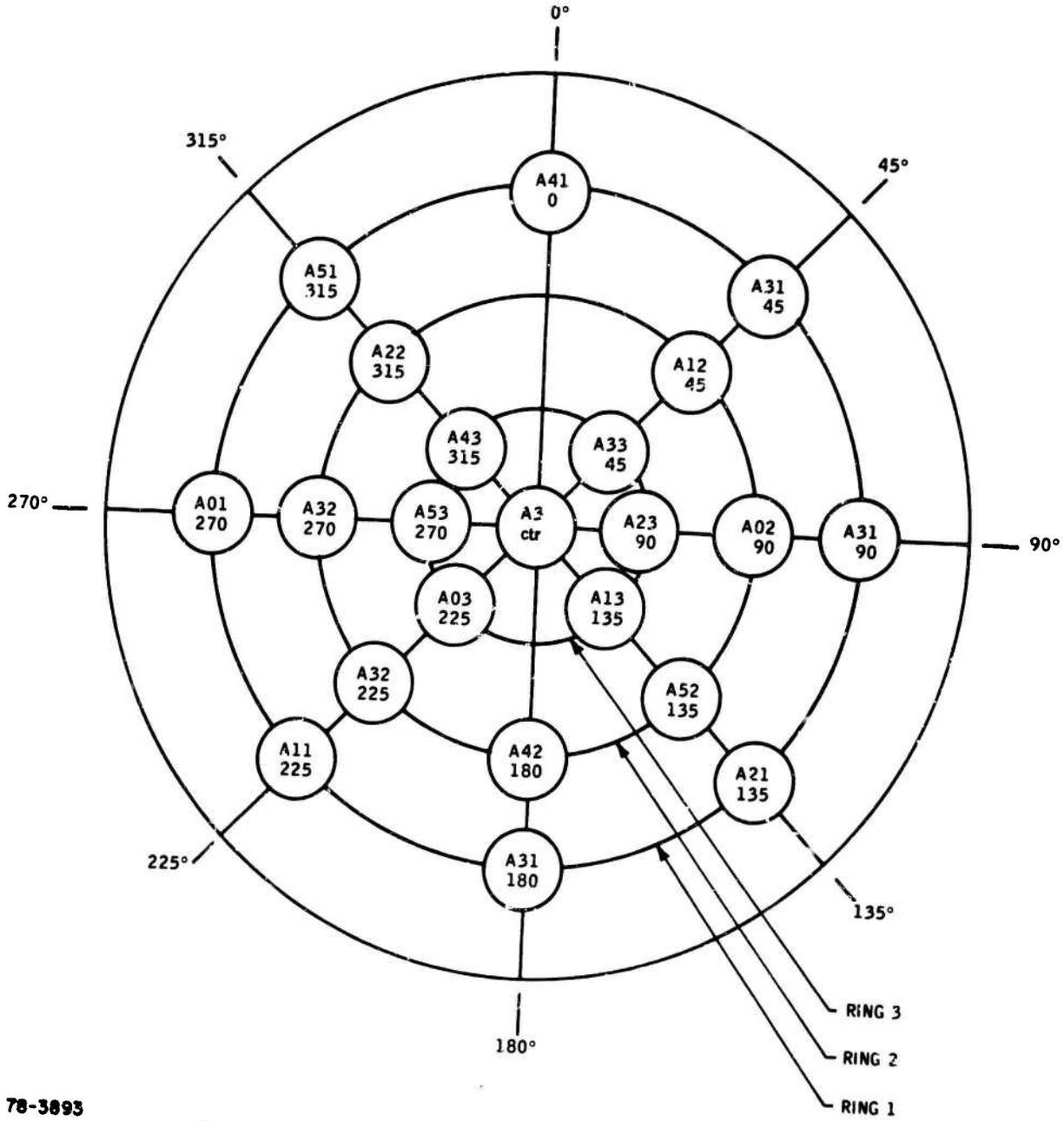

78-3893

Figure 48 CUTTING PLAN FOR ACROSS-GRAIN TENSILE COUPONS, ATJS BILLET L-1-11, VIEWED FROM TOP FACE OF BILLET

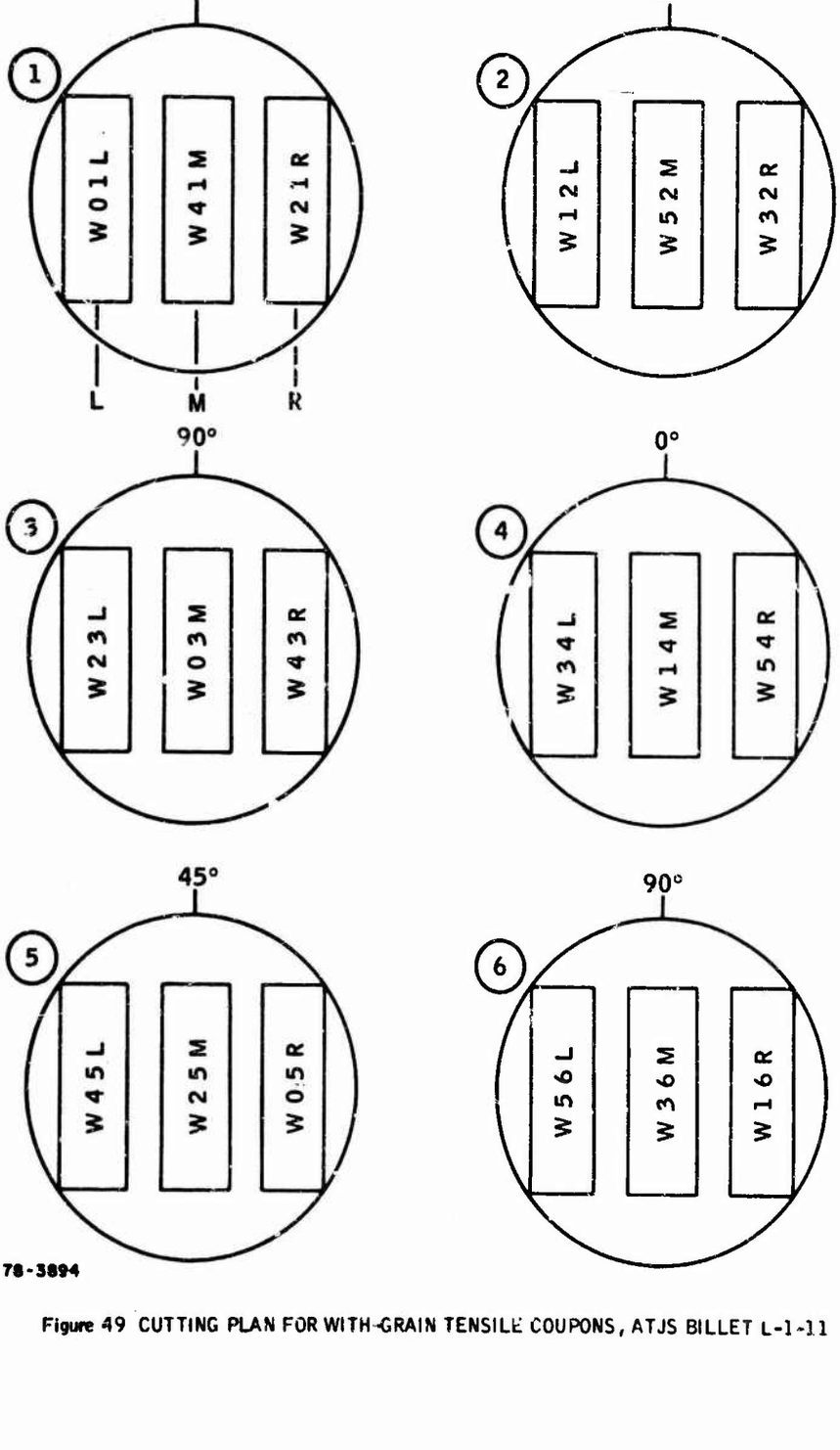

Figure 49 CUTTING PLAN FOR WITH-GRAIN TENSILE COUPONS, ATJS BILLET L-1-11

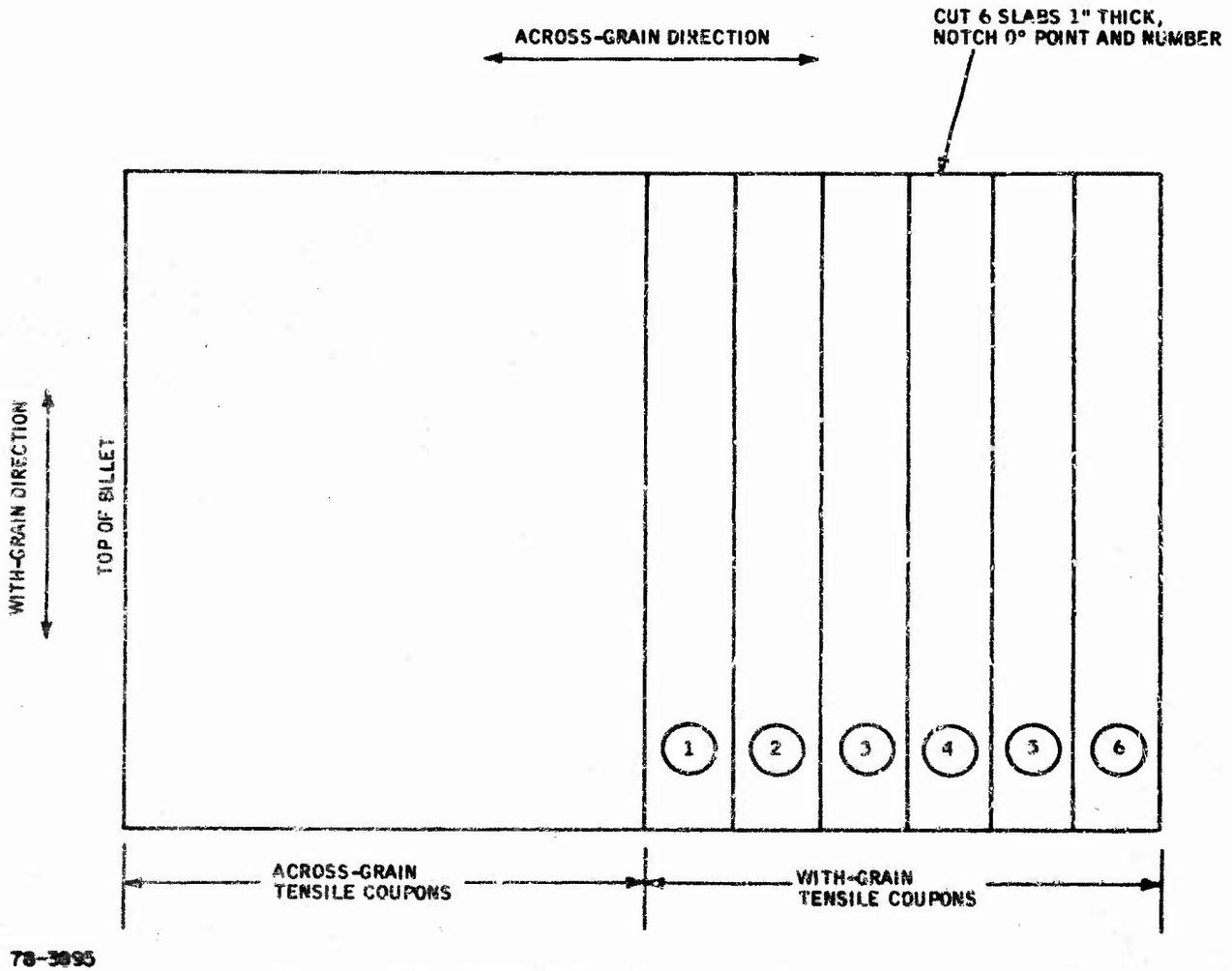

Figure 50 CUTTING PLAN FOR ATJS GRAPHITE BILLET L-1-11, VIEWED FROM SIDE OF BILLET

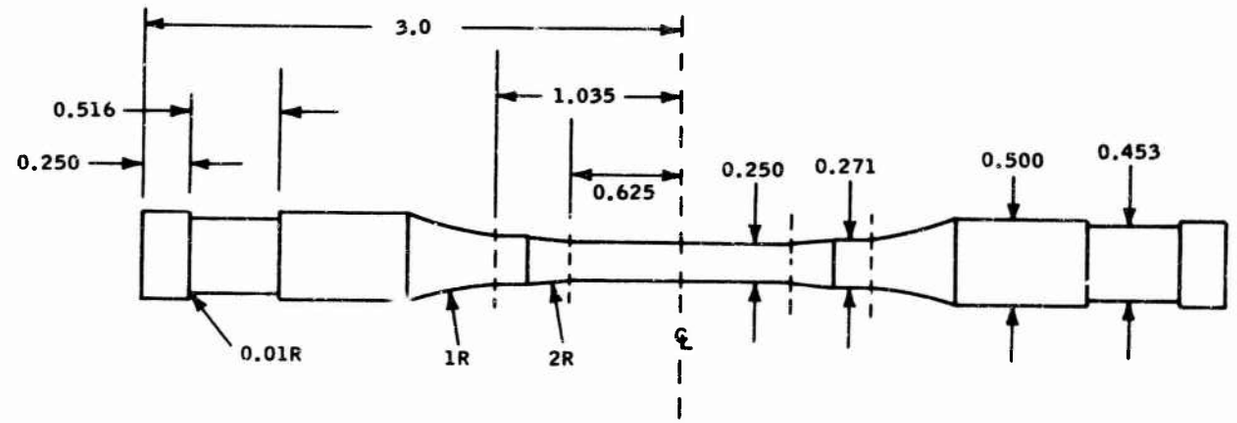

Figure 51 TENSILE COUPON USED AT SOUTHERN RESEARCH INSTITUTE, TO DEVELOP DATA ON BILLET L-1-11

values quoted in the table for the radial directions are the averaged values predicted for the nearest appropriate position in the billet. Further, it must be remembered that all predicted values in the axial direction are the integrated values for the full length of the billet while the measured values were obtained from specimens cut through only about half of the billet length.

The majority of the test coupons cut from billet No. L-1-11 were tested at elevated temperatures; therefore, the only valid correlations that can be carried out at this time are those for the specimens that were measured at room temperature.

C. PROPERTY CORRELATIONS, BILLET L-1-11 ATJ-S

In the axial direction, only three test coupons were destructively tested at room temperature; however, all density values can be compared and this has been done in the following. All axial specimens were taken from the billet at points which correspond with NDT data points.

Density Comparisons, Against the Grain, L-1-11, Southern Research Data

Specimen No.		Density		
Philco-Ford	Avco	Predicted	Measured	Percent Variation
A01-270	A9007	1.795	1.814	1.06
A03-225	A4505	1.805	1.802	0.17
A02-90	A9002	1.795	1.799	0.22
A12-45	A4502	1.805	1.795	0.56
A11-225	A4507	1.818	1.819	0.06
A13-135	A3503	1.801	1.801	
A21-135	A3502	1.801	1.810	0.50
A23-90	A9003	1.813	1.800	0.72
A22-315	A3506	1.804	1.802	0.11
A32-225	A4506	1.798	1.807	0.50
A33-45	A4503	1.794	1.801	0.39
A32-270	A9006	1.806	1.804	0.11
A52-135	A3502	1.801	1.800	0.06
A31-180	A0007	1.809	1.815	0.33
A31-45	A4501	1.805	1.805	
A3 -CTR	A0004	1.802	1.802	
A41-00	A0001	1.803	1.809	0.33
A43-315	A3505	1.802	1.801	0.06
A42-180	A0006	1.809	1.801	0.44
A51-315	A3507	1.801	1.808	0.39
A31-90	A9001	1.816	1.806	0.55
A53-270	A9005	1.797	1.800	0.17

Modulus Comparison - Against the Grain, L-1-11, Southern Research Data

Specimen No.		Modulus x 10^6 psi		
Philco-Ford	Avco	Dynamic V_L^2	Measured Initial	Percent Variation
A01-270	A9007	1.23	1.08	13.9
A03-225	A4505	1.22	1.13	8.0
A02-90	A9002	1.23	0.99	24.2

Tensile Strength Comparison, Against the Grain L-1-11 - SoRI Data
(At STF of 0.0045 inch per inch)

Specimen No.		Tensile Strength, psi		
Philco-Ford	Avco	Predicted	Measured	Percent Variation
A01-270	A9007	3160	4120	30.4
A03-225	A4505	3127	3480	11.3
A02-90	A9002	3184	3700	16.2

Note: The tensile strength values shown above were predicted on the basis of a strain to failure value of 0.0045 inch per inch. The same table is presented again below showing tensile strength values computed on the Philco-Ford measured values of strain to failure for each individual coupon.

Tensile Strength Comparisons, Against the Grain L-1-11 - SoRI Data

Specimen No.		Tensile Strength, psi			
Philco-Ford	Avco	Predicted	Measured	STF Measured	Percent Variation
A01-270	A9007	4424	4120	0.0063	7.4
A03-225	A4505	3196	3480	0.0046	8.9
A02-90	A9002	3750	3700	0.0053	1.4

Density Comparisons, With the Grain L-1-11, Southern Research Data

Specimen No.	Density Predicted	Density Measured	Percent Variation
W03-M	1.788	1.797	0.50
W04-R	1.802	1.812	0.55
W01-L	1.793	1.802	0.50
W14-M	1.790	1.800	0.56
W16-R	1.813	1.826	0.72
W12-L	1.793	1.801	0.45
W25-M	1.796		
W21-R	1.793	1.799	0.33
W23-L	1.790	1.799	0.50
W34-L	1.792	1.800	0.45
W32-R	1.793	1.801	0.45
W36-M	1.807	1.825	1.00
W41-M	1.797	1.797	0.06
W43-R	1.790	1.808	1.01
W45-L	1.797	1.812	0.83
W56-L	1.813	1.827	0.77
W54-R	1.792	1.801	0.50
W52-M	1.793	1.797	0.22

Modulus Comparisons, With the Grain, L-1-11, SoRI Data

Specimen No.	Modulus x 10^6 Predicted (Av) Dynamic Mod. (V_L^2)	Modulus x 10^6 Measured (initial)	Percent Variation
W03-M	1.74	1.56	11.5
W05-R	1.75	1.46	19.9
W01-L	1.72	1.45	18.6

Tensile Strength Comparisons, With the Grain, L-1-11, SoRI Data
(at strain-to-failure of 0.0034 inch per inch)

Specimen No.	Tensile Strength, psi Predicted (Av)	Tensile Strength, psi Measured	Percent Variation
W03-M	3702	4520	22.1
W05-R	3735	4560	22.1
W01-L	3664	4750	29.6

The tensile strength comparison table is repeated again to indicate what the predicted values would be using the individually measured strain-to-failure on each coupon.

Tensile Strength Comparisons, With the Grain, L-1-11, SoRI Data

Specimen No.	Tensile Strength, psi Predicted (Av)	Tensile Strength, psi Measured	STF inch per inch	Percent Variation
W03-M	4900	4520	0.0045	8.4
W05-R	5273	4560	0.0048	15.6
W01-L	4634	4750	0.0043	2.5

Graphite billet No. L-1-5 was cut into a nose tip and six test coupons as shown in the cutting plans Figures 52 and 55. In this case, the three axial specimens correspond very closely with NDT test data points except that once again they are limited to about one-half of the billet length. The coupons cut in the "with the grain" direction, however, are cut across a chord of the circle rather than a diameter so that the predicted values appearing in the following tables represent averaged values for the appropriate level in the billet.

Density Comparisons L-1-5 - Philco-Ford Data

Specimen No.		Density		
Philco-Ford	Avco	Predicted	Measured	Percent Variation
A001 (7-12)	A0001	1.795	1.815	1.1
A451 (7-12)	A4501	1.816		
A457 (2-7)	A4507	1.806		
RO-90-1		1.795	1.812	0.95
RO-90-3		1.794		
RO-90-5		1.786		

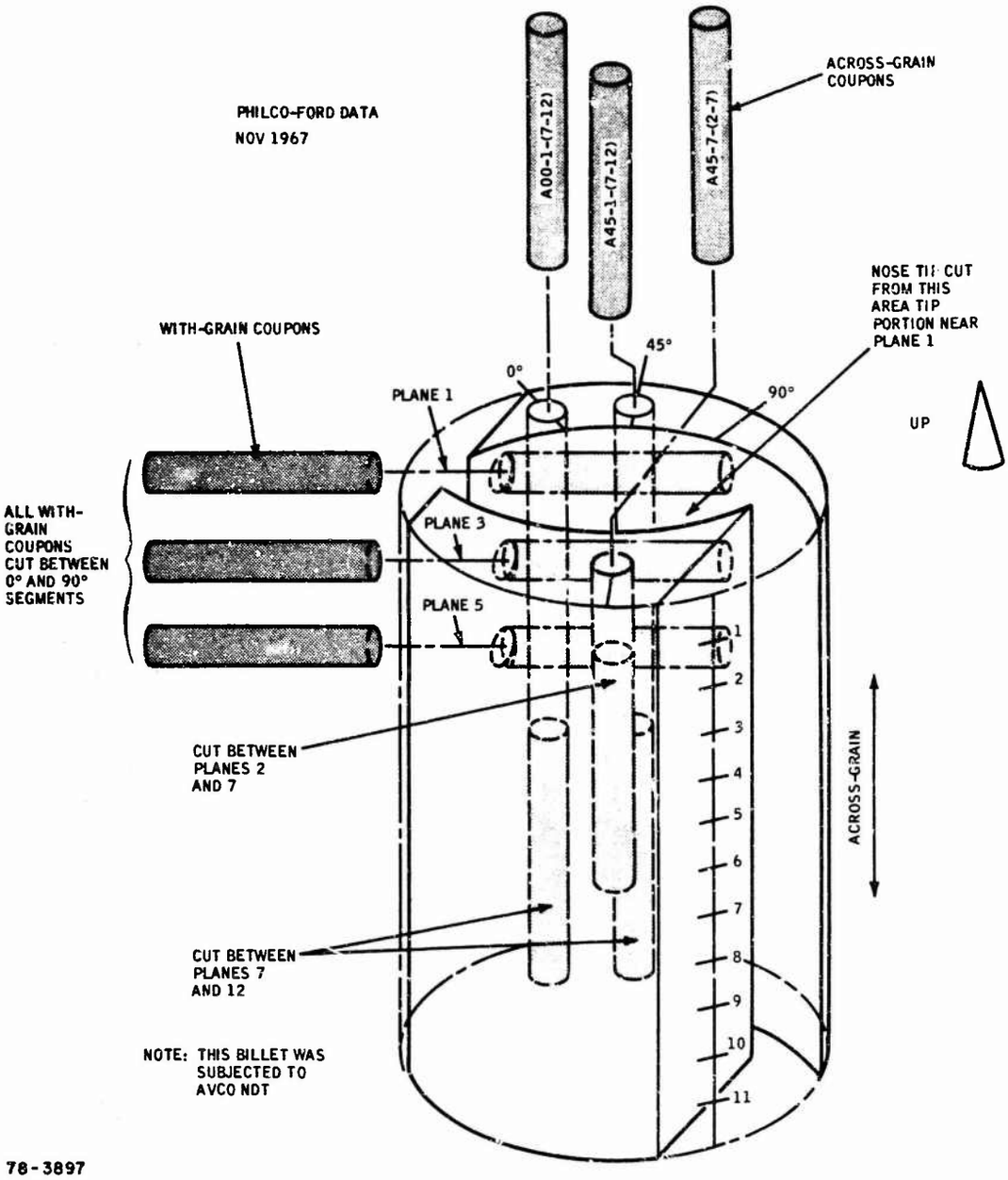

Figure 52 ATJS BILLET L-1-5 TESTED AT PHILCO-FORD

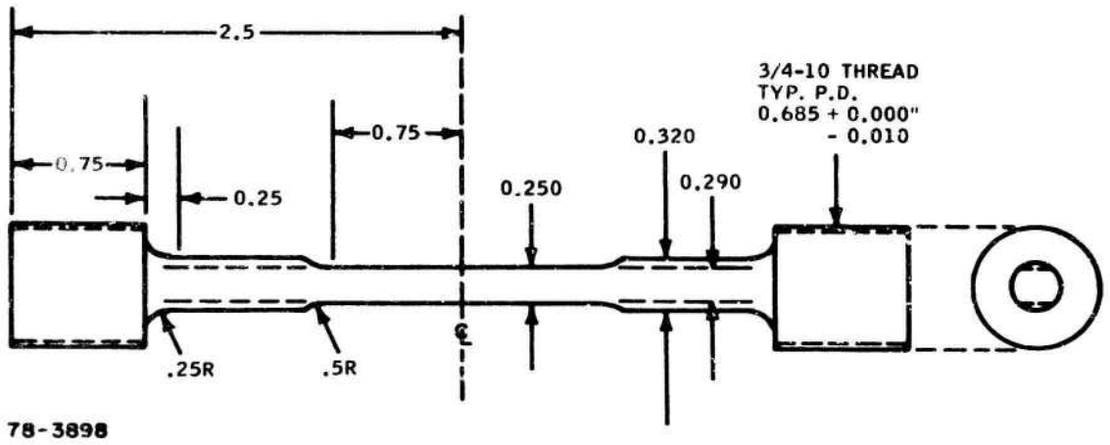

Figure 53 TENSILE COUPON USED AT PHILCO-FORD, TO DEVELOP DATA ON BILLETS L-1-5, L-11-7, AND L-14-2

Density Comparisons, L-11-7, Philco-Ford Data

Specimen No.		Density		
Philco-Ford	Avco	Predicted	Measured	Percent Variation
A180-1 (2-7)	A0007	1.823	1.826	0.16
A135-1 (7-12)	A3501	1.835		
A90-1 (7-12)	A9001	1.818		
R45-135-1		1.824	1.83	0.33
R45-135-3		1.813		
R45-135-5		1.818		

Modulus Comparisons, L-11-7, Philco-Ford Data

Specimen No.		Modulus x 10^6 psi		
Philco-Ford	Avco	Predicted (V_L^2)	Measured Initial Tensile	Percent Variation
A180-1 (2-7)	A0007	1.273	1.25	1.84
A135-1 (7-12)	A3501	1.284	1.27	1.10
A90-1 (7-12)	A9001	1.291	1.26	2.46
R45-135-1		1.857	1.33	39.62
R45-135-3		1.841	1.30	41.62
R45-135-5		1.909	1.28	49.14

Tensile Strength Comparisons, L-11-7, Philco-Ford

Specimen No.		Tensile Strength, psi			
Philco-Ford	Avco	Predicted	Measured	STF inch per inch	Percent Variation
A180-1 (2-7)	A0007	33.7	3940		18.8
A135-1 (7-12)	A3501	3358	3700	0.0045	10.2
A90-1 (7-12)	A9001	3382	3780		11.8
R45-135-1		4016	4550		13.3
R45-135-3		3975	4070	0.0034	2.4
R45-135-5		4152	4650		12.0

In the table below, the tensile strength comparisons are repeated using the individual strain-to-failure values measured for each specimen.

Tensile Strength Comparisons, L-11-7, Philco-Ford

Specimen No.		Tensile Strength, psi			
Philco-Ford	Avco	Predicted Avco	Measured Philco-Ford	STF inch per inch	Percent Variation
A180-1 (2-7)	A0007	3902	3940	0.0053	0.97
A135-1 (7-12)	A3501	3852	3700	0.0052	4.11
A90-1 (7-12)	A9001	4178	3780	0.0051	10.53
R45-135-1		6260	4550	0.0040	37.6
R45-135-3		6079	4070	0.0039	49.4
R45-135-5		6228	4650	0.0042	

TABLE X

ATJS TENSILE DATA (BILLET L-1-11)

Loading Direction	Test Temperature (°F)	Loading Rate (psi/min)	Specimen Number	Coupon Bulk Density (g/cm^3)	Ultimate Tensile Strength (psi)	Initial Elastic Modulus (x 10^6 psi)	Total Unit Axial Strain (in/in)	Remarks
Across Grain	70	10,000	A01-270	1.814	4120	1.08	0.0063	Strain gages used for strain meas.
			A03-210	1.802	3480	1.13	0.0046	
			A02-90	1.799	3700	0.99	0.0053	
	1500		A12-45	1.795	4420	1.06	0.0061	
			A11-225	1.819	5000	0.92	0.0073	
			A13-150	1.801	4100	1.01	0.0053	
	2500		A21-135	1.810	5000	1.08	0.0061	
			A23-90	1.800	4880	1.17	0.0056	
			A22-315	1.802	4700	1.15	0.0053	
	3500		A32-225	1.807	5950	1.10	0.0074	
			A33-30	1.801	5700	1.23	0.0060	
			A32-270	1.804	>5400	1.52	>0.0048	Head broke off specimen
			A52-135*	1.800	4800	1.66	0.0037	
			A31-180	1.815	6250	1.40	0.0075	
			A31-45	1.805	5180	1.25	0.0055	
			A3-CTR	1.802	5450	1.23	0.0058	
	4500		A41-0	1.809	6390	1.02	0.0152	Head broke off specimen
			A43-330	1.801	>7100	0.88	>0.040	
			A42-180	1.801	6900	1.22	0.0194	
	5000	10,000	A51-315	1.808	6500	0.90	0.0355	
			A31-90	1.806	7130	0.90	>0.040	Head broke off
			A53-270	1.800	6630	0.70	>0.035	

*Coupon designated for 5000°F test was tested at 3500°F as indicated.

TABLE XI

ATJS TENSILE DATA (BILLET L-1-11)

Loading Direction	Test Temperature (°F)	Loading Rate (psi/min)	Specimen Number	Coupon Bulk Density (g/cm^3)	Ultimate Tensile Strength (psi)	Initial Elastic Modulus (x 10^6 psi)	Total Unit Axial Strain (in/in)	Remarks
With Grain	70	10,000	W03-M	1.797	4520	1.56	0.0045	Strain gages
			W05-R	1.812	4560	1.46	0.0048	used for
			W01-L	1.802	4750	1.45	0.0043	strain meas.
	1500		W14-M	1.800	4450	1.67	0.0035	
			W16-R	1.826	6250	1.49	0.0053	
			W12-L	1.801	5070	1.37	0.0042	
	2500		W25-M	-	5660	1.59	0.0043	Specimen broke
			W21-R	1.799	> 5350	1.89	> 0.0031	Outside gage
			W23-L	1.799	6400	1.63	0.0049	in radius
	3500		W34-L	1.800	5650	1.79	0.0036	
			W32-R	1.801	5630	1.72	0.0036	
			W36-M	1.825	8310	1.96	0.0070	
	4500		W41-M	1.796	8630	1.36	0.0184	
			W43-R	1.808	9200	1.46	0.025	
			W45-L	1.812	8290	1.33	0.0168	
	5000	10,000	W56-L	1.827	> 11250	0.87	0.035 at 6500 psi	Head broke off
			W54-R	1.801	> 9750	1.03	0.025 at 7300 psi	Head broke off
			W52-M	1.797	> 9150	1.07	0.035 at 7800 psi	Head broke off

TABLE XII

ATJS TENSILE DATA (BILLET L-1-5)*

Loading Direction	Test Temp (°F)	Loading Rate	Specimen No.	Coupon Bulk Density (g/cm^3)	Ultimate Tensile Strength (psi)	Initial Elastic Modulus (x 10^6 psi)	Total Unit Axial Strain (in/in)	Remarks
With-Grain	70	0.020 in/min	RO-90-1	1.812	4020	1.3	> 0.0038**	*See Figure 54 for cutting plan.
			RO-90-3	-	3220	1.23	> 0.0030**	
			RO-90-5	-	3870	1.27	> 0.0033**	**2.0-inch extensometer used
Across Grain	70	0.020 in/min	A00-1-(7-12)	1.815	4000	-	-	L-1-5 was evaluated at Avco
	70	0.020 in/min	A45-1-(7-12)	-	3640	-	-	
	70	0.020 in/min	A45-7-(2-7)	-	4040	-	-	

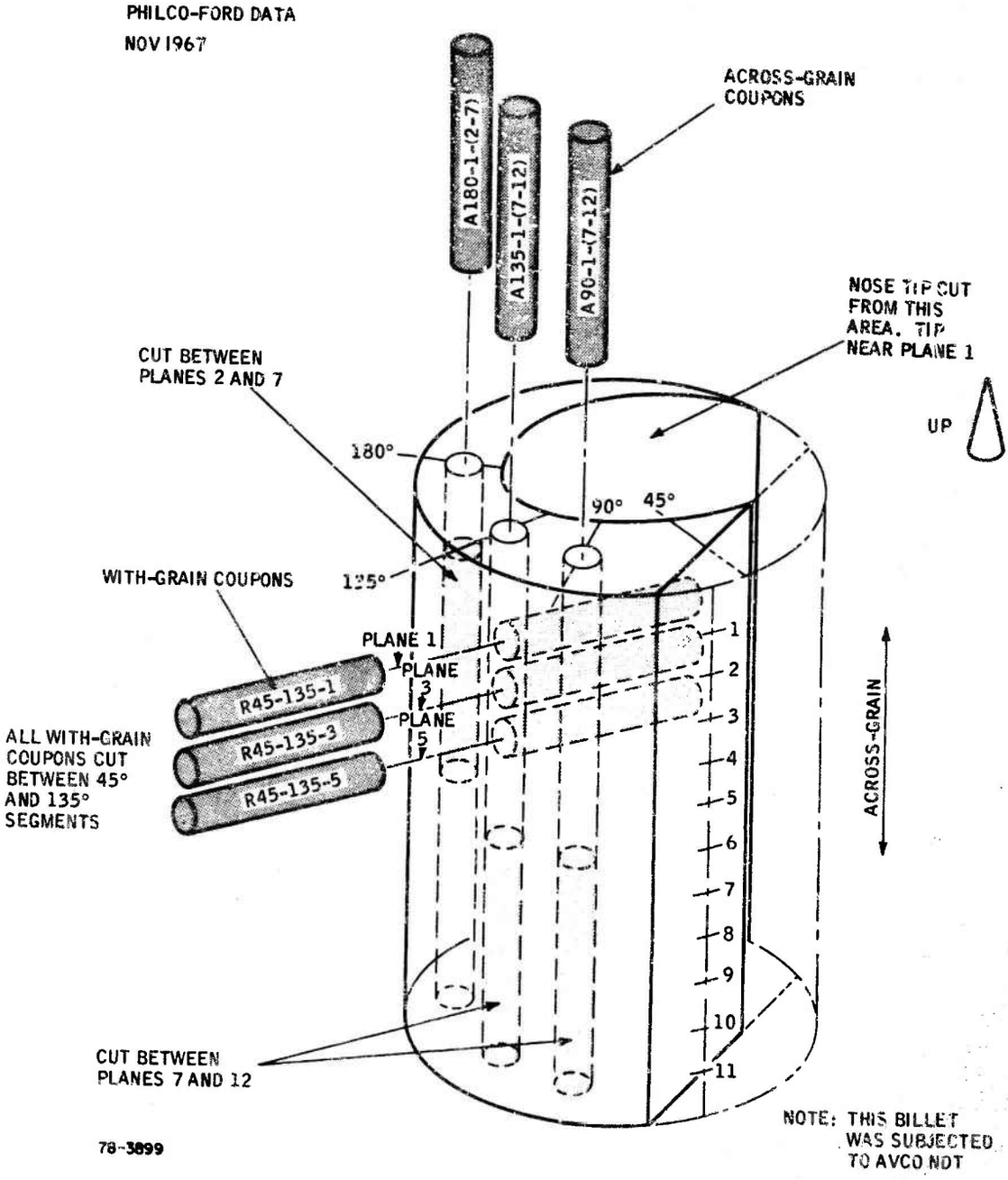

Figure 54 ATJS BILLET L-11-7 TESTED AT PHILCO-FORD

TABLE XIII

ATJS TENSILE DATA BILLET (L-11-7)*

Loading Direction	Test Temp (°F)	Loading Rate	Specimen Number	Coupon Bulk Density (g/cm^3)	Ultimate Tensile Strength (psi)	Initial Elastic Modulus (x 10^6 psi)	Total Unit Axial Strain (in/in)	Remarks
With-Grain	70	0.02 in/min	R45-135-1	1.83	4550	1.33	> 0.0040**	*See Figure 55 for cutting plan
	70	0.02 in/min	R45-135-3	-	4070	1.30	> 0.0039**	
	70	0.02 in/min	R45-135-5	-	4650	1.28	> 0.0042**	**2.0-inch extensometer used.
								***1.0-inch extensometer used.
Across Grain	70	0.02 in/min	A180-1-(2-7)	1.826	3940	1.25	0.0053***	L-11-7 was evaluated at Avco
	70	0.02 in/min	A135-1-(7-12)	-	3700	1.27	> 0.0052**	
	70	0.02 in/min	A90-1-(7-12)	-	3780	1.26	0.0051***	

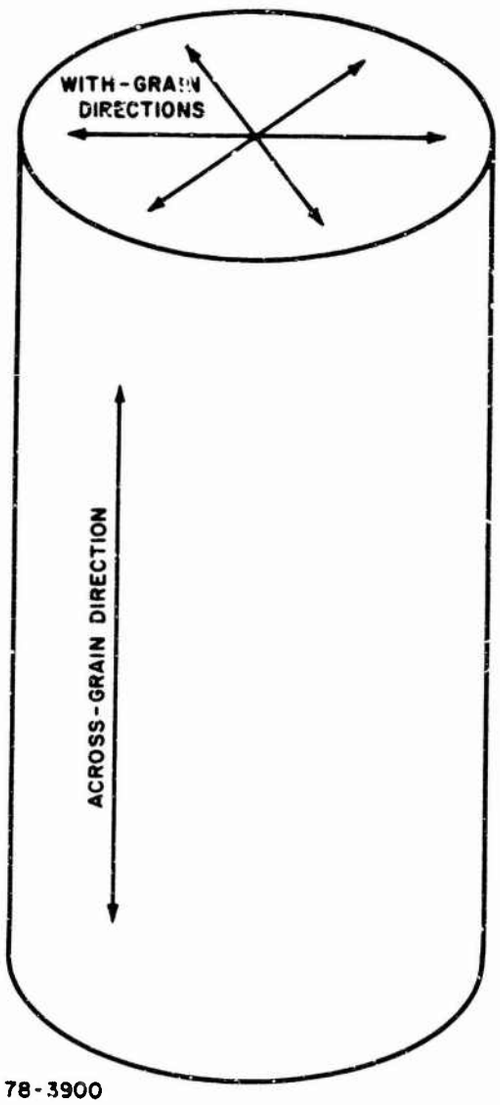

Figure 55 MATERIAL GRAIN DIRECTION IN A TJS GRAPHITE BILLET

III. SUMMARY

In an attempt to answer the question of how well NDT predicted the properties of graphite, it must be pointed out that not only is the sampling quantity rather small, but also in none of the data reported can there be claimed to be a complete one-to-one relationship between the destructive and the nondestructive test data. Even in the cases where the test coupon was cut from the billet at the NDT data points, as was the case with all axial and some radial specimens, the length of the coupon was considerably shorter than the billet dimension so it did not contain all the material that was included in the NDT characterization.

In all cases where the test coupon was taken from a position between two NDT test points, the indicated predicted values represent the averaged values from these two data points. In the case where the test coupon has been cut across a chord of the billet, the predicted property values represent the average values of all the test points evaluated at the particular level in the billet from which the coupon was cut. All instances in which averaged property values are indicated can be identified in the tables by the fact that no Avco test point number is identified.

It is apparent from the destructive data that the strain-to-failure values of the graphite do vary over wide limits, and in view of the fact that the Philco-Ford nose tip design is based on this property, it may prove that computer tabulations of strain-to-failure might be more important than the more conventional ultimate tensile strength computations. Such a computation would have to be based on experimentally determined values of tensile strength. Before such a procedure could be justified, however, it would have to be shown that variability in tensile strength is less than variability in strain-to-failure for the material in question. Such a determination could not be made from the data available in this report as the applicable strain-to-failure values are based in many cases on 2-inch extensiometers rather than strain gages. Furthermore, it should be noted that many of the experimentally determined values of strain-to-failure are reported as being greater than a specified value, thus a further element of uncertainty is introduced.

A. PROPERTY CORRELATIONS

1. Density

In general, the comparisons between predicted and measured densities agree to within ±1 percent. The few minor exceptions noted can probably be attributed to the lack of a complete one-to-one correspondence in the material tested by the two methods. It is believed, however, that the radiometric density procedures now being followed are capable of determining incremental densities quantitatively with an accuracy of 1 percent. The results reported here appear to verify this conclusion.

2. Modulus

The comparisons reported between the predicted and measured modulus values, at first sight, appear to indicate some fairly wide discrepancies. However, a combination of several factors is involved here which unless taken into consideration, could prove to be misleading.

The most obvious of these factors is the lack of a one-to-one relationship between the samples of material being evaluated, particularly as the experimental determination is made over a relatively short gage length in the center of the tensile bar.

It must be also pointed out that most of the tensile bars cut in the "with grain" direction are cut along a chord rather than a diameter of the billet, thus the nondestructive and the experimental moduli are being determined on different samples of the material, and in different direction.

Another factor which must be taken into consideration is the nature of the property being measured. The nondestructive determination of modulus computed from the expression $E_D = V_L^2$ is a measure of the dynamic modulus of the material whereas the experimentally determined value is a measure of the initial tensile modulus, or the initial slope of the tensile stress-strain curve. These values are not the same as can be seen by reference to Figure 56.

Note that in the figure, the slope of the line denoting E_D or dV_L^2 is greater than the slope of the tensile modulus or E_T line which is the initial slope of the stress-strain curve. The dynamic modulus, by its very nature, will always be larger than the initial tensile modulus.

The relationship between these two moduli, as determined nondestructively and experimentally, is not a constant value, but a variable function of specimen geometry, including gage length, and characteristics of the tensile test machine on which the determination is carried out. It is for these reasons then that the predicted value of dynamic modulus is always expected to be higher than the experimentally determined initial tensile modulus, and by an indeterminate and variable factor.

A further factor which contributes to uncertainty in the measurement of the initial tensile modulus is a human one. This modulus is defined as the slope of the initial part of the tensile stress strain curve. Individual interpretations of the exact value of this slope can vary considerably.

An examination of the data reported here indicates that the nondestructively determined value of dynamic modulus is considerably more consistent than the destructively measured values. Lockyer[2] has shown a large spread in data in his comparison of dynamic modulus and tensile modulus, whereas his comparisons of sonic resonance modulus and ultrasonic wave velocity indicate a high degree of consistency. It must be noted that data scatter evident in correlations between dynamic and tensile moduli is considered to be associated with limitations involved in tensile modulus determinations.

3. Ultimate Tensile Strength

When comparing predicted and measured tensile strengths, it becomes immediately obvious that the predicted values are consistently low, or unduly pessimistic. When considering the reasons for this apparent discrepancy, it appears anomalous at first that these values should be low, in view of the fact that the predicted moduli all tended to be unduly high as compared to the measured values of initial tensile modulus. However, it must be pointed out that the factors

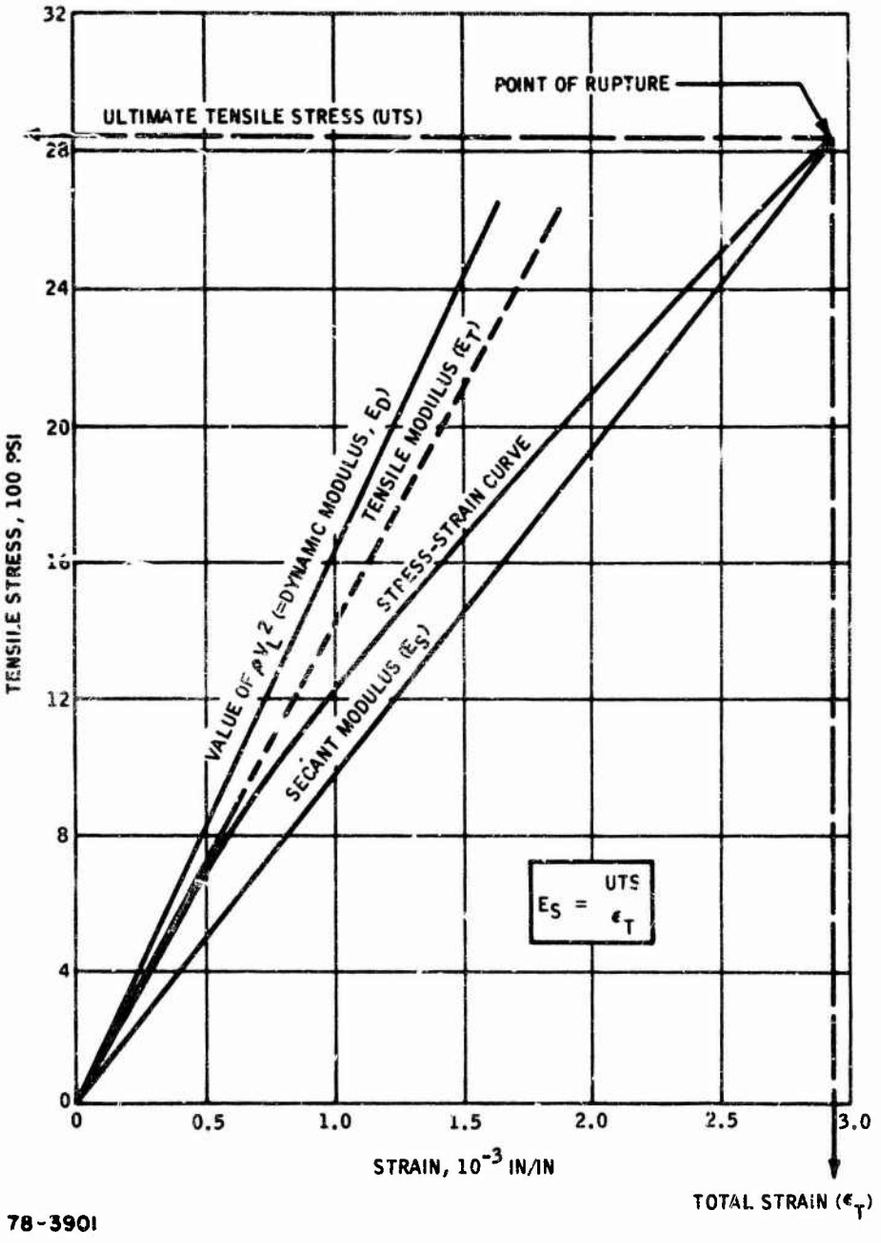

78-3901

Figure 56 RELATIONSHIPS CONSIDERED IN DEVELOPMENT OF NONDESTRUCTIVE TENSILE STRENGTH DETERMINATION

of proportionality used for the determination of the secant modulus are applied to the value of the dynamic rather than the initial tensile modulus, and are not related to the difference between them.

In connection with the relationship between the dynamic and the secant moduli, it must be pointed out that the factors of proportionality were originally determined for grades of graphite which characteristically exhibited strain-to-failure values which were not only relatively constant, but were also considerably lower than has proved to be the case for the ATJ-S involved here. Experimental evidence now being accumulated appears to indicate that the extrapolation of these factors of proportionality into the less brittle grades of graphite, such as ATJ-S cannot be done without introducing a margin of error.

Another factor which must be pointed out is that the reported values of strain-to-failure for the graphite involved here appear not only to be considerably higher than the values used for computation purposes, but they also vary over a wide range. Much of this variation can probably be attributed to the variable factors involved in making the measurements such as the manner in which the specimen is supported in the tensile machine, geometric considerations pertaining to the tensile specimen, and the manner in which the measurement of strain is accomplished. It appears, however, that in this grade of graphite, the strain-to-failure values are not constant; but vary over a range considerably wider than that found in the grades exhibiting lower strain-to-failure values. Wherever possible in the tables, the predicted tensile strength has been recomputed on the basis of the measured strain-to-failure. It will be noted that in all these cases, the correlation between predicted and measured tensile strengths are closer.

It must be remembered that tensile strength is only predicted on the basis of flaw-free materials; therefore, complete correspondence can not be expected.

B. EFFECT OF POISSON'S RATIO

It has been shown that the expression $E_D = dV_L^2$ can only be considered to be valid in the case of materials for which the effects of Poisson's ratio can be neglected as is the case with the more brittle grades of graphite. However, for grades of graphite exhibiting relatively higher strain-to-failure values, this may no longer be the case, as these grades tend to depart further and further from the concept of a completely brittle material. Under these conditions, not only would the quantitative value of dynamic modulus be subjected to error, but also the relationship between dynamic modulus to both initial tensile and secant moduli will become more uncertain.

When considering the influence of Poisson's ratio on the measured modulus of graphite, it is important to consider the effects of material anisotropy. A tensile test bar cut with its axis parallel to the with grain direction will have normal to its axis conditions of "with the grain" in one direction, and "against the grain" perpendicular to this direction.

Under such conditions, an axial stress on a test specimen of round cross section will tend to alter the cross section to an elliptical configuration. Such an effect could lead to considerable confusion, in the direct measurement of Poisson's

ratio which would vary depending upon the direction in which the meaaurements were taken. It seems quite possible that, in a material with sufficient anisotropy, and with the thickness measurement taken in the direction of the major axis of the eclipse, that an apparent negative value could be obtained for Poisson's ratio. The influence of such an effect on the relationship given by $E_D = V_L^2$ is unknown.

Any factor which influences the validity of the relationship between dynamic modulus and the density-velocity squared product will not only effect the value of the predicted modulus, but will also influence the predicted tensile strength of the material which is derived from this value.

C. RELATIONSHIP BETWEEN DYNAMIC AND INITIAL TENSILE MODULI

In an attempt to establish a relationship between the predicted dynamic modulus and the measured initial tensile modulus,* it must be pointed out that the data available are limited to only those measurements made at room temperature. The sampling size is thus extremely small.

It will be noted from the tablea that from the data generated by Southern Research Institute, the factor of proportionality between the two moduli ranges from 0.81 to 0.93 with an average of about 0.86. No significant difference appears to exist with respect to grain direction. However, only a total of six samples are involved.

When examining the data from Philco-Ford, this factor varies from 0.67 to 0.77 with an average of about 0.73 for the with grain directions whereas against the grain comparisons yield a factor of 0.98.

It is perhaps very significant that the SoRI measurements of initial tensile modulus appear to be relatively independent of grain direction, whereas the Philco-Ford data tends to indicate a strong dependence on grain orientation. A possible explanation of this fact could lie in the fact that it is difficult if not impossible to support a specimen in a tensile testing machine in such a manner that no bending torque is introduced. The Southern Research Institute tensile machine supports the specimen by means of the "air bearing" which theoretically eliminates this problem.

* This relationship is defined by the expression, $E_T = K E_D$, where E_T and E_D are the two moduli, and K is the relationship factor.

IV. CONCLUSIONS AND RECOMMENDATIONS

In retrospect, it can now be said that this joint effort has not been particularly effective as an effort to correlate nondestructively determined properties with service performance of graphite hardware. In any future program conducted with this end in view, the following recommendations are made:

1. All sampling for destructive tests should be accomplished in accordance with NDT test positions in order that the same volume of material be evaluated by both methods.

2. Definitive data with respect to Poisson's ratio and strain to failure values should be established for the NDT program. Lack of such data may seriously affect the NDT modulus determinations, in addition to invalidating the tensile strength determinations.

3. Test bars should be cut from the billet with full regard to NDT findings. The material tested should cover a range of characteristics, including defects. Defects are important, and an effort to determine their influence on material characteristics should be made.

4. For the most meaningful correlations, the test bars and hardware, after being cut from the billet should be individually characterized by nondestructive means prior to any destructive testing.

It is realized that this particular test program was fully planned and initiated before the question of nondestructive characterization was brought up. As a result, it was a matter of considerable difficulty to reorient the planning with a view towards injecting broader objectives within the allowable time frame.

V. REFERENCES

1. Lockyer, G. E., E. Lenoe, and A. W. Schultz, Investigation of Nondestructive Methods for the Evaluation of Graphite Materials, (AFML-TR-66-101), Contract No. AF33(615)-1601.

2. Lockyer, G. E., Investigation of Nondestructive Methods for the Evaluation of Graphite Materials, Technical Report AFML-TR-65-113.

Unclassified
Security Classification

DOCUMENT CONTROL DATA - R & D

(Security classification of title, body of abstract and indexing annotation must be entered when the overall report is classified)

1. ORIGINATING ACTIVITY (Corporate author) Avco Government Products Group Space Systems Division, 201 Lowell St., Wilmington, Massachusetts 01857	2a. REPORT SECURITY CLASSIFICATION None 2b. GROUP

3. REPORT TITLE

Investigation of Nondestructive Methods for the Evaluation of Graphite Materials

4. DESCRIPTIVE NOTES (Type of report and inclusive dates)
Technical Report, 15 April 1967 to 15 May 1968

5. AUTHOR(S) (First name, middle initial, last name)
R. C. Stinebring
A. W. Schultz
J. W. Orner

6. REPORT DATE	7a. TOTAL NO. OF PAGES	7b. NO. OF REFS
February 1969	128	9

8a. CONTRACT OR GRANT NO. AF33(615)-3942 b. PROJECT NO. 7360 c. d.	9a. ORIGINATOR'S REPORT NUMBER(S) AVSSD-0236-68-RR 9b. OTHER REPORT NO(S) (Any other numbers that may be assigned this report) AFML-TR-67-128, Part II

10. DISTRIBUTION STATEMENT
This document is subject to special export controls and each transmittal to foreign governments or foreign nationals may be made only with prior approval of the AF Materials Laboratory, Wright-Patterson AFB, Ohio 45433.

11. SUPPLEMENTARY NOTES	12. SPONSORING MILITARY ACTIVITY
	Air Force Materials Laboratory Air Force Systems Command Wright-Patterson Air Force Base, Ohio

13. ABSTRACT

The objective of the program was to utilize the nondestructive testing information, correlations, and techniques, developed during the previous year, for characterizing and evaluating zirconium and hafnium diboride systems and aerospace graphite materials.

The program was divided into three distinct phases:

A. Characterization and Evaluation of Diboride Materials
B. Analysis of the Nondestructive Infrared Method for Measuring the Thermal Inertia ($k\rho C\rho$)
C. Application of NDT Techniques for Evaluating and Predicting Properties in Aerospace Graphite Billets

During Phase A, over 800 billets of diboride systems were evaluated and characterized. Several important correlations are presented relating nondestructive test results to billet quality as well as mechanical and thermal behavior. Among the most effective NDT techniques for evaluating the diborides are ultrasonic velocity, ultrasonic pulse-echo, radiography, gamma radiometry, eddy current, thermoelectric and dye penetrant.

Phase B was concerned with the determination of limitations and influencing variables on the performance of the infrared radiometric techniques for determining thermal inertia ($k\rho C\rho$). This technique offers several advantages, such as increased speed, non-contact with specimen and ability to evaluate actual structures.

The geometrical limitations, such as curvature, thickness, edge effects, as well as range of thermal conductivities, etc., are discussed. Suggestions are made for improvements in the apparatus and for adapting it for field use.

Aerospace graphite (ATJ-S) used in a Philco-Ford nose cone program was characterized in the billet form in Phase C of the contract. The use of gamma radiometry and ultrasonic velocity data in a computer program allowed modulus to be monitored and density changes to be noted. Some work was also done on detection and characterization of flaws and anomalies, such as "calcium" deposits, parting lines, etc.; but their effects on material behavior were not studied. Recommendations are presented for improving this type of effort. These include the judicious use of such destructive test data as strain to failure, Poisson's ratio, ultimate tensile strength, modulus and effects of flaws for obtaining the most meaningful nondestructive test correlations.

DD FORM 1 NOV 68 1473

Unclassified
Security Classification

14. KEY WORDS	LINK A		LINK B		LINK C	
	ROLE	WT	ROLE	WT	ROLE	WT
Graphite						
Ceramics						
Zirconium Diboride						
Hafnium Diboride						
Nondestructive Testing						
Dynamic Modulus						
Ultrasonic Velocity						
Ultrasonic Flaw Detection						
Infrared Radiometry						
Thermal Inertia						
Thermoelectric Test						
Radiography						
Eddy Current Test						
Dye Penetrant						
Gamma Radiometry						